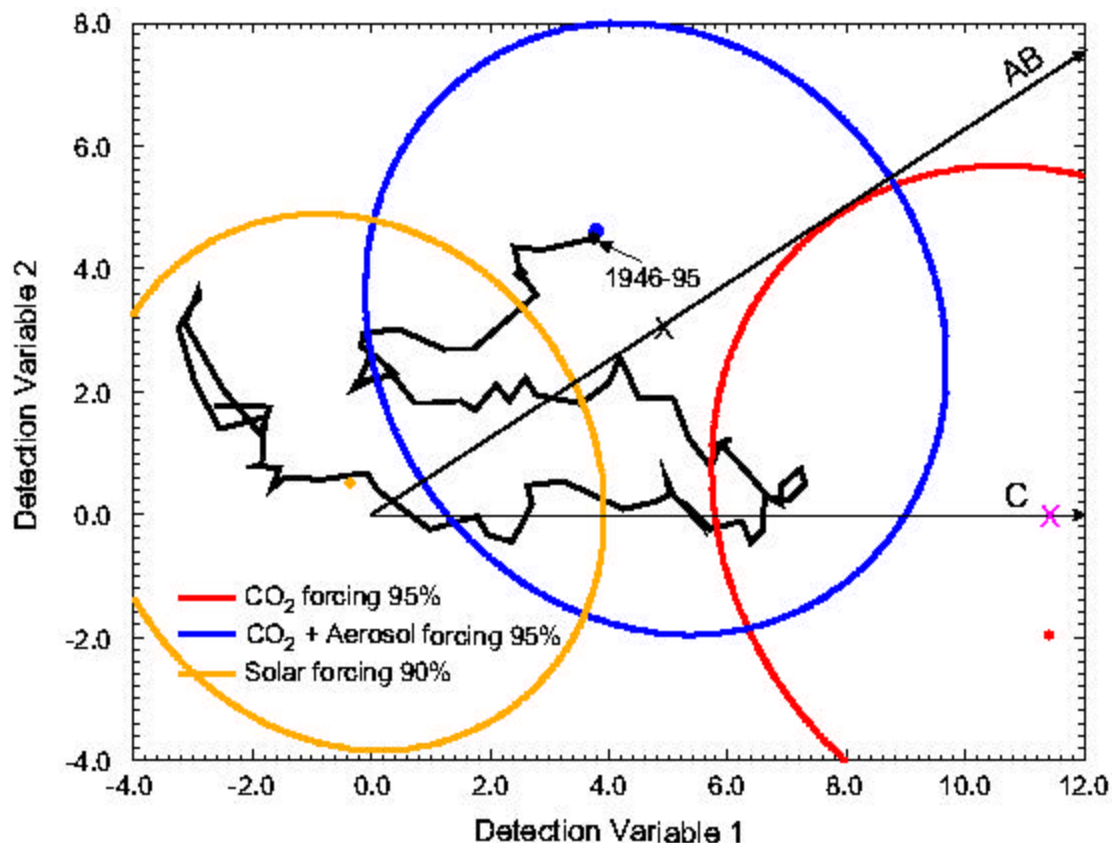


# Summary Report of the Project

## Simulation, Diagnosis and Detection of the Anthropogenic Climate Change (SIDDAKLICH)

ENV4-CT95-0102

Ulrich Cubasch, Myles Allen, Martin Beniston, Cédric Bertrand, Sabine Brinkop, Jean-Yves Caneill, Jean-Louis Dufresne, Laurent Fairhead, Marie-Angèle Filiberti, Jonathan Gregory, Gabriele Hegerl, Guido Hoffmann, Tim Johns, Gareth Jones, Carine Laurent, Ruth McDonald, John Mitchell, David Parker, Josef Oberhuber, Chantal Poncin, Robert Sausen, Ulrich Schlese, Peter Stott, Simon Tett, Herve leTreur, Uwe Ulbrich, Sophie Valcke, Reinhard Voss, Martin Wild, Jean-Pascal Ypersele



# Simulation, Diagnosis and Detection of the Anthropogenic Climate Change (SIDDAKLICH)

## ENV4-CT95-0102

Ulrich Cubasch<sup>1</sup>, Myles Allen<sup>4</sup>, Martin Beniston<sup>8</sup>, Cédric Bertrand<sup>3</sup>, Sabine Brinkop<sup>9</sup>, Jean-Yves Caneill<sup>2</sup>, Jean-Louis Dufresne<sup>10</sup>, Laurent Fairhead<sup>6</sup>, Marie-Angèle Filiberti<sup>6</sup>, Jonathan Gregory<sup>4</sup>, Gabriele Hegerl<sup>7</sup>, Guido Hoffmann<sup>5</sup>, Tim Johns<sup>4</sup>, Gareth Jones<sup>4</sup>, Carine Laurent<sup>6</sup>, Ruth McDonald<sup>4</sup>, John Mitchell<sup>4</sup>, David Parker<sup>4</sup>, Josef Oberhuber<sup>1</sup>, Chantal Poncin<sup>3</sup>, Robert Sausen<sup>9</sup>, Ulrich Schlese<sup>1</sup>, Peter Stott<sup>4</sup>, Simon Tett<sup>4</sup>, Herve leTreut<sup>6</sup>, Uwe Ulbrich<sup>5</sup>, Sophie Valcke<sup>10</sup>, Reinhard Voss<sup>1</sup>, Martin Wild<sup>8</sup>, Jean-Pascal Ypersele<sup>3</sup>

small numbers indicate institute, for which the work was performed under this contract (not present affiliation)

### List of project partners

1. U. Cubasch (**coordinator**), Deutsches Klimarechenzentrum GmbH (DKRZ), Bundesstr. 55, D-20146 Hamburg, Germany; Tel: +49 40 41173-376, Fax: +49 40 41173 400, email: [cubasch@dkrz.de](mailto:cubasch@dkrz.de)
2. J.-Y. Caneill, EDF, 6, quai Watier, F-78401 Chatou cedex, France; Tel: +33 1 30 87 79 60, Fax: +33 1 30 87 83 34, email: [jean-yves.caneill@der.edf.fr](mailto:jean-yves.caneill@der.edf.fr)
3. J. P. van Ypersele, UCL/ASTR, 2, Chemin du Cyclotron, B-1348 Louvain-la-Neuve, Belgium; Tel: +32 10 473296, Fax: +32 10 474722, email: [vanypersele@astr.ucl.ac.be](mailto:vanypersele@astr.ucl.ac.be)
4. T. Johns, Hadley Centre (UKMO), London Rd, Bracknell, RG 12, 2SZ, UK; Tel: +44 1344 856 901, Fax +44 1344 854 898, email: [tcjohns@meto.gov.uk](mailto:tcjohns@meto.gov.uk)
5. P. Speth, IGM, Kerpener Str. 13, D-50937 Köln, Germany; Tel: +49 221 470 3679, Fax: +49 221 4705 161, email: [speth@meteo.uni-koeln.de](mailto:speth@meteo.uni-koeln.de)
6. H. le Treut, IPSL, 24, Rue Lhomond, F-75 231 Paris Cedex 05, France, Tel. +33 1 44 32 22 37, Fax +33 1 43 36 83 92, email: [letreut@lmd.ens.fr](mailto:letreut@lmd.ens.fr)
7. K. Hasselmann, MPI für Meteorologie (MPIHH), Bundesstr. 55, D-20146 Hamburg, Germany; Tel. +49 40 41173 236, Fax: +49 40-41173 250, email: [klaus.hasselmann@dkrz.de](mailto:klaus.hasselmann@dkrz.de)
8. Martin Beniston, Institute of Geography, University of Fribourg, Perolles, CH-1700 FRIBOURG, Switzerland, Tel 0041 26 300 90 10 (Sekr.), Fax 0041 26 300 97 46, email: [martin.beniston@unifr.ch](mailto:martin.beniston@unifr.ch); Martin Wild, Eidgenössische Technische Hochschule Zürich, Abteilung Klimatologie, Winterthurstr. 190, CH 8057 Zürich, Schweiz, Tel 0041 1 257-5236, Fax 0041 1 362 5197, email: [wild@geo.umnw.ethz.ch](mailto:wild@geo.umnw.ethz.ch)
9. R. Sausen, DLR, D-82 234 Oberpfaffenhofen, Germany; Tel: +49 8153 282500, Fax: +49 8153 28 1841, email: [robert.sausen@dlr.de](mailto:robert.sausen@dlr.de)
- 10 O. Thual, CERFACS, 42, Avenue G. Coriolis, F-31057 Toulouse, France; Tel: +33 61 193070, Fax: +33 61 19 3000, email: [thual@cerfacs.fr](mailto:thual@cerfacs.fr)

<b>ABSTRACT</b>	<b>4</b>
<b>1. INTRODUCTION</b>	<b>5</b>
<b>2. MODEL DEVELOPMENT</b>	<b>6</b>
2.1. THE HADLEY CENTRE MODELS	8
2.1.1. <i>HadCM2</i>	8
2.1.2. <i>HadCM3</i>	8
2.2. THE DKRZ/MPI MODELS	8
2.2.1. <i>Atmospheric component: ECHAM</i>	9
2.2.2. <i>Oceanic component: LSG</i>	9
2.2.3. <i>Oceanic component: OPYC</i>	9
2.3. THE CERFACS MODEL	9
2.4. THE IPSL MODEL	10
2.4.1. <i>Atmospheric component</i>	10
2.4.2. <i>Oceanic component</i>	10
2.5. THE UCL-ASTR MODEL	11
2.5.1. <i>Atmospheric component</i>	11
2.5.2. <i>Oceanic component</i>	11
2.6. MODEL COUPLING	12
<b>2.7. INITIALISATION AND SPIN UP</b>	<b>12</b>
<b>3. MODEL EXPERIMENT RESULTS</b>	<b>15</b>
3.1. MEAN CLIMATE OF THE CONTROL SIMULATIONS	15
3.1.1. <i>Sea-surface temperature</i>	17
3.1.2. <i>Overturning of the North-Atlantic circulation</i>	17
3.1.3. <i>Mean meridional climate</i>	20
3.2. MEAN CLIMATE OF THE CLIMATE CHANGE SIMULATIONS	22
3.2.1. <i>Response in anthropogenic and natural forcing experiments</i>	22
3.2.1.1. Coupled GCM simulations	22
3.2.1.2. Two-dimensional transient simulations	27
3.2.2. <i>Possible irreversible changes in the Atlantic ocean circulation</i>	32
3.2.2.1. during the next 200 years	32
3.2.2.2. in the longer term	34
3.2.3. <i>Flux-adjusted versus non flux-adjusted responses</i>	37
3.2.4. <i>The role of individual air-sea flux components</i>	38
3.3. MID-LATITUDE STORM TRACKS AND THE NORTH-ATLANTIC-OSCILLATION	40
3.3.1. <i>Changes of cyclone- and upper air storm tracks</i>	40
3.3.2. <i>Variability and anthropogenic changes of the NAO</i>	45
3.4. CONVECTIVE ACTIVITY	49
3.5. HIGH LATITUDE PROCESSES	50
<b>4. DETECTION AND ATTRIBUTION OF CLIMATE CHANGE</b>	<b>54</b>
4.1. FINGERPRINT ANALYSIS	57
4.2. CAUSES OF TWENTIETH CENTURY TEMPERATURE CHANGE:	59
<b>5. SUMMARY AND CONCLUSIONS</b>	<b>59</b>
<b>6. EXPLOITATION OF MODEL RESULTS</b>	<b>62</b>
<b>7. REFERENCES</b>	<b>63</b>

## Abstract

Climate responses under various anthropogenic and natural forcing scenarios have been studied and intercompared with several independent models and with different experimental strategies.

The model simulated patterns of temperature and precipitation responses to increases in the greenhouse gas concentration are related to the model feedbacks, and therefore differ in detail between models. Nevertheless, some broad features of the responses with a surface- and lower tropospheric warming in high latitudes, marked land-sea contrast with land warming more than the ocean surface, and intensified hydrological cycle (more evaporation and rainfall, with largest increases in the Tropics), are common to all models.

The models produce a 10-15% increase of winter storm track activity over the north-western Europe at the time of CO<sub>2</sub>-doubling. This increase is caused by an increasing baroclinicity over the entire north-east Atlantic with main changes occurring in the upper troposphere. In a warmer climate increases in storm intensity is due to a larger amount of water vapour in the atmosphere.

The observed close relationship between the NAO index and the Atlantic storm track intensity is confirmed in the model simulations

During the summer and winter season, the global mean convective rain rate decreases by about 4-5 % resulting from a strong decrease of the frequency of deep convective events. Globally, for rain rates between 5 and 40 mm/day a decrease of both frequency and the respective mean daily rain rates is found. However, for convective rain rates larger than 40 mm/day both frequency and mean daily rain rate increase indicating an increase of strong rain events.

There is no agreement about the net influence of glacier mass gain in Antarctica and mass loss in Greenland on sea level change between the different simulations.

Common to all stabilising experiments, in which the greenhouse gas concentration is kept constant after an initial rise to 2\*CO<sub>2</sub> or 4\*CO<sub>2</sub>, is a strong warming during the years, while the greenhouse gas concentration is still increasing, followed by a weaker, but still considerable, warming during the period with fixed concentrations. This long-term adjustment is also visible in the sea-level change due to thermal expansion. The overturning circulation in the North Atlantic weakens during the first 100 years of these experiments by 15% to 20%. In these runs the intensity slowly recovers after reaching the minimum, once the greenhouse gas concentration has stabilised. In the CO<sub>2</sub>-quadrupling experiments the reduction is so strong that at the end of the runs even after the recovery the intensity is still significantly weaker than in the control simulation. Nevertheless, in the quadrupling experiments an Atlantic conveyor belt-type overturning circulation pattern is present throughout the full simulation period. This reduction is caused by thermal effects, while the relative contribution of momentum and freshwater fluxes is less than 25%.

With a 2D-model it can be shown that it is impossible to simulate the 20th century climate warming without the inclusion of the greenhouse-gas releases connected to human activities,

Applying an optimal detection strategy to the model experiment results one finds that while the observations are consistent with greenhouse gas and aerosol forced climate change, they disagree significantly from greenhouse gas only climate change and marginally from solar forced climate change. No significant change was found on timescales of 10 years. For trends of length 30 years only the global mean change was found to be significant. Only for trends of 50 years were significant sub-global scale changes found and even so the changes are only significant for spatial scales greater than 5,000 km. The results further suggest that the unusually strong global mean warming in the middle of this century may have been influenced by an early greenhouse gas response, and possibly also by a solar irradiance increase.

## 1. Introduction

At the start of this project, climate change calculations had only been carried out with resolutions of typically 500 km (T21) and coarser (Gates et al, 1993; IPCC, 1996). Higher resolutions could so far not be used because of limitations in the available computing resources. On the other hand users of the model data like impact researchers, hydrologists and ecologists demand a higher resolution for their particular models.

Simulations done with higher resolution (T42 = ca. 250 km) models in the time-slice mode (Cubasch et al, 1995; Parey, 1994; Mahfouf et al, 1994) clearly show that the higher resolution improves the simulation of regional climate parameters. However, no transient simulations have been carried out with such a resolution so far. Tests have been done in the time-slice mode with the very high resolution T106 (= ca. 110 km) resolution, but only for too short integration times to give a sufficient large sample for a statistical meaningful evaluation.

Furthermore, Wang et al (1991) indicated in their study that the other greenhouse gases besides the CO<sub>2</sub> have different horizontal distributions than CO<sub>2</sub> which influences the regional heating distribution and therefore the climate change. Their results clearly show that running an experiment with equivalent CO<sub>2</sub>-forcing does not give the same results as a repetition of the experiment with the individual greenhouse gases used as forcing.

Another effect, which has only recently been estimated to be of great importance are the sulphate aerosols. Equilibrium studies by Roeckner et al (1995) and Taylor and Penner (1994) done with mixed layer models clearly show that the sulphate-aerosols cause a cooling in the Northern hemisphere, which masks the warming by the greenhouse gases. Hegerl (1994) and Santer et al (1995) show that experiments done with the sulphate aerosols included are rather able to represent the currently observed climate trends than the simulations considering only the greenhouse gases.

Other phenomena, like solar variability or volcano eruptions, influence the climate as well. An estimate of these effects has so far only been done by statistical methods (Schönwiese et al, 1990; Friis-Christensen and Lassen, 1991), with simplified models (Fichefet, 1995) or in case studies (Graf and Kirchner, 1993). A transient climate simulation which includes these effects will enhance our possibilities to detect the anthropogenic climate change.

The first experiments have all been started with present day conditions. It soon became clear, that this starting point led to an underestimation of the greenhouse warming since the warming from the beginning of the industrialisation until now had been neglected. (Hasselmann et al, 1992; Fichefet and Tricot, 1992, Cubasch et al, 1995). It is therefore planned to start all experiments at 1890 conditions, at which time the industrialisation had not advanced that much that it causes a major problem in the climate simulations (Fichefet and Tricot, 1992).

Cubasch et al (1994) have shown that the internal variability of the climate system makes it necessary to run several *Monte-Carlo* type experiments in order to assess the uncertainty of the modelled climate change.

In order to try to answer those open questions,

- a number of climate models have been developed by the participating groups as tools (**section 2**);

- with these models the present day climate and the future climate has been simulated, the results have been evaluated and intercompared (**section 3**);
- it has been studied, to what extent observed climate anomalies can be attributed to anthropogenic emissions or to natural fluctuations of the climate system (**section 4**).

After the summary (**section 5**) it is discussed to what extent the results of this project have been exploited (**section 6**)

## **2. Model Development**

As well as improving existing models and their physical and technical capabilities, several new models have been developed during SIDDACLICH giving a greater diversity of coupled models within Europe. This chapter gives details of the models themselves, with a summary of model characteristics, experimental set-up, and experiments conducted in **Tables 1 and 2**.

As computers have increased in capacity it has been possible for more experiments to be performed in ensemble mode; typically 2 to 4 independent realisations with the same model and forcing. This adds information on the signal-to-noise, and hence significance, of climate changes.

Also, proper warm up periods from pre-1900 are now standard practice in forced experiments using reconstructed historical forcings in UKMO and DKRZ models.

The most important characteristics of each model, including their grid and resolution, and the main references where they are described can be found in **Table 1**.

MODEL (Partner)	ATMOSPHERE		OCEAN		SEA ICE	REFERENCES
	RESOLUTION (lat*lon*lev)	REMARKS	RESol. (lat*lon*lev)	REMARKS		
HADCM2 (Hadley Centre)	2.5°x3.75°x19L (hybrid coordinates) B-grid	Unified forecast/climate model *quasi-hydrostatic version of the full primitive equations *equivalent CO <sub>2</sub> *sulphate aerosols: direct effect modelled as change in surface albedo *usually run with flux adjustment	2.5°x3.75°*20L rigid lid	* Bryan-Cox type * isopycnal mixing	zero-layer thermodynamic s + advection and idealized ice resistance	Johns et al. (1997) Johns (1996)
HADCM3 (Hadley Centre)	2.5°x3.75°x19L	* radiative effect of GHG now computed separately * new land surface scheme (incl. stomatal resistance) * revised orographic and gravity wave drag *new cloud parameterizations *revised boundary layer mixing *sulphur cycle	1.25°x1.25°*20 L rigid lid	* ocean mixing: Gent & McWilliams (1990) * variable thickness diffusion parameterization *mixed layer: Kraus & Turner (1967); Pacanowski & Philander (1981)	Same as in HADCM2	Gordon et al. (1999)
ECHAM 3- LSG (MPI- DKRZ)	T21 (5.6° for physics)*19L (hybrid $\sigma$ -p coordinates)	ECMWF model modified for climate applications, diurnal cycle included	5.6°x5.6°*11L, free surface E grid	LSG : PE for large scale geostrophic motion. Implicit time integrat.	thermodynamic s	Roeckner et al. (1992) LSG : Maier Reimer et al. (1993)
ECHAM 4- OPYC (MPI- DKRZ)	T42 (2.8° for physics) *19L	*high order horizontal diffusion *modified cumulus convection *separate GHG radiative effect	2.8° if $\phi > 36^\circ$ meridional resolution down to 0.5° at equator 9 layers B-grid free surface	OPYC: primitive equations, isopycnal layer. Mixed layer: TKE budget. Implicit time- stepping	viscous-plastic rheology	ECHAM 4: Roeckner et al. (1996) OPYC : Oberhuber (1993a, 1993b)
ARPEGE- Climat V2 - OPAICE (CERFACS)	T31 (3.75° for physics) x 19L (hybrid $\sigma$ -p coordinates)	*ARPEGE-Climat: Météo-France forecast model modified for climate applications *Deep convection: mass-flux scheme (Bougeault, 1985) *fast radiation code based on Ritter and Geleyn (1992) *4-layer soil scheme	~ 2°x1.5°x31L rigid lid C-grid	OPAICE (from LODYC): * tensorial formalism ensures second- order accuracy on any curvilinear orthogonal grid (Martí et al., 1991) * isopycnal param. *TKE of order 1.5	* thermo- dynamical * 3 ice-thick- ness classes	Déqué et al. (1994) Météo-France (1996) Madec & Imbard (1996) Filiberti et al. (1997)
LMD5.3 - OPAICE (IPSL)	64 pts in longitude (5.6°) 50 pts in sine of lat. 15L (sigma) C-grid	* LMD5.3: random-maximum cloud overlapping * Kuo (1965) convection scheme * Le Treut & Li (1991) cloud param.*surface = bucket model	~ 2°x1.5°x31L rigid lid C-grid	OPAICE (see above)	Same as above	Sadourmy & Laval (1984) Harzallah & Sadourmy (1995)
LMD-CLIO (UCL- ASTR)	64 pts in longitude (5.6°) 50 pts in sine of latitude 15L (sigma) C-grid	LMD5.2 modified: *residual turbulent kinetic energy in stable case and large scale condensation scheme adapted to better represent low stratiform clouds * cold cloud precip. rate reduced to improve the tropical regions	3° x 3°x20L free surface two spherical grids connected in equatorial Atlantic to avoid North Pole singular..	CLIO (developed at UCL-ASTR): - mixed layer turbulent closure scheme : Mellor & Yamada (1974) 2.5	* 3-layer thermodyn. * viscous- plastic rheology * snow-ice formation * brine pocket param.	Grenier (1997) Fichefet & Morales Maqueda (1997) Campin & Goosse (1999)
LLN 2-D (UCL- ASTR)	2.5-dimensional: 5° in latitude 2 levels (10 to 15 for radiation) 5 surface types in each zonal band	* quasi geostrophic potential vorticity * full radiation code similar to that used in LMD5.3 AGCM	5° in latitude	integral mixed layer and diffusive deep ocean following Hansen et al. (1988)	* zero-layer thermodynamic s * lead para- meterization	Gallée et al. (1991) Bertrand & van Ypersele (1999a,b)

**Table 1: The SIDDACLICH model characteristics**

## **2.1. The Hadley Centre models**

### **2.1.1. HadCM2**

HadCM2, which uses the Unified Model system developed at the UK Met office, was developed during the previous contract - Anthropogenic Climate Change - and is described in some detail in the report for that contract. A full description is in the paper by Johns et al. (1997) and the technical report by Johns (1996). Only an outline description is given here. The model consists of atmospheric and ocean GCMs using finite difference representations. A simple sea ice model representing the thermodynamics of ice and snow, and sea ice advection by ocean surface currents with an idealised representation of internal resistance to compression, is embedded within the ocean model.

### **2.1.2. HadCM3**

The HadCM3 model was developed from HadCM2, but various improvements to the atmosphere and ocean components allow it to be run with no artificial flux adjustments without excessive climate drift. The primary reference for the HadCM3 model is Gordon et al. (1999).

The atmospheric component of the model is the same resolution as HadCM2, but includes a number of important changes as follows. A new radiation scheme is included with 6 and 8 spectral bands in the short-wave and long-wave. The radiative effects of minor greenhouse gases as well as CO<sub>2</sub>, water vapour and ozone are explicitly represented (Edwards and Slingo, 1996). A simple parameterisation of background aerosol (Cusack et al., 1998) is also included. A parameterisation of the direct impact of convection on momentum (Gregory et al., 1997) is now used.

The new land surface (Cox et al., 1998) includes a representation of the freezing and melting of soil moisture and the formulation of evaporation includes the dependence of stomatal resistance to temperature, vapour pressure and CO<sub>2</sub> concentration. Parameterisations of orographic and gravity wave drag are revised (Milton and Wilson, 1996; Gregory et al., 1998). Several parameters in the cloud and precipitation schemes have been tuned to optimise top of atmosphere radiative flux balances. Some significant revisions to boundary layer mixing are present in HadCM3, including removal of a non-local mixing scheme which degraded transport and sinks of aerosols. The atmosphere component of the model also optionally allows the transport, oxidation and removal by physical deposition and rain out of anthropogenic sulphur emissions to be included interactively.

An important improvement in HadCM3 is an increase in the ocean horizontal resolution from 2.5° x 3.75° to 1.25° x 1.25°, while the vertical resolution is unaltered. The ocean simulation is further improved by the inclusion of various revised parameterisations for oceanic mixing. Horizontal mixing of tracers uses a version of the Gent and McWilliams (GM, 1990) adiabatic diffusion scheme. A variable thickness diffusion parameterisation (Wright, 1997; Visbeck et al., 1997) is used.

Near surface vertical mixing is parameterised partly by a Kraus-Turner mixed layer scheme for tracers (Kraus and Turner, 1967), and a K-theory scheme (Pacanowski and Philander, 1981) for momentum.

## **2.2. The DKRZ/MPI models**

The coupled models developed by DKRZ and MPI are based upon two versions of the atmospheric

model ECHAM (version 3 and 4) and two different oceanic models, LSG and OPYC. Whereas the LSG model is a low resolution model (similar resolution than the T21-version of ECHAM), OPYC has been employed in a higher resolution (corresponding to the T42 Gaussian grid in the extra-tropics and a refinement between  $30^{\circ}$  N and  $30^{\circ}$  S in north-south direction up to  $0.5^{\circ}$  near the equator). The LSG is coupled to the T21 version of ECHAM3 and the OPYC to the T42 version of ECHAM4. For the time slice experiments an ECHAM4 version with a horizontal resolution of T106 ( $1.1^{\circ}$  in the grid space) has been applied.

### **2.2.1. Atmospheric component: ECHAM**

The atmosphere component ECHAM (Roeckner et al., 1992; Roeckner et al., 1996) is a spectral general circulation model used for climate applications. The prognostic variables are vorticity and divergence, temperature, surface pressure, water vapour and cloud water. The diurnal cycle is included. Sub-grid scale physical processes such as radiation, cloud formation, precipitation, convection and turbulent mixing are parameterised. Additionally for the coupled runs, the runoff into the ocean is calculated using a simple surface hydrology model.

### **2.2.2. Oceanic component: LSG**

The ocean component LSG is based on a numerical formulation of the primitive equations (Maier-Reimer et al., 1993) appropriate for large-scale geostrophic motion. The non-linear advection of momentum is neglected and fast gravity waves are strongly damped by an implicit time integration scheme using a time step of 30 days. Vertical convective mixing is applied whenever the stratification becomes unstable. Sea ice is computed from the ice heat balance. A realistic bottom topography is included.

### **2.2.3. Oceanic component: OPYC**

The ocean general circulation model OPYC (Oberhuber, 1993a, 1993b) consists of three sub-models for the interior ocean, the surface mixed layer and the sea ice.

The model for the interior ocean employs the primitive equations in the flux form of the conservation laws for momentum, mass, heat and salt in isopycnal layers. These quantities as well as the sea level are prognostic variables. Horizontal mixing for momentum is a function of the local Rossby deformation radius, while horizontal diffusion for temperature and salinity involves some dependence on flow deformation. Vertical mixing follows the concept of entrainment/detrainment for which budgets of turbulent and mean potential energy are solved. A standard convection scheme is used which instantaneously removes vertical instabilities.

The model for the interior ocean is coupled to a mixed layer model, as the concept of isopycnal coordinates breaks down near the surface when strong turbulence is present.

The sea-ice model solves for ice momentum, ice and snow thickness and their concentration. The viscous-plastic rheology is chosen to parameterise the stress tensor while the thicknesses of ice and snow and the concentration of ice are computed from the respective continuity equations.

## **2.3. The CERFACS model**

The global coupled model ARPEGE/OASIS/OPAICE used at CERFACS was developed in the framework of the SIDDACLICH project.

The atmosphere model is ARPEGE-Climat V2 from Météo-France (1996) in Toulouse. A T31 spectral truncation is used, corresponding to an horizontal resolution of  $3.75^{\circ}$ . The Geleyn radiation scheme has been used. Convective and stratiform cloudiness are calculated using respectively the

precipitation rates and the humidity profile. The deep convection uses the mass-flux scheme described by Bougeault (1985) while the shallow convection is parameterized through a modification of the Richardson number. A gravity wave drag parameterisation is also included. The model includes a four-layer prognostic soil scheme, with no restoring term. Model river flows are parameterised simply by taking all excess runoff in a river basin and discharging it instantly into the ocean at a reduced set of weighted outflow grid points.

The ocean model coupled is OPAICE, described in **section 2.4.2**.

## **2.4. The IPSL model**

### **2.4.1. Atmospheric component**

The atmospheric model is the LMD AGCM developed at the Laboratoire de Météorologie Dynamique and described in Sadourny and Laval (1984). The version being used is LMD5.3 (cycle 5), described in Harzallah and Sadourny (1995).

The model is a finite difference general circulation model. Grid points are regularly spaced in longitude and in sine of latitude. The grid has equal area meshes, with a better latitudinal resolution in low latitudes.

Primitive equations are expressed in terms of  $u$  and  $v$  wind components, potential enthalpy, specific humidity and surface pressure. Time stepping is a combination of Matsuno and leap-frog schemes. The advection scheme is designed to conserve potential enstrophy for divergent barotropic flow (Sadourny 1975a and 1975b). Lateral diffusion is modelled by a mixed bi-Laplacian operator.

Short-wave radiation is modelled after an updated version of the scheme of Fouquart and Bonnel (1980) and distinguishes two spectral intervals: visible and near infrared. Long-wave radiation is computed after the method of Morcrette (1990) over 7 spectral intervals. A new release of the Morcrette's scheme has been introduced. The cloud overlapping is then random-maximum instead of being only random in the previous version. Some other minor modifications on clear sky affect slightly the radiative transfer. An iterative method is used in which saturation is tested downward starting from the top layer to allow the falling droplets to evaporate. Kuo's scheme (1965) deals with convection due to large scale moisture convergence. Manabe and Strickler's (1964) moist convective adjustment occurs when the air is super-saturated (small-scale convection). The Le Treut and Li's (1991) cloud parameterisation is based on a cloud water budget equation. The interaction with radiation makes explicit use of the computed cloud fraction and cloud water content but uses prescribed equivalent droplet radius.

Hydrological exchanges between the soil-vegetation system and the atmosphere are determined by the parameterisation SECHIBA (Ducoudré et al., 1993).

### **2.4.2. Oceanic component**

The oceanic model used by IPSL and CERFACS is the OPA OGCM developed at the Laboratoire d'Océanographie Dynamique et de Climatologie (Delecluse et al., 1993) to study large-scale ocean circulation and its interaction with atmosphere and sea-ice. The version used is OPA7G onto a global ocean domain (Madec and Imbard, 1996). The model solves the primitive equations with a non-linear equation of state (Unesco, 1983). A rigid lid approximation is made at the surface. A distinctive feature of the model grid is that, in the southern hemisphere, it is regular, while in the northern hemisphere, the grid is stretched with the pole centred on Asia to overcome the North pole singularity (Madec and Imbard, 1996). The horizontal mesh is orthogonal and curvilinear on the

sphere. In the version used, the diffusion is isopycnal. The horizontal eddy viscosity depends on the geographical position (it is reduced near the western coasts and near the equator). The vertical eddy viscosity and diffusivities are computed by a 1.5 order Turbulent Kinetic Energy (TKE) closure scheme (Blanke and Delecluse, 1993). An implicit scheme is used for vertical diffusive processes. The solar radiation penetrates in the top meters of the ocean (Blanke and Delecluse, 1993), taking the selective absorption of radiation in the ten first meters of the ocean into account. This simulation has a sea-ice thermodynamic scheme. The version of the ocean OPA containing this sea-ice thermodynamic scheme is called OPAICE and is described in Filiberti et al. (1997) and briefly in Barthelet et al. (1998a).

## **2.5. The UCL-ASTR model**

### **2.5.1. Atmospheric component**

The coupled AOGCM developed at UCL-ASTR in Belgium in the framework of the SIDDACLICH project contains an improved version of the LMD5.2 AGCM. Each greenhouse gas is taken into account separately. The aerosol impact is modelled as a change in surface albedo under clear sky conditions. In the UCL-ASTR's version, the surface drag coefficients are computed according to Louis (1979). This model is therefore similar to the LMD5.3 AGCM (see **section 2.4.1**). Furthermore, in order to implicitly increase resolution, each grid box is divided for the turbulent processes in the planetary layer into appropriate fractions of land, ocean and sea ice (Grenier, 1995). This allows flux conservation between the atmospheric and oceanic models as the oceanic surfaces and masks are identical in those models. The residual turbulent kinetic energy in stable case has been reduced to retain more humidity in the surface boundary layer. Then, the width of the imposed statistical distribution of water content has been adapted inside the boundary layer to condense more efficiently this humidity. These changes have led to a better representation of stratiform clouds. By reducing the cold cloud precipitation rate, more humidity is kept in the tropical atmosphere, and it reduces the overestimation in the surface evaporation. In the LMD's model, a diagnostic of ice versus liquid water content is done to compute the precipitation rate and the cloud radiative impact; the transition temperatures between liquid and ice clouds have also been adapted. Finally, the so-called max/random overlapping of clouds is used in this version whereas clouds are assumed to overlap randomly in the LMD5.2 model.

### **2.5.2. Oceanic component**

The new ocean/sea ice model (CLIO) developed at UCL-ASTR is a primitive-equation, free-surface model. Its horizontal resolution is of  $3^\circ$  by  $3^\circ$ . To avoid any singularity at the North Pole, two spherical grids connected in the equatorial Atlantic are used (Deleersnijder et al., 1993; Goosse et al., 1997a). The Mellor and Yamada's (1974, 1982) level 2.5 turbulence closure scheme as modified by Kantha and Clayson (1994) is employed to compute the vertical eddy viscosity and diffusivity. When static instability occurs, the vertical eddy diffusivity is strongly increased to simulate convection. Moreover, the Campin's (1997) scheme for the export of dense waters formed over continental shelves is used. The sea-ice component (Fichefet and Morales Maqueda, 1997) incorporates parameterisations of the most relevant thermodynamic and dynamic sea-ice processes. An improved version of Semtner's (1976) 3-layer model determines the vertical growth and decay of the ice due to thermodynamic processes. To take into consideration the existence of leads and polynyas, we introduce a concentration variable related to the heat budget of the open water area (Fichefet and Morales Maqueda, 1997). For the momentum balance, the ice is considered as a two-dimensional viscous-plastic continuum following Hibler (1979).

## 2.6. Model coupling

The atmosphere and ocean/sea-ice GCMs are coupled by the air-sea-ice fluxes of radiation, heat, momentum and freshwater (evaporation minus precipitation, plus runoff along coastal boundaries). As the resolution of both components are different for all models, interpolation and/or area averaging is needed. All laboratories involved in SIDDACLICH except the Hadley Centre and UCL-ASTR use the OASIS (Ocean Atmosphere Sea Ice Soil) coupler developed at CERFACS (Terray et al., 1995, 1998). The role of any coupler software is to ensure the time synchronisation of the two GCMs and to interpolate the surface heat fluxes, the water fluxes and the wind stresses from the atmosphere model grid to the ocean model grid, and the sea surface temperature and the sea-ice characteristics from the ocean model grid to the atmosphere model grid. The models exchange time-averaged fields once a day. To avoid the drift simulated in certain coupled models, a flux correction (Sausen et al., 1988) can be applied. This is equivalent to coupling the atmosphere and ocean in anomaly response experiments by the anomalies of the fluxes computed relative to the equilibrium states of the uncoupled sub-systems. The flux correction has no impact on the computed response for small perturbations about the mean state of the model climate, provided the individual sub-systems reproduce the mean climate reasonably well. Flux correction is used in HADCM2 and the DKRZ/MPI models, while all other models run without it.

A few specific remarks follow about the Hadley Centre models.

**HadCM2:** The atmosphere and ocean/ice models are coupled once a day. As the grids of atmosphere and ocean are congruent, the coupling routines transfer grid box average values directly without interpolation.

**HadCM3:** As in HadCM2, atmosphere-ocean coupling occurs once per day. As there are six ocean grid boxes per atmosphere grid box, interpolation and/or area averaging is used in HadCM3, with weightings computed to preserve precise conservation.

As the ocean model has a rigid lid formulation, water fluxes do not lead to volume changes in the water column. The potential effect of this on global salinity drift is counteracted in HadCM3 by assuming that water fluxes can be converted to surface salinity changes using a fixed (rather than in situ) reference salinity of 35 ppt. This slightly distorts the local effects of P-E fluxes depending on the salinity. Two additional potential sources of salinity drift also arise from the treatment of land surface runoff of water and snow. Not all the river catchments lead back to the world ocean, so some runoff disappears into inland drainage basins. A small correction (about 0.01 mm/day) is therefore made to global water fluxes into the ocean to account for this. And since there is no explicit representation of glaciers, snow can build up on land and ice sheets. A simple representation of the calving of icebergs via a fixed water flux into the ocean, at a rate balancing the net snowfall accumulation, and with a geographical pattern designed to mimic the locations for iceberg melting (Bigg et al. 1996) is therefore used to close this part of the water budget. These terms were calibrated from a prior model integration. These salinity conservation issues are not masked by water flux adjustments as was the case in HadCM2, so have to be addressed directly in HadCM3.

## 2.7. Initialisation and spin up

Two techniques are been employed to spin-up the models before the actual start of an experiment: a) the start from an ocean as close as possible to equilibrium (UKMO-HadCM2 and MPI/DKRZ) and b) from an ocean state as close as possible to the observation (UKMO-HadCM3, IPSL, CERFACS, UCL-ASTR). In details, however, the methods differ considerably.

UKMO:

HadCM2: A long coupled spin-up of about 500 years was performed prior to running climate change experiments with HadCM2. Flux adjustments to oceanic surface heat and water fluxes derived from the spin-up phase are applied in most experiments to reduce climate drift, but a limited number of sensitivity experiments without flux adjustments have also been conducted. The radiative effect of sulphate aerosols is simply modelled as a change in surface albedo under clear sky conditions (an approximation to the 'direct' effect of sulphate aerosols alone).

HadCM3: The model is simply initialised directly from the Levitus and Boyer (1994) observed ocean state at rest, with a suitable atmospheric and sea ice state. No spin-up with surface or interior ocean relaxation is used - the model runs freely from the start. A prior integration of the model was used to calibrate the water flux terms required for global salinity conservation, as outlined above.

DKRZ/MPI:

ECHAM3/LSG: The spin-up procedure of the uncoupled models is based upon the experience obtained during the development of the AOGCMs ECHAM1/LSG (Cubasch et al., 1992) and ECHAM2/OPYC (Lunkeit et al., 1996a). Before coupling, both models were spun-up with boundary conditions taken from observed climatological data sets. The oceanic model was integrated over 27000 years and the atmospheric component over 20 years (for details see Voss, 1996).

After the preparation of the uncoupled components the synchronously coupled model was integrated over 115 years starting from the state which was reached by the uncoupled models at the end of the spin-up procedure. All runs investigated in this study were started from the state of the coupled model reached after the 115-year integration.

ECHAM4/OPYC: Prior to coupling, the OGCM has been spun up for about 1000 years by prescribing a combination of observed and AGCM simulated fluxes and variables. While the dynamical components such as wind stress and friction velocity have been derived from the AGCM forced with observed climatological sea surface temperatures (SSTs), the fluxes of heat and freshwater are based on a combination (1) of observed climatology (Oberhuber 1988), (2) a bulk flux parameterisation (Oberhuber 1993a,b) and (3) additional relaxation towards observed SSTs (AMIP climatology) and surface salinity (Levitus 1982), respectively. The drift induced by the 'coupling shock' when the restoring boundary conditions are replaced by the fluxes computed in the CGCM can be reduced considerably if flux correction (or adjustment) techniques are applied (e.g., Sausen et al. 1988). However, the methods which have been employed so far are not totally satisfactory since the SST still tends to drift by typically 0.5 K in the global mean within the first 100 years after coupling (Cubasch et al. 1992; Lunkeit et al. 1996a). It is also contended by some modelling groups (see Neelin et al. 1992) that the seasonal correction, particularly if SST itself undergoes a correction independent from the heat flux (Lunkeit et al. 1996a), tends to reduce and/or spectrally modify ENSO variability. In the current model, an alternative approach is applied. It differs from the traditional one basically in two aspects, namely, (1) the flux correction is computed by gradual updating during a 100-year spinup of the CGCM, and (2) only the annual mean of heat and freshwater is corrected while the respective annual cycles and the wind stress (and all other coupling variables as well) remain unchanged. Denoting  $F_A$  the flux (of heat or freshwater) computed by the AGCM,  $F_O$  the flux resulting from the OGCM bulk parametrization under the same surface conditions and  $F_R$  an additional Haney (1971) type restoring term (zero for heat where ice

exists), the flux  $F$  seen by the OGCM after the CGCM spinup is

$$F = F_A + \langle F_O + F_R - F_A \rangle$$

where the flux correction term  $\langle \dots \rangle$  represents a long-term annual mean which has been obtained from the time series of the respective fluxes during the CGCM spinup. More details on ocean spinup and flux correction will be presented in a separate study.

In a 100-year control experiment of the present-day climate, with the flux correction as defined in the equation, a relatively small secular drift is found with a cooling trend of the ocean (all layers) of about 0.1 K, a freshening of the upper ocean by typically 0.02 psu and a salinity increase with about the same rate in the deep ocean.

CERFACS:

The atmospheric initial state results from a forced integration of the atmospheric model by climatological Sea Surface Temperature (SST). The ocean is initially at rest, with temperature and salinity prescribed from the Levitus (1982) atlas. From this initial state, the coupled model is integrated for a few years with a Newtonian restoring term for oceanic temperature and salinity at the surface and under the mixed layer. After 7 years of integration, the wind-driven circulation is established and the sea-ice extent cycle stabilises close to observations. In the control simulation, the coupled model is then integrated with no more internal restoring terms for a period of 130 years, the CO<sub>2</sub> concentration being held constant at the 1990 measured value (353 ppmv). After 15 years of this free coupled simulation, the dynamics at the air-sea interface stabilises and from that point an 80-year scenario experiment, in which the CO<sub>2</sub> concentration is increased by 1 %/year, is started.

IPSL:

This control run starts for the ocean from Levitus observations and from the 1st January 89 of an AMIP run for the atmosphere. Then a period of 8 years is forced towards climatology. From year 9 and after a rapid initial drift, the model reaches a quasi-equilibrium at year 15. The coupled simulation lasts 225 years.

UCL-ASTR:

As many other AOGCMs without flux correction, the UCL's coupled model drifts away from realistic climatology. To reduce this drift during the scenario simulation, the model components have been improved and the following spin-up procedure is employed. The oceanic model is run in forced mode for 1000 years to reach a quasi-equilibrium state. The main features of the oceanic model drift away from Levitus' observations are then present in the oceanic state. This trend associated to deficiencies in the oceanic model will therefore not occur in coupled mode. A similar approach is used for the atmospheric model; but the time scale being shorter, it is run in forced mode for only 10 years to reach an equilibrium state.

The atmospheric and oceanic models are then coupled without any flux correction or restoring terms. After a 25-year period the main part of the model drift is over and the control and scenario simulations start.

The whole spin-up and control runs are performed according to the atmospheric conditions of 1970 for the greenhouse gases and aerosol concentrations. This choice is a compromise between the computer time and the cold start effect.

### 3. Model experiment results

#### 3.1. Mean climate of the control simulations

Seven coupled models in following configurations have been used to carry out the climate (change) experiments (c. f. **Table 1 and 2**):

Two of them are based on the ECHAM models. ECHAM3 is coupled to the ocean LSG model, whereas ECHAM4 is coupled to the OPYC ocean model. All those models include a flux correction.

Two models of the HadCM family have been considered: HadCM2 is flux-corrected, whereas HadCM3 is not.

Finally two models (IPSL and CERFACS) share the same ocean (OPA), but differ through the atmospheric model (LMD5.3 at the IPSL, ARPEGE/Meteo-France at CERFACS). Both are non-flux corrected.

The LMD-CLIO model developed at UCL-ASTR uses also the LMD AGCM, coupled to a new ocean/sea-ice model (CLIO). Only shorter simulations without flux correction have been performed. A 15 year control simulation has been followed by many sensitivity experiments to reduce the model drift before launching century-long simulations.

no	institute	model	1	2	3	4	5	6	7	8
			control	obs. CO <sub>2</sub> from 19th century to today, 1% equiv. CO <sub>2</sub> or similar for future	like 2, but with prescribed aerosol effect	like 2, the greenhouse gases are treated individually	like 1, but with observed solar variability and/or volcanoes	like 2, the GHGs are treated individually, direct effect of aerosols calculated from emissions	like 2, the GHGs are treated individually, direct and indirect effect of aerosols calculated from emissions	stabil. exp., i. e. 1% increase or scenario up to a certain CO <sub>2</sub> -level, afterwards stabilization at this level
1	DKR Z/M PI	ECHAM 3/LSG T21	2000 years	205 years	2*170 years		4*292 years (no volcanoes)			period. synch. 1*CO <sub>2</sub> , 2*CO <sub>2</sub> and 4*CO <sub>2</sub> , 850 years each
2	MPI/ DKR Z	ECHAM 4/OPYC T42	300 years			240 years		190 years	190 years	
3	DKR Z/M PI	ECHAM 4/HOPE T30	500 years still running							
4	UCL/ AST R	ASTR 2D	100 years	500 years	500 years		500 years			
5	UCL/ AST R	UCL/AS TR/LM D	15 years							
6	CERF ACS	ARPEGE /OASIS/ OPA LAHO no flux corr.	130 years	102 years starting from 1990, 1% increase						
7	IPSL	LMD/O ASIS/O PA LAHO no flux corr.	210 years	150 years						
8	UKM O	HadCM 2	1700 years	4*240 years	4*240 years		4*195 solar (1700-1995); 4* 149 volcanic (1850-1999) 3*105 solar (1890-1995)			
9	UKM O	HadCM 2 no flux corr.	1000 years	3*80 years (1% scenar io)						
10	UKM O	HadCM 3 no flux corr.	200 years started directly (Levitus)			240 years			240 years	
11	ETH Z/DK RZ	ECHAM 4 T106 time- slice	10 years	10 years						
12	DLR	ECHAM 4 T106 time- slice	0.5 years		0.5 years					

**Table 2: The model experiments**

### 3.1.1 Sea-surface temperature

The evolution of the global SST is displayed separately over a period of up to 300 years (for all models, **Fig. 1**) and up to 2000 years (for the models that have been carried out longer than 300 years, **Fig. 2**). The flux-corrected models remain all within  $0.5^{\circ}$  of the observed climate. HadCM3 is the only non-flux corrected model which remains completely stable. The IPSL model tends to warm initially (mainly at high latitudes, the tropical regions are subject to a cooling) and then recovers gradually toward more realistic global temperatures, although regional errors tend to persist. The CERFACS model tends to warm strongly during the very first years, and then gets much more stable. These results reflect largely the initialisation procedure. Both the IPSL and CERFACS models are directly integrated from the Levitus conditions, with only a minor adjustment period of about 15 years during which the SST is restored toward observations. The models are then very sensitive to small initial imbalances of the surface fluxes.

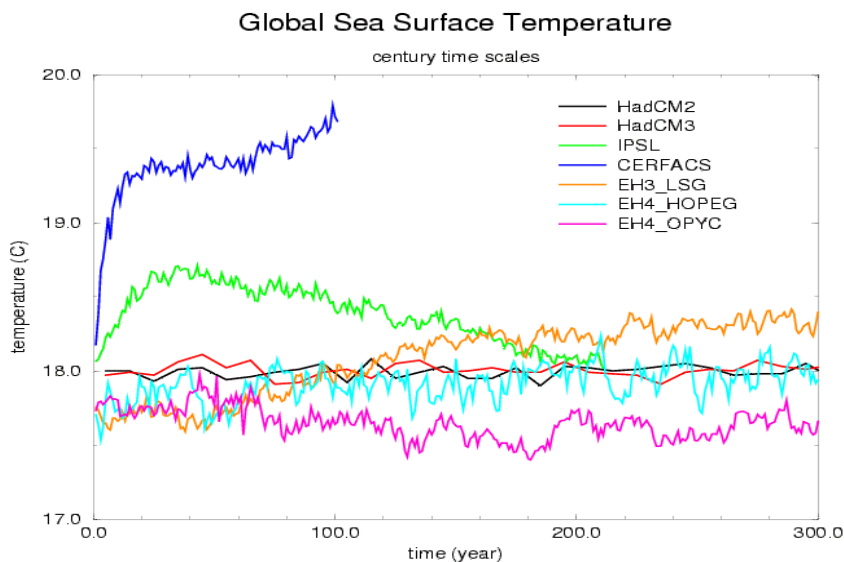


**Figure 1:** The global mean sea surface temperature during the first 300 years of the control simulations. The data for the HadCM model are 10 year averages (Note: ECH4-HOPEG represents an additional experiment with the coupled ECHAM4 T30 model coupled to the HOPEG ocean model. So far no climate change experiments have been carried out with this model).

### 3.1.2 Overturning of the North-Atlantic circulation

The divergence between the different models is quite significant, with values ranging from slightly less than 15 to slightly more than 30 Sverdrups (**Fig. 3**). The most extreme cases (IPSL and CERFACS) are obtained with models sharing the same ocean, which indicates the large influence of the atmosphere model coupled to the ocean model on the maintenance of this overturning. The drift of this overturning appears comparatively small, even in models run for a thousand years or more (**Fig. 4**).

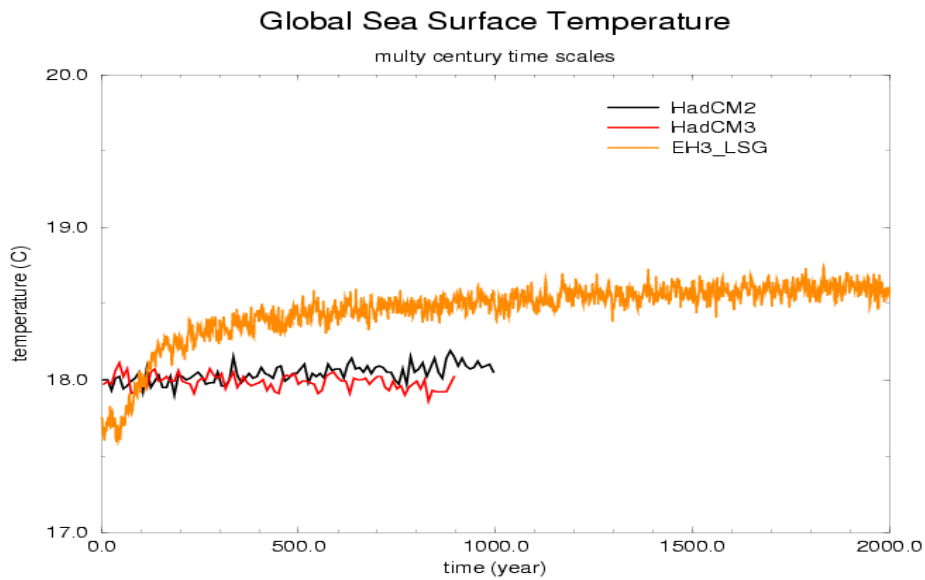


**Figure 2: The global mean sea surface temperature of the 1000 year + control simulations. The data for the HadCM model are 10 year averages.**

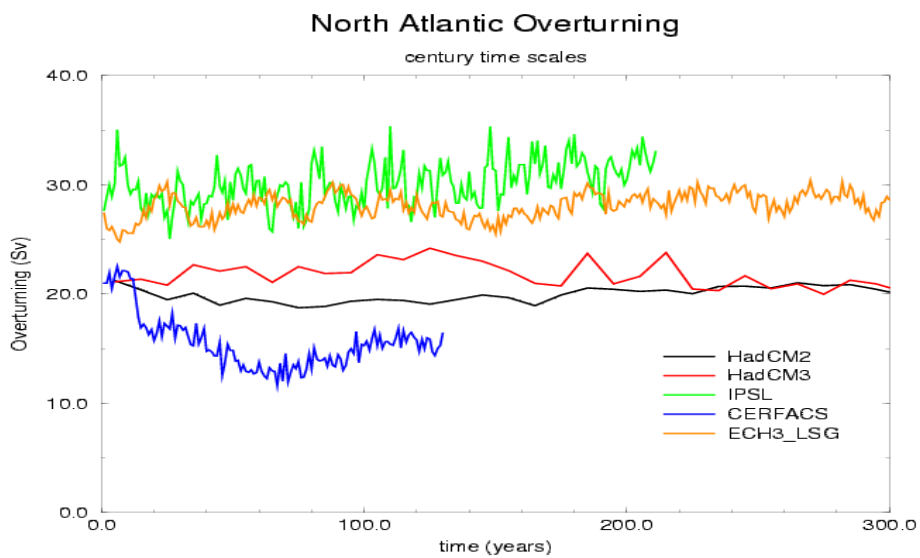


**Figure 3: The North Atlantic overturning during the first 300 years of the control simulations. The data for the HadCM model are 10 year averages. unit: Sv).**

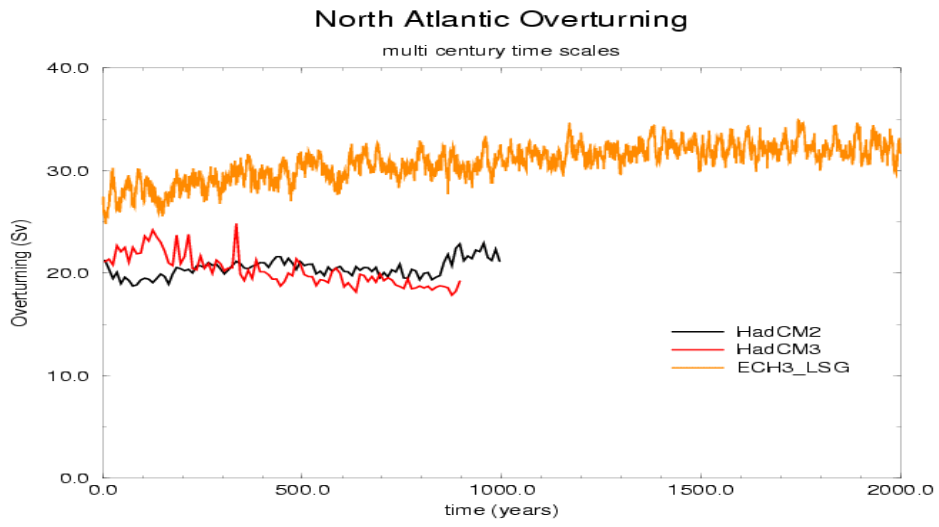


**Figure 4: The North Atlantic overturning of the 1000 year+ control simulations. The data for the HadCM model are 10 year averages.**

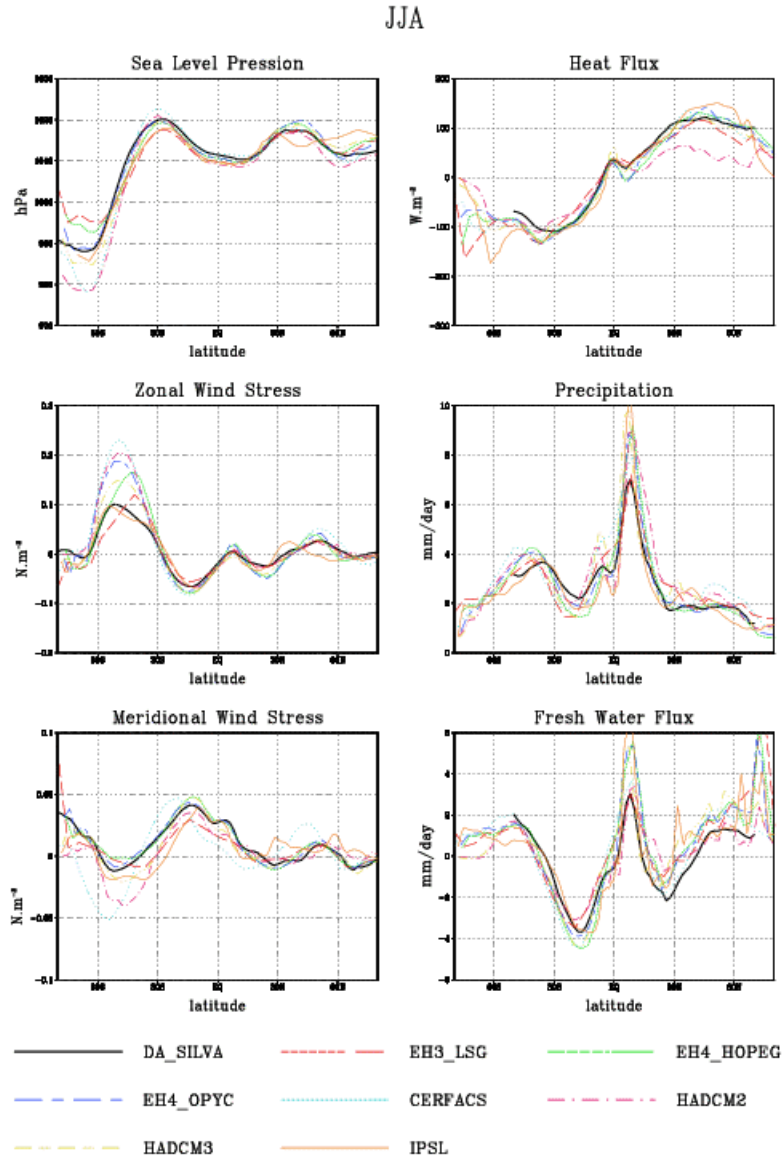
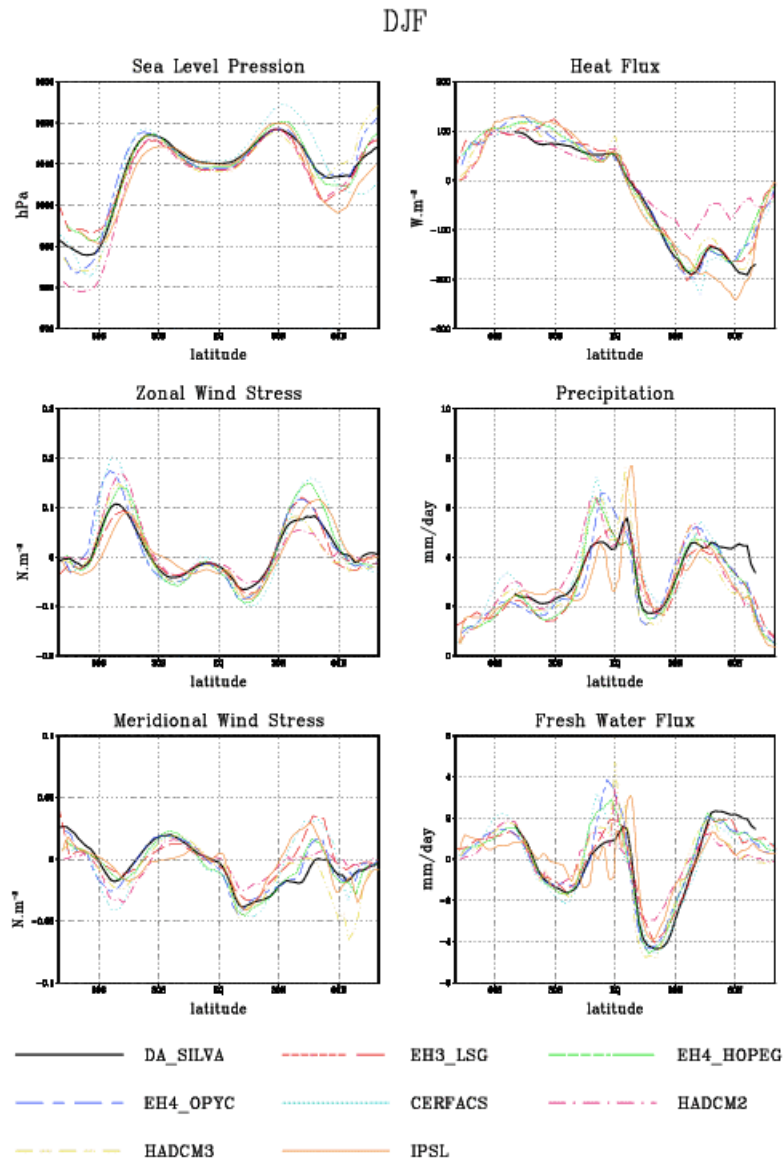


Figure 5: zonally averaged sea level pressure, zonal and meridional wind stress, heat flux, precipitation and fresh water flux of the control simulations for June-July-August. Observations are according to DaSilva et al, (1995).

### 3.1.3 Mean meridional climate

Meridional distributions of several atmospheric fields are shown, averaged over JJA (June-July-August, **Fig. 5**) and DJF (December-January-February, **Fig. 6**) conditions, and compared to the Da Silva climatology (DaSilva et al., 1995). The sea-level pressure agreement is quite good in the whole intertropical area. As shown by prior intercomparisons (IPCC Report, 1996) the models tend to diverge slightly at higher latitudes, especially in the Southern Hemisphere. The precipitation shows relatively systematic errors common to several models: in JJA the precipitation maximum in the Northern Hemisphere near the Equator tends to be overestimated by at least half the models, whereas in DJF, there tends to occur a double ITCZ, with a maximum at about  $15^{\circ}$  S much larger than in the observations, which develops at the expense of the ITCZ in the Northern Hemisphere. In the subtropical and extratropical areas the agreement between the

models is on the contrary quite striking. The same systematic errors are apparent in the fresh water flux into the ocean. The structure of the errors in the surface heat flux are quite different in the two hemispheres. In the Southern Hemisphere all models tend to overestimate (at least compared to the available climatologies) the summer (DJF) heat flux into the ocean. In the Northern Hemisphere the situation appears more model-dependent, with the seasonal cycle of the surface flux being reduced in HadCM2, and increased in the IPSL.



**Figure 6: Zonally averaged sea level pressure, zonal and meridional wind stress, heat flux, precipitation and fresh water flux of the control simulations for December, January and February. Observations are according to DaSilva et al, (1995).**

The zonal wind stress simulated by most models is in quite close agreement, and also in good general agreement with the evaluation of Da Silva (1995). There still is some discrepancy

concerning the size of the mid-latitude maxima. In JJA this can be noted in the Southern Hemisphere, and in DJF this appears in the Northern Hemisphere. The simulation of the meridional wind stress appears slightly worse. Although the values of the stress are smaller, and therefore the absolute errors are also smaller, the relative agreement between the models is generally weaker.

## **3.2. Mean climate of the climate change simulations**

### **3.2.1 Response in anthropogenic and natural forcing experiments**

#### ***3.2.1.1. Coupled GCM simulations***

The simplest benchmark for intercomparison of model responses is with a 1%-per-annum increase of carbon dioxide relative to a control run in which CO<sub>2</sub> is held fixed. Three independent models; HadCM2, ARPEGE-OPAICE and LMD-OPAICE; have been run using this simple scenario. In the case of HadCM2, an ensemble of 3 runs has been averaged. The LMD-OPAICE model run was extended to stabilise at either 2\* or 4\*CO<sub>2</sub> (c.f. **Table 3**)

Global mean temperature responses in the three experiments (**Fig. 7a**) are similar - about 2 K after 70 years (the time of CO<sub>2</sub>-doubling) - but the initial responses are more varied, with a larger cold start delay in the LMD-OPAICE case. The global warming sensitivity of the LMD model is about 5 K to a quadrupling of CO<sub>2</sub> at equilibrium (or an equilibrium sensitivity to doubled CO<sub>2</sub> of about 2.5 K). In fact, all of these European models appear to cluster near the centre of the quoted IPCC climate sensitivity range 1.5-4.5 K. These experiments are included in phase 2 of the larger international model intercomparison project CMIP.

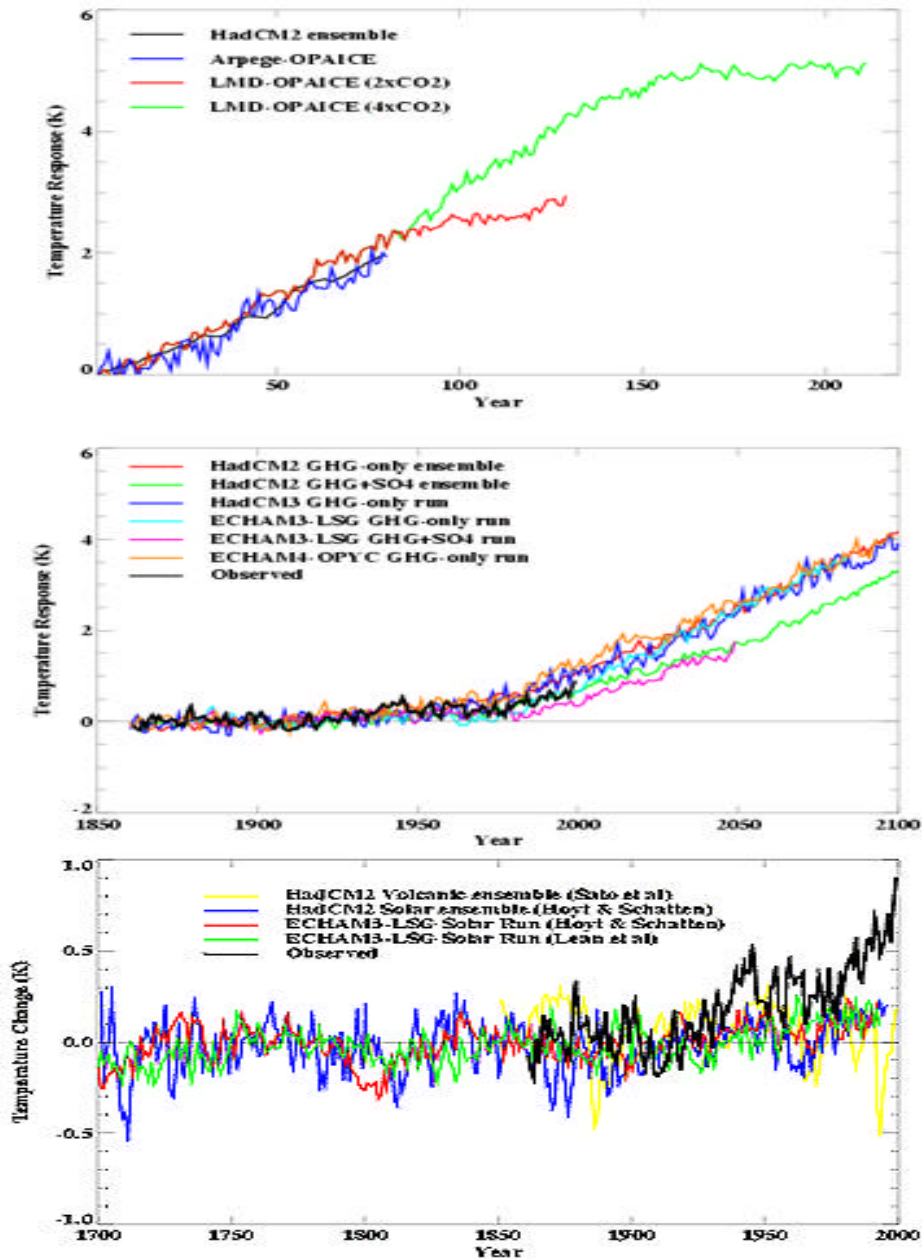


Figure 7: Global mean temperature response versus time in coupled model experiments with anthropogenic and natural forcings. (top) 1%-per-annum cold start experiments with models HadCM2 (4-member ensemble), ARPEGE-OPAICE and LMD-OPAICE (stabilising at  $2 \times \text{CO}_2$  and  $4 \times \text{CO}_2$ ). (middle) Warm start experiments with slow increase of greenhouse gases (and aerosols in some cases) from 19th century to present, then 1%-per-annum or IS92a scenario, compared to observed temperature changes. Changes are computed relative to the start of the 20th century. (bottom) Experiments with HadCM2 and ECHAM3-LSG from pre-industrial to present day with variations in solar irradiance following Hoyt and Schatten (1993) and Lean et al. (1995), and stratospheric aerosol optical depth variations based on observed volcanic activity. [Note: Just one HadCM2 solar run was performed for 1700-1890; the curve represents a single run up to 1890, but an ensemble average of four realisations thereafter.] Changes are computed relative to the start of the 20th century.

More realistic anthropogenic forcing scenarios, including the historical build up of greenhouse

gases since the last century together with other related forcings, have been modelled by UKMO (Hadley Centre) and DKRZ. **Fig. 7b** shows the outcome of several such experiments including greenhouse gases and sulphate aerosols compared to observed temperatures. In addition, these two centres have run experiments with 'natural forcings' due to variations in solar irradiance (Hoyt and Schatten 1993; Lean, Beer and Bradley 1995), and volcanically induced stratospheric optical depth changes (Sato et al. 1993). Such experiments (**Fig. 7c**) provide alternative hypotheses to test as explanations of observed climate changes in the context of detection and attribution studies (see also **chapter 4**). In terms of global mean temperature it seems clear that the recent observed warming is outside the range predicted from natural forcings, and no simulations with purely natural forcings (solar and volcanic) have yet reproduced past observed global or large scale patterns of variation in temperature convincingly - some anthropogenically forced response appears to be necessary. However, there is still scope for refining reconstructed solar and volcanic forcings and their physical representations in models in attempts to attribute observed climate changes more accurately.

Both UKMO and DKRZ have also run some scenarios with newly developed models (HadCM3 and ECHAM4-OPYC) as well as older models (HadCM2 and ECHAM3-LSG). The effects of refinements in model physics and forcings (and the removal of flux adjustments in the case of HadCM3) on the response have been examined. While there appears to be some convergence in global climate sensitivity, at least among European coupled models, the models' internal physical behaviours are markedly different.

To illustrate this, **Fig. 8** shows the relationship between changes in net radiative short-wave (SW) input and long-wave (LW) output at the top of the atmosphere plotted against global mean warming for different models. In general, as the planet warms, incoming solar radiation increases due to increased absorption, but the relationship varies considerably from model to model. As regards outgoing LW radiation, the relationship with global warming is even less consistent, even in terms of the sign of the changes. The behaviour of clouds, particular their radiative feedbacks in response to warming, is very important in explaining some of this variation but other feedbacks such as ice/snow albedo also contribute.

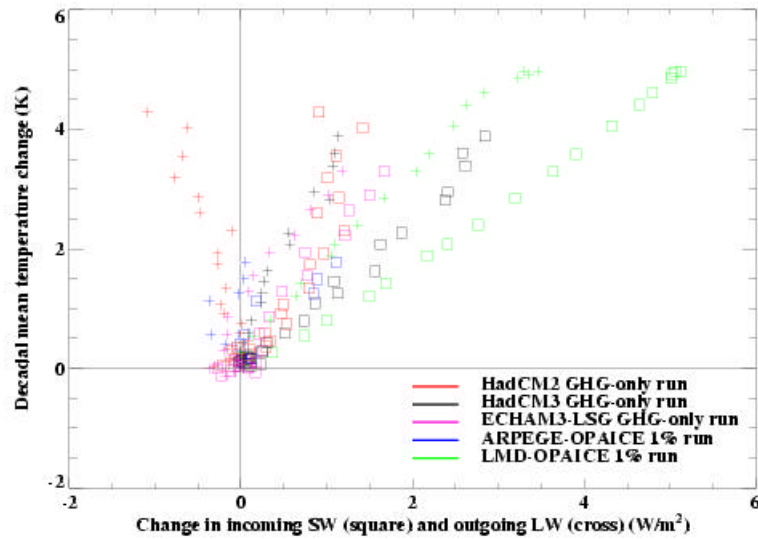


**Figure 8:** Change in decadal mean global average top-of-atmosphere incoming short-wave and outgoing long-wave radiation response plotted against global warming, for selected coupled model experiments with greenhouse gas forcing only [HadCM2, HadCM3, ECHAM3-LSG, ARPEGE-OPAICE and LMD5.3-OPAICE].

For example, at the time of CO<sub>2</sub>-doubling in the ARPEGE-OPAICE experiment (Barthelet et al. 1998; Barthelet, Terray and Valcke 1998) there is an increase of 1.3 W/m<sup>2</sup> as compared to the control from an increase in absorbed SW due to a general reduction of the cloud cover (except at high latitudes) plus a general decrease in the planetary albedo due to ice and snow melting. In the LW component, there is almost a balance between a water vapour increased greenhouse effect (+1.1 W/m<sup>2</sup>) and a cloud reduced greenhouse effect (-1.2 W/m<sup>2</sup>) giving a negative net imbalance of just -0.1 W/m<sup>2</sup>. However, in the LMD-OPAICE model, both incoming SW and outgoing LW increase strongly (almost linearly) as the climate warms. In this example, the atmospheric feedbacks are most likely the cause of differences as the two models share a similar ocean model component.

In general, as well as sensitivities to atmospheric feedbacks via clouds, sea ice and snow albedo etc., there are additional coupled feedbacks operating through oceanic heat uptake, interior mixing and transport processes which can affect both the initial and long term climate responses. Continued work is needed to understand these effects, and to refine the model representations of crucial physical mechanisms and feedbacks.

The model simulated patterns of temperature and precipitation responses to doubled CO<sub>2</sub> (see **Fig. 9** for examples from the LMD-OPAICE (IPSL) model) are related to the model feedbacks, and therefore differ in detail between models (others not shown). Nevertheless, some broad features of the responses; amplification of warming in high latitudes, marked land-sea contrast with land warming more than the ocean surface, and intensified hydrological cycle (more evaporation and rainfall, with largest increases in the Tropics); are common to all models.

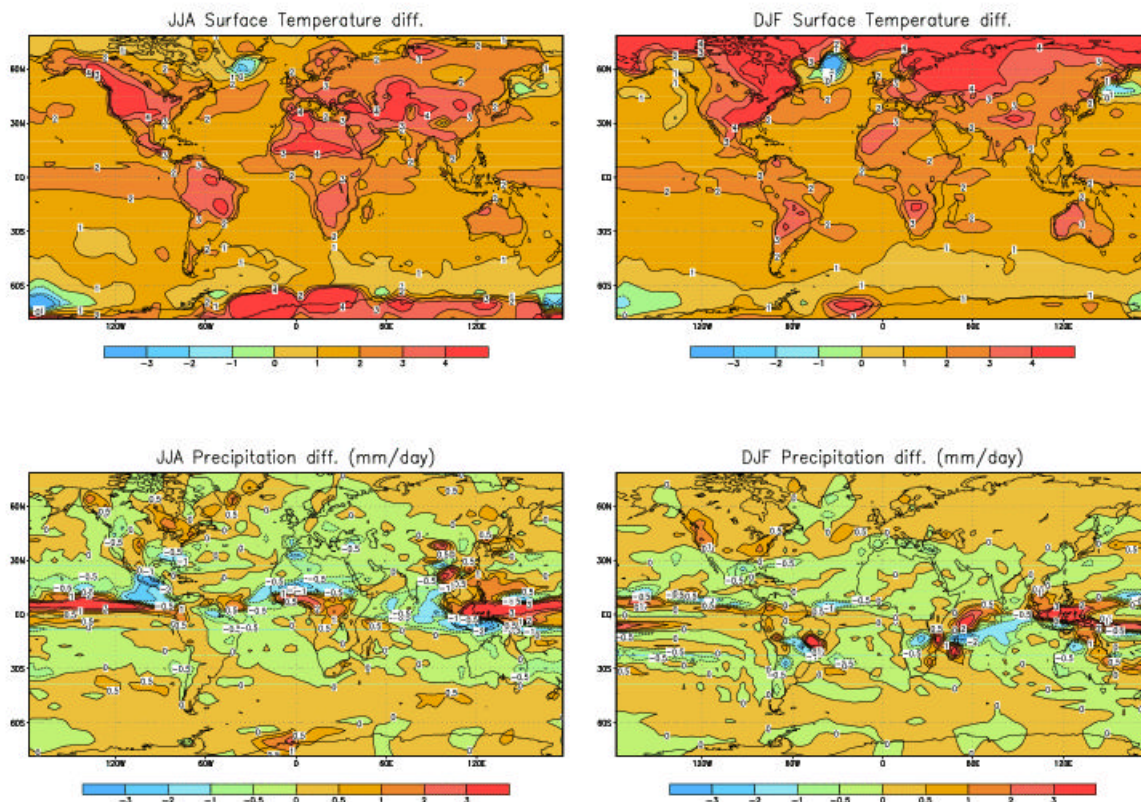


**Figure 9:** Seasonal temperature (K) and corresponding precipitation (mm/day) response for DJF and JJA for a 20-year period around time of  $\text{CO}_2$ -doubling relative to the control climate for the LMD-OPAICE model.

On the regional scale significant differences remain in many land areas, particularly regarding precipitation changes, which translate into marked differences in the implied local impacts from climate change. This is so even when considering just greenhouse gas-forced responses. Additionally, it was established from initial experiments with HadCM2 and ECHAM3-LSG that inclusion of sulphate aerosol forcing in models tends to reduce the strength of the monsoon flow in response to the direct aerosol cooling effect over land with a marked effect on seasonal response patterns. Recent preliminary experiments with ECHAM4 and HadCM3, using revised estimates of sulphate aerosol forcing with indirect as well as direct aerosol forcing effects included, suggest that the direct effect was probably overestimated in the initial studies and the strong land-sea contrast in aerosol forcing overall may not be so marked, reducing the damping effect on the monsoon flow. Nevertheless some significant, though rather uncertain, regional responses to aerosol forcing are almost certain to occur, placing emphasis on future work to improve understanding of sulphate aerosol forcing effects.

Comparison of transient model responses with actual observed climate changes over the 20<sup>th</sup> century offers some prospect of checking whether model response patterns are realistic and thereby indirectly constraining models. The signal-to-noise is better for temperature than for precipitation, so this is conventionally used in detection and attribution studies. Also, vertical temperature cross sections provide less noisy patterns to compare with observations than surface patterns (e.g. see **Fig. 10**). In the attribution context, the aim is to determine the best causal explanation of observed

changes in terms of forcings, but assuming that a model simulation has approximately the correct representation of the historical forcing it is possible to attempt a time-dependent ‘validation’ of the model against observed climate change in order to check the realism of its feedbacks. Attempts to undertake such time-dependent validation studies are so far at an early stage (for a diagnostic example looking at precipitation patterns in HadCM2 ensembles see Hulme, Osborne and Johns, 1998).

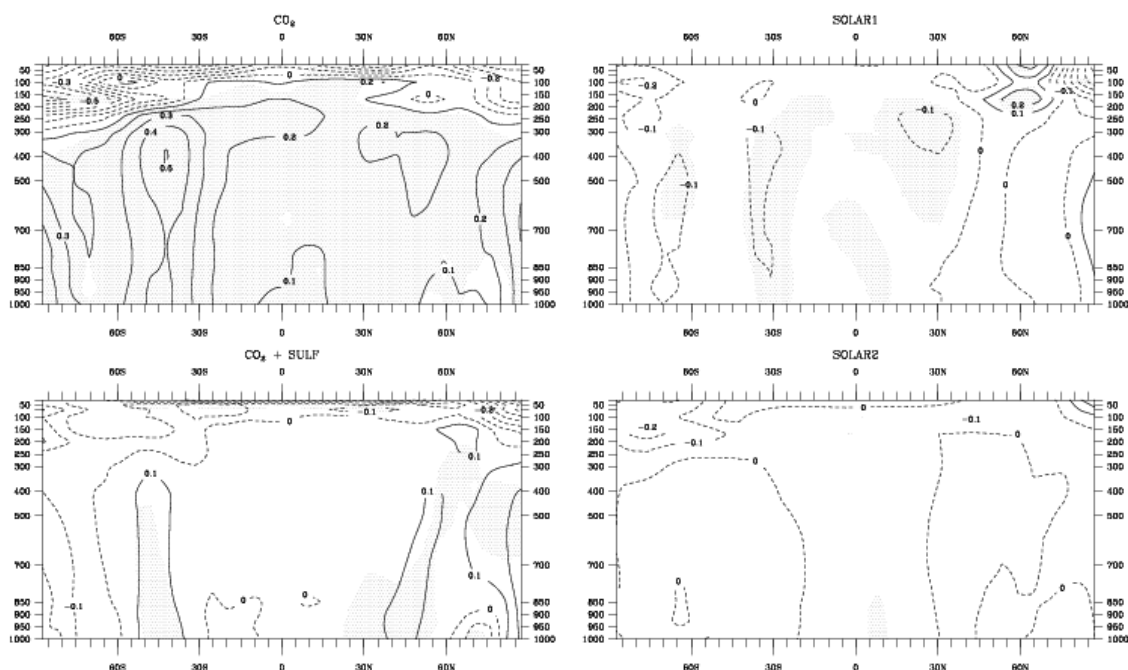


Figure 10: Height-latitude temperature trends (K/decade) over a 30-year period from 1961-1990 in ECHAM3-LSG experiments with  $CO_2$  forcing,  $CO_2$ +aerosol forcing, and solar forcing (Solar1 = forcing based on Hoyt and Schatten 1993; Solar 2 = forcing based on Lean et al. 1995). In the latter 3 examples the pattern is averaged over ensembles of two runs each.

### 3.2.1.2. Two-dimensional transient simulations

In addition to these GCMs transient climate simulations, numerical experiments have been carried out by using the LLN-2D sector-averaged climate model of Gallée et al. (1991) extended to both hemispheres and coupled to a diffusive deep ocean as done in Bertrand et al. (1999) and Bertrand and van Ypersele (1999a,b) to assess the potential impact of four hypothesised mechanisms of decadal to century-scale climate variability, both natural and anthropogenically-induced. More specifically, to investigate the potential role of solar variability as an agent for climate change since 1850, the transient model response to the variations in solar radiation caused by the orbital

forcing (Berger, 1978) ("MIL." in **Fig. 11 to 13**) as well as by the changes intrinsic to the Sun ("SOL.") have been assessed while solar total irradiance variations have been computed following the Hoyt and Schatten (1993) reconstruction. The potential impact of large volcanic eruptions ("VOLC.") on the Earth's climate variations since the second half of the last century has been taken into account by the short-wave radiative transfer perturbations resulting from the changes in the latitudinal and temporal stratospheric aerosol optical depths as compiled by Sato et al. (1993 updated). And finally, based on Bertrand and van Ypersele (1997), the direct anthropogenic sulphate perturbation ("SUL.") has been computed using the monthly mean sulphate abundances simulated by the Moguntia model (Langner and Rodhe, 1991).

As displayed in **Fig. 11 a** and **b**, neither the individual responses nor the combined natural ("NAT.") or anthropogenic forcings ("ANT.") allow to reproduce all of the recorded major temperature fluctuations since the latter half of the 19th century. Half of these forcings have contributed to a long-term warming (largely dominated by the greenhouse gas forcing) and the other half to a long-term cooling (dominated by anthropogenic sulphate forcing and episodic volcanic events) (**Fig. 11a**). The influence of the orbital elements on the global air surface temperature variations are clearly insignificant at this time scale. Moreover, while prior to about 1930, natural externally-driven climate forcings ("SOL+VOL") were the major forcings of the climate system; the combination of these forcings is clearly unable to induce the rapid warming observed after 1970. **Fig. 11b** indicates that the lack of volcanism between 1925 and 1960 certainly could account, at least partly, for the warming trend in this period. By contrast, the combination of the cooling attributed to the anthropogenic sulphate aerosols with the warming due to the greenhouse gases gives a simulation close to the observations in recent decades, while prior to that, the modelled surface temperature response ("ANT.") is too smoothed to reproduce the details of the recorded surface temperature fluctuations. Additionally, a simulation involving anthropogenic factors only is unable to simulate the steep rise of around 0.3°C in global mean during the 1930s and 1940s (see **Fig. 11b**).

As shown in **Fig. 11c**, the model response to the combination of all forcings ("ALL", natural and anthropogenic perturbations) suggests that the observed temperature trends are the result of a subtle combination between naturally driven climate fluctuations and effects of industrialisation. As an example, the warming trend 1920-1940 which coincides with a warm stage of a Gleissberg cycle (an 80- to 90-year quasi-periodic variation in sunspot number and other solar indices) and with the lack of large volcanic events after the Katmai eruption (Alaska) in 1912 is strengthened by industrialisation in Western Europe and the US. The period of relatively low volcanic activity holds until the Agung eruption (Bali) in 1963. This resurgence of volcanic activity combined with a decreasing solar output allows to offset and overcome the greenhouse warming signal (partly counteracted by sulphate aerosols) during a few years. The rapid warming after 1970 appears to be the response to accelerated greenhouse warming and a slower rate of increase in cooling from sulphate aerosols. This last period is clearly dominated by the greenhouse warming which seems to be the largest climate forcing except for short time periods linked with volcanic events like El Chichon (Mexico, 1982) or Pinatubo (Philippines, 1991). Therefore, it seems impossible to simulate the 20th century climate warming without the inclusion of the greenhouse-gas releases connected to human activities, unless this warming is due to the internally driven natural variability of the climate system.

As illustrated in **Fig. 11b**, a large discrepancy between the model response to the natural forcings and the observation occurs in the model response to the Krakatau eruption (Indonesia, 1883). Such a discrepancy is reduced to some extent when forcing the model with half a Krakatau forcing (NAT. 1/2 Kra). Justification to this sensitivity experiment can be found in Sato et al. (1993) which

subjectively estimate a typical error in their reconstructed stratospheric aerosol optical depth of about 50 % for the period 1850-1915.

Based on these results, this climate model of intermediate complexity has also been used to perform transient climate simulations up to 2100. **Fig. 12** presents climate projections that explore the response of the climate system to the IPCC IS92a emission scenario with and without including changes in aerosol beyond 1990. For IS92a carbon emission scenario, the annual and global temperature increase by 2100 relative to 1990 is 2.5°C with constant aerosols after 1990 (IS92a GHG). Including the anthropogenic sulphate forcing according to the IS92a SO<sub>2</sub> emission scenario leads to a reduction in global warming by only 0.2°C at the end of next century (IS92a GHG + SUL). By contrast, reducing the anthropogenic sulphur emission to their 1880 level increases the global warming by 0.17°C in 2100 (IS92a GHG - SULF). Clearly, if direct anthropogenic sulphate forcing has been able to counteract part of the greenhouse-gas forcing over this century, its expected influence on the global air surface temperature at the end of the next century seems insignificant compared to the warming induced by the greenhouse gas forcing.

In addition to these simulations forced by projected changes in anthropogenic perturbations, the model has also been forced by scenarios concerning externally-driven natural climate forcing. Were natural climatic variations of the sort that have characterised the last centuries to recur in the next 100 years, they could modify the expected effects of increased anthropogenic perturbations: either masking an underlying upward trend or accelerating the rate at which it occurs. The climate response to two extreme scenarios concerning the solar forcing have been investigated. Based on the larger magnitude of the total solar irradiance reconstruction of Hoyt and Schatten (1993), the model was forced by a total solar irradiance of  $\pm 0.36$  % in 2100 relative to the 1990 value; the increase (decrease) being obtained by simple linear interpolation between the solar total irradiance values in 1990 and 2100. Future volcanic perturbations being unpredictable, the model was forced by reproducing for the 21st century, the period of maximum volcanic perturbations which has occurred over the last four centuries, i.e., the period from 1800 to 1900 (Zielinski, 1995). **Fig. 13** presents the results. Clearly, these natural climate forcing which have probably modulated the air surface temperature variations over the past centuries (e.g., Overpeck et al., 1997; Briffa et al., 1998; Bertrand et al., 1999), appear either weak or short-lived compared to the greenhouse gas forcing. The transient model response to these changes, expressed in terms of global mean surface temperature change, appears like background noise (less than 0.5°C compared to the model response to the greenhouse gas forcing over the same period (2.5°C)).

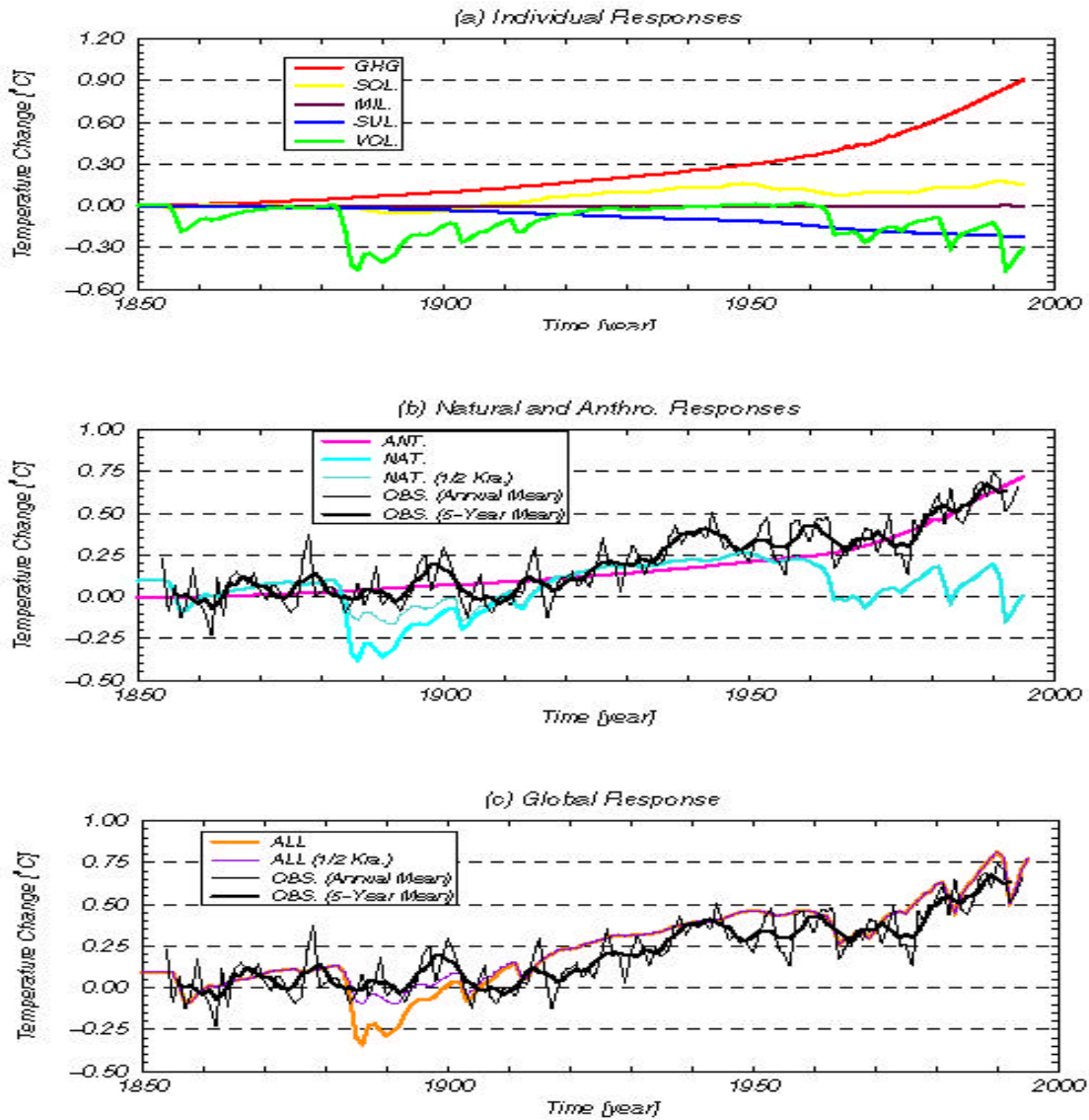


Figure 11: Results from the UCL-ASTR LLN-2D model: Transient response of (a) the annual global mean air surface temperature to the greenhouse gas, (GHG), solar irradiance, (SOL.), Milankovitch, (MIL.), direct sulphate, (SUL.), and volcanic forcings, (VOL.). The temperature anomalies are given relative to the equilibrium state. Comparison between (b) the transient response of the annually globally averaged surface temperature to the anthropogenic forcings (ANT.: anthropogenic sulphate aerosol and greenhouse gas forcing combined), the natural climate forcings (solar and volcanic forcings combined with the Krakatau correction, NAT. (1/2 Kra.), and without it, NAT.), and (c) the combined anthropogenic and natural climate forcings (ALL) with the observed temperature variations from Jones (1988 updated). The anomalies are calculated relative to 1854-1863.

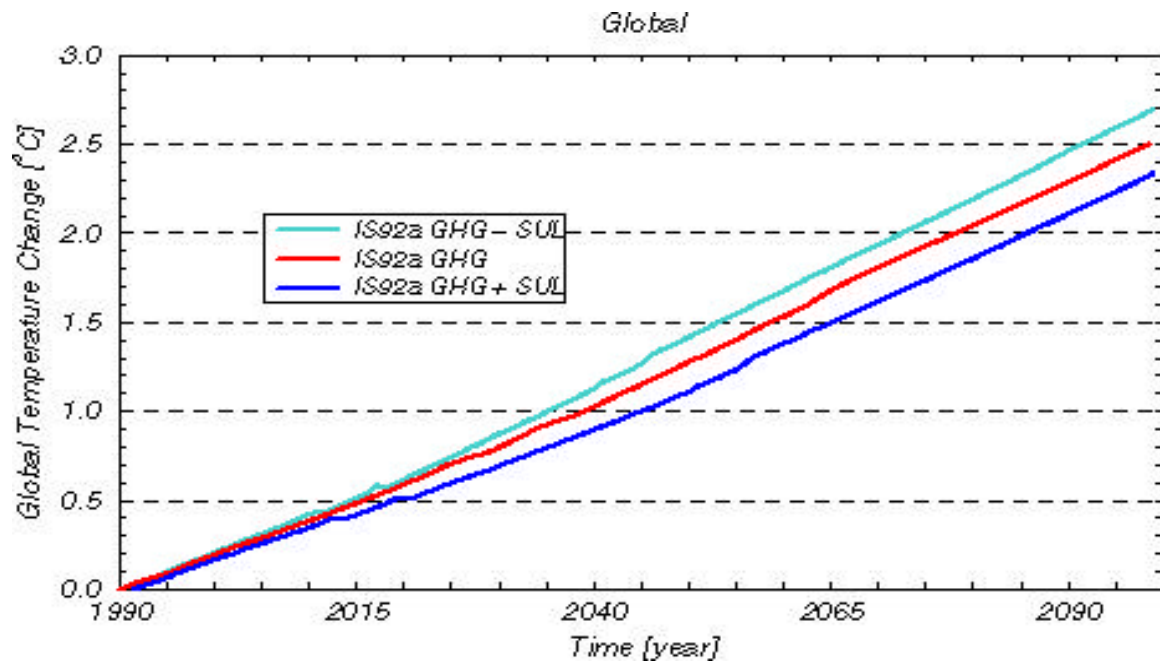


Figure 12: Results from the UCL-ASTR LLN-2D model: Global mean temperature changes from 1990 for IPCC scenario IS92a with changing aerosol concentrations (decreasing: IS92a GHG - SUL, and increasing: IS92a GHG + SUL) and constant (IS92a GHG) beyond 1990.

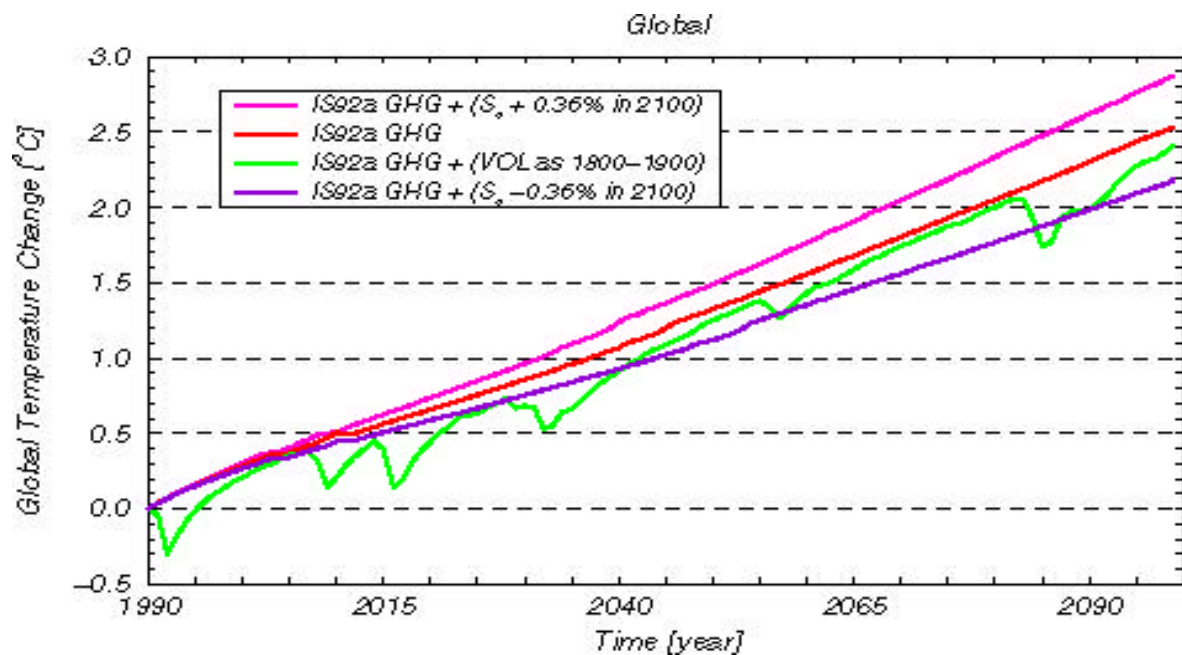


Figure 13: Results from the UCL-ASTR LLN-2D model: Global mean temperature changes from 1990 for IS92a (GHG) combined with a  $\pm 0.36\%$  variations in solar total irradiance in 2100 relative to 1990 value or by assuming the same volcanic activity as that reconstructed over the time period 1800-1900.

### 3.2.2 Possible irreversible changes in the Atlantic ocean circulation

The irreversible changes in the Atlantic ocean circulation have been analysed for the short time scale, which is still within the reach of today's mankind, and for the very long timescale in order to investigate the stability of the results.

Institute	Model	CO <sub>2</sub> -scenario	Length [years]	Flux correction	Coupling
ISPL	LMD-5.3/ OPA-ICE	1% increase up to approximately CO <sub>2</sub> -doubling after 80 years, then fixed	130	no	synchronous
		1% increase up to CO <sub>2</sub> -quadrupling after 140 years, then fixed	210	no	synchronous
Hadley Centre	HADCM2	1% increase up to CO <sub>2</sub> -doubling after 70 years, then fixed	550	yes	synchronous
		IPCC scenario S550 (Houghton et al., 1995)	260	yes	synchronous
DKRZ	ECHAM3/ LSG	IPCC scenario A (Houghton et al. 1990) up to CO <sub>2</sub> -doubling after 60 years, then fixed	850	yes	periodically synchronous
		IPCC scenario A (Houghton et al. 1990) up to CO <sub>2</sub> -quadrupling after 120 years, then fixed	850	yes	periodically synchronous

Table 3: Stabilisation experiments

#### 3.2.2.1 during the next 200 years

Of particular relevance to European climate is the possibility of a collapse in the oceanic conveyor belt circulation provoked by global warming, which might be irreversible beyond some threshold. Theoretically, this possibility is well established using simplified models (e.g. Rahmstorf, 1994, 1995), but its occurrence under real climate change conditions is expected to be sensitive to details of the present climate state as well as temperature and hydrological responses to climate change.

Therefore, the comprehensive coupled models within SIDDACLICH provide an important new database for examining the stability question in a more realistic context.

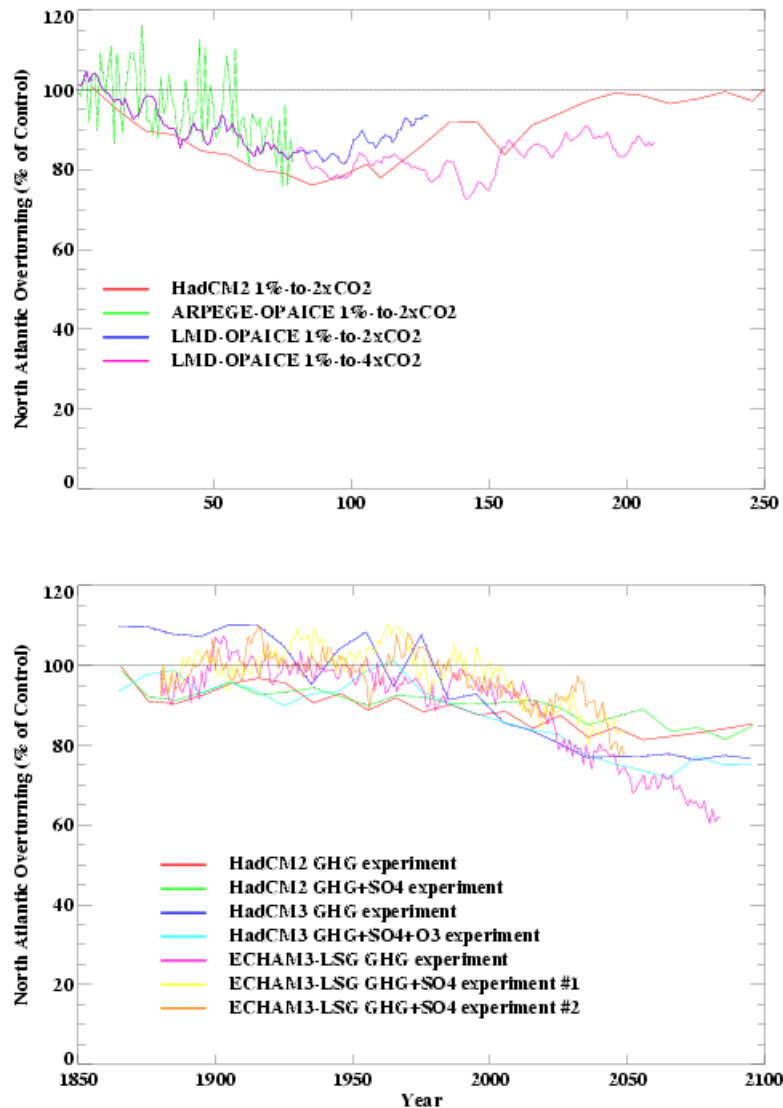


Figure 14: Strength of the Atlantic overturning streamfunction as a percentage of the control simulation for various greenhouse gas forced experiments for (top) idealised forcing, cold start experiments; and (bottom) warm start experiments. The normalisation is with respect to a representative long term mean of the respective control runs except for ARPEGE-OPAICE which is normalised on a year-by-year basis due to large transient changes in both the control and 1%-per-annum simulations.

Interestingly, even though the absolute strength of the Atlantic thermohaline circulation (THC) varies by about a factor of 2 between the models in their present day (control) state, between about 14 to 29 Sv, the relative sensitivities to climate warming are rather similar. In the case of idealised CO<sub>2</sub> increases at 1%-per-annum (Fig. 14a), the three models show a reduction of between 15-20% relative to their control state at the time CO<sub>2</sub> doubles (70 years). HadCM2 and LMD-OPAICE runs which subsequently stabilise at 2\*CO<sub>2</sub> both show a gradual recovery back towards the control

level, with an almost total recovery after about 200 years in the case of HadCM2. In the LMD-OPAICE run which continues up to 4\*CO<sub>2</sub> before stabilising, the circulation does not decline much further beyond 2\*CO<sub>2</sub>, again recovering slightly after CO<sub>2</sub> stabilises.

This general pattern of a modest but not catastrophic decline in the Atlantic THC is confirmed in the more realistic forcing scenarios using a historical warm up period to present followed by a standard forcing scenario to 2100 including GHGs and other forcing factors. Seven different runs with three models (**Fig. 14b**) give a range of between 15-30% reduction by 2050. The HadCM3 and ECHAM3-LSG models are slightly more sensitive than HadCM2, but none of them collapses completely on this timescale and the global warming signal tends to dominate over any local cooling trend in NW Europe due to the weakened Gulf Stream.

The evolution of the THC in response to such representative future forcing scenarios is a topic requiring further study. It should be noted in particular that these scenario experiments do not presently model the possible effects of significant fresh water input arising from changes in land ice sheets (Greenland and Antarctic ice caps) and mountain glaciers, which might well lead to stronger reductions in the THC. So it is too early to say with confidence whether irreversible collapse in the THC is likely or not, or at what threshold it might occur. The realism of the representation of oceanic mechanisms involved in the THC changes also needs to be carefully evaluated in the models.

### ***3.2.2.2. in the longer term***

Two groups (Hadley Centre and DKRZ) have extended their stabilisation scenario calculations for more than 500 years (see **Table 3**).

The ECHAM3/LSG model used for this extended experiment has been run in a periodically synchronously coupled mode. This coupling scheme consists of alternating synchronous and ocean-only integrations. The switching off of the atmospheric component during the ocean-only periods results in a considerable reduction of the computer time. In the presented simulations synchronously coupled periods of 15 months alternate with ocean-only periods of 48 months. With this choice of the period lengths the periodically synchronously coupled ECHAM3/LSG consumes only 30% of the computer time of the synchronously coupled model version. The comparison of the results obtained with both model versions shows that the mean state and the climate change pattern are satisfactory reproduced by the periodically synchronously coupled model (Voss et al., 1998).

The results of the stabilising experiments are compared to corresponding control simulations with fixed present-day conditions (see **section 3.1**). More details of the ECHAM3/LSG stabilising experiments are presented in Voss and Mikolajewicz (1999).

As mentioned before, common to all stabilising experiments is a strong warming during the years, while the CO<sub>2</sub>-concentration is still increasing, followed by a weaker warming (ca. 1 K) during the period with fixed concentrations. This warming continues to the end of the long simulations (i.e. in one case even 850 years).

This continuing slow increase is due to adjustment processes of the ocean. For instance, in the ECHAM3/LSG runs the temperature increase in the deep ocean is much stronger during the last hundred years (751-850) than in the first century. The long-term adjustment is also visible in the sea-level change due to thermal expansion. After 850 years the rise of the sea level in the ECHAM3/LSG runs is more than 75 cm in the CO<sub>2</sub>-doubling case and 150 cm in the CO<sub>2</sub>-quadrupling case (**Fig. 15b**). Due to the large heat capacity of the deep ocean the changes are still

strong at the final century of the experiments (5 cm/century in the CO<sub>2</sub>-doubling run and 12 cm/century in the CO<sub>2</sub>-quadrupling run). The Hadley Centre model shows a similar behaviour with a slightly stronger sea-level rise (**Fig. 16b**).

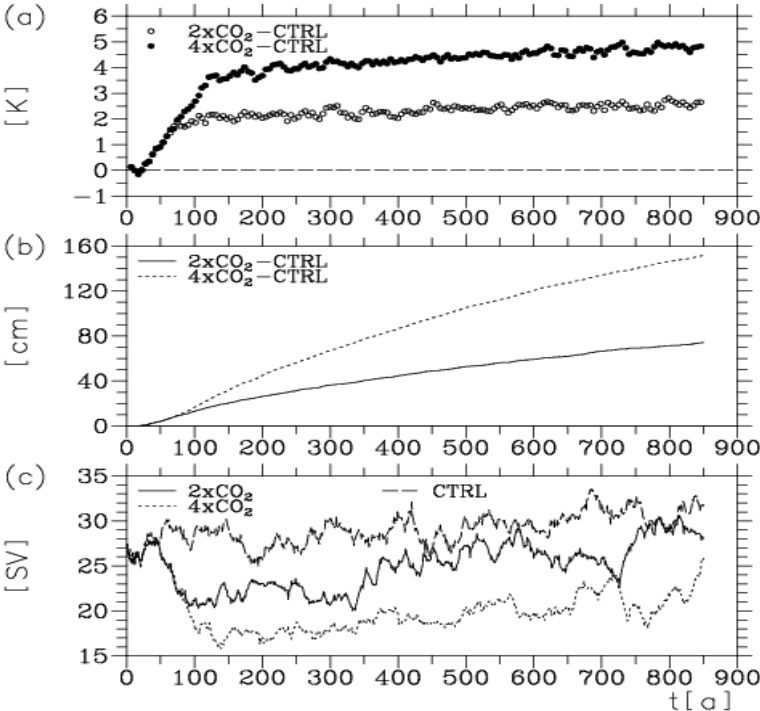


**Figure 15:** Time evolution of (a) the global mean sea surface temperature, (b) the global mean sea level change due to thermal expansion, and (c) the maximum of the meridional stream function for the Atlantic simulated by the ECHAM3/LSG model. In (a) the annual means of the synchronously coupled periods are shown.

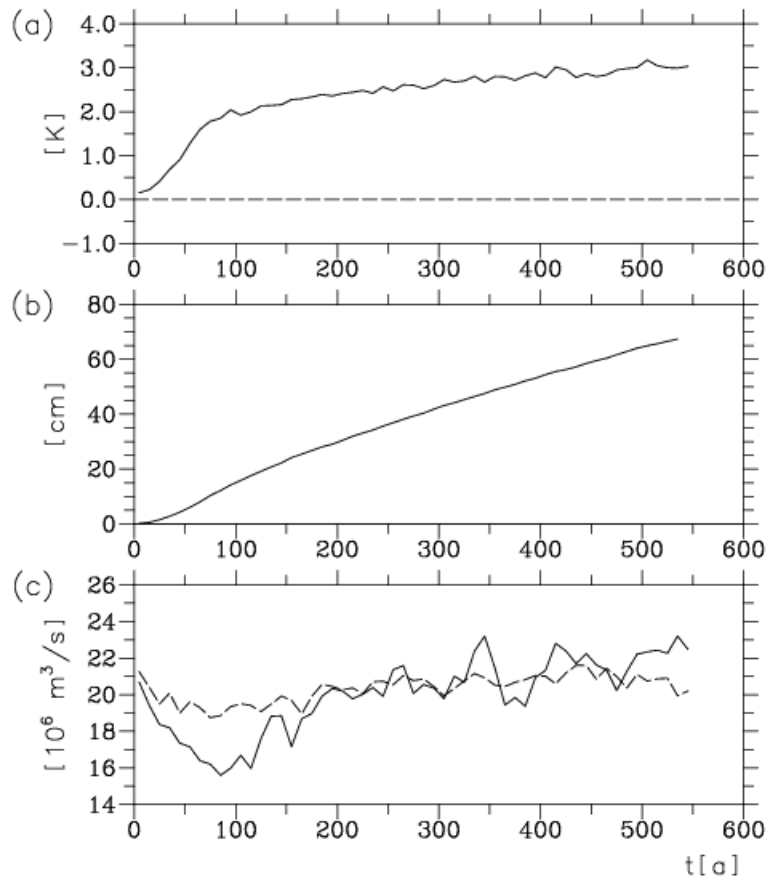


**Figure 16:** Time evolution of (a) the global mean sea surface temperature, (b) the global mean sea level change due to thermal expansion, and (c) the maximum of the meridional stream function for the Atlantic simulated by the HADCM2 model for the CO<sub>2</sub>-doubling scenario. In (a) and (b) the decadal mean anomalies to the control run values are displayed. The dashed curve in (c) represents the control run values.

The thermohaline circulation also exhibits remarkable changes. As an example the time series of the maximum of the meridional stream function for the North Atlantic are shown in **Fig. 15c** and **Fig. 16c**. In the control simulation as well as in the climate change experiments this measure of the intensity of the overturning circulation is characterised by decadal to centennial variability.

The overturning circulation weakens during the first 100 years of the CO<sub>2</sub>-doubling experiments by 15% to 20%. In these runs the intensity slowly recovers after reaching the minimum. In the Hadley Centre simulation it reaches the control run value after ca. 200 years whereas in the DKRZ-

run it is slightly below the control run value after 850 years. In the CO<sub>2</sub>-quadrupling experiments of IPSL and DKRZ the reduction is stronger. At the end of both runs the intensity is still significantly weaker than in the control simulation, but it tends to increase. Nevertheless, in the quadrupling experiments an Atlantic conveyor belt-type overturning circulation pattern is present throughout the full simulation period. This is in contrast to a corresponding CO<sub>2</sub>-quadrupling experiment of Manabe and Stouffer (1994) where the thermohaline circulation totally collapses.

### 3.2.3 Flux-adjusted versus non flux-adjusted responses

Several of the models in SIDDACLICH run without flux adjustments (see Chapter 2). There are both advantages and disadvantages to this approach. The absence of flux adjustments allows easier identification of the causes of initial drifts in the simulation, enabling underlying biases in the present day climate simulation of the model to be systematically improved via a focussed model development program. Provided present day climate is well represented, omitting artificial terms is highly beneficial in terms of allowing a clean experimental set-up, and lessens the possibility that climate change sensitivity is distorted or damped in some way.

An example of the non flux adjusted approach is HadCM3 which has proved to be highly successful in that it uses no flux adjustments yet maintains a realistic climate state with generally small drifts, but there remain some problem areas that still need improvement. Drifts in any model can become a source of difficulty if they are large, as they can distort climate change responses and make analysis difficult. For example, the absence of flux adjustments in the ARPEGE-OPAICE model leads to some climate drift at high latitudes in the control simulation which suppresses deep water formation in the Labrador and Irminger seas (Barthelet, Terray and Valcke, 1998). The additional sea surface freshening that occurs in the 1%-per-annum CO<sub>2</sub>-experiment results in a further weakening of the THC. One can argue that if the initial bias was corrected, convection in the Labrador and Irminger seas would be maintained in the control simulation. Thus, as the freshening due to anthropogenic forcing is particularly large in these regions, the deep water formation would be further reduced and the THC would be affected to a larger extent in the transient experiment as compared to the control.

The exact impact of using or omitting flux adjustments is very difficult to measure, but some experiments with HadCM2 with and without flux adjustments (Gregory and Mitchell 1997) tend to support the view that flux adjustments themselves do not grossly distort climate sensitivity or the patterns of response. Rather, as is their intention, they are largely a device for constraining the drifts in the control climate state. So the zonal mean temperature response to CO<sub>2</sub>-doubling shows a similar pattern with or without flux adjustment in HadCM2 (**Fig. 17**), the main difference being a reduction of about 30% in the global average warming which can be related to more efficient vertical transport in the ocean in the different control state when flux adjustments are omitted. Analysis of differences in climate change responses under GHG forcing between HadCM2 (with flux adjustments) and HadCM3 (see Mitchell, Johns and Senior 1998) provides limited insight into the role of flux adjustment. Most of the differences in response patterns between HadCM2 and HadCM3 are probably related to improvements

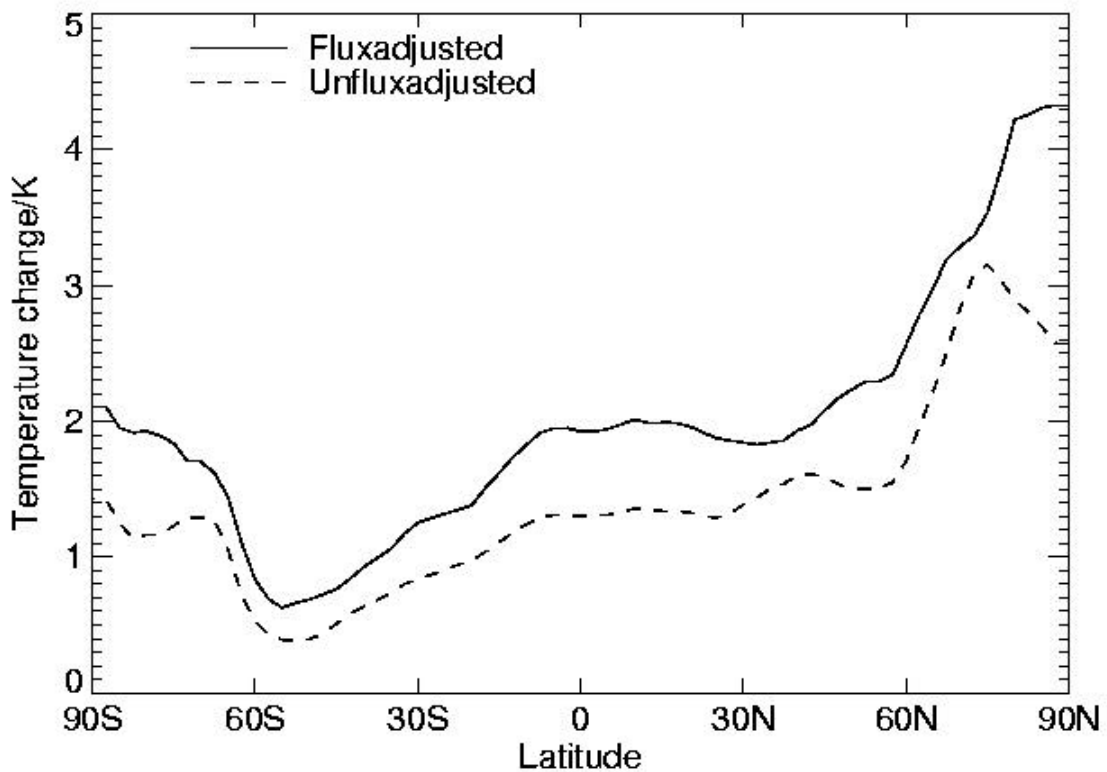


Figure 17: Comparison of zonal mean temperature response in HadCM2 experiments at the time of CO<sub>2</sub>-doubling with and without flux adjustment (Gregory and Mitchell 1997).

in the model physics rather than to flux adjustment, but the global climate sensitivity and land-sea contrasts remain almost identical in HadCM3 despite the fairly wide-ranging model changes from HadCM2 to HadCM3.

### 3.2.4 The role of individual air-sea flux components

The role of heat, freshwater and momentum fluxes in changing the oceanic climate and thermohaline circulation as a consequence of increasing atmospheric CO<sub>2</sub>-concentration has been investigated (Mikolajewicz and Voss, 1998). Two baseline integrations with the fully coupled ocean atmosphere general circulation model ECHAM3/LSG with either fixed or increasing atmospheric CO<sub>2</sub> concentrations have been performed. The runs represent the first 150 years of the 850-year control and CO<sub>2</sub>-quadrupling runs described in **section 3.2.2**.

In a set of sensitivity experiments (of 150 years length each) either freshwater and/or momentum fluxes were no longer simulated, but prescribed according to one of the fully coupled baseline experiments (see **Table 2**). This approach gives a direct estimate of the contribution from the individual flux components. The direct effect of surface warming and the associated feedbacks in ocean circulation are the dominant processes in weakening the Atlantic thermohaline circulation in the model. The relative contribution of momentum and freshwater fluxes to the total response turned out to be less than 25% (**Fig. 18**).

Experiment	CO <sub>2</sub> -concentration	Freshwater flux	Wind stress
FSS	Fixed present-day	Simulated	Simulated
ISS	Increasing	Simulated	Simulated
IFS	Increasing	from FSS	Simulated
FIS	Fixed present-day	from ISS	Simulated
IFF	Increasing	from FSS	from FSS

Table 4: List of surface flux sensitivity experiments

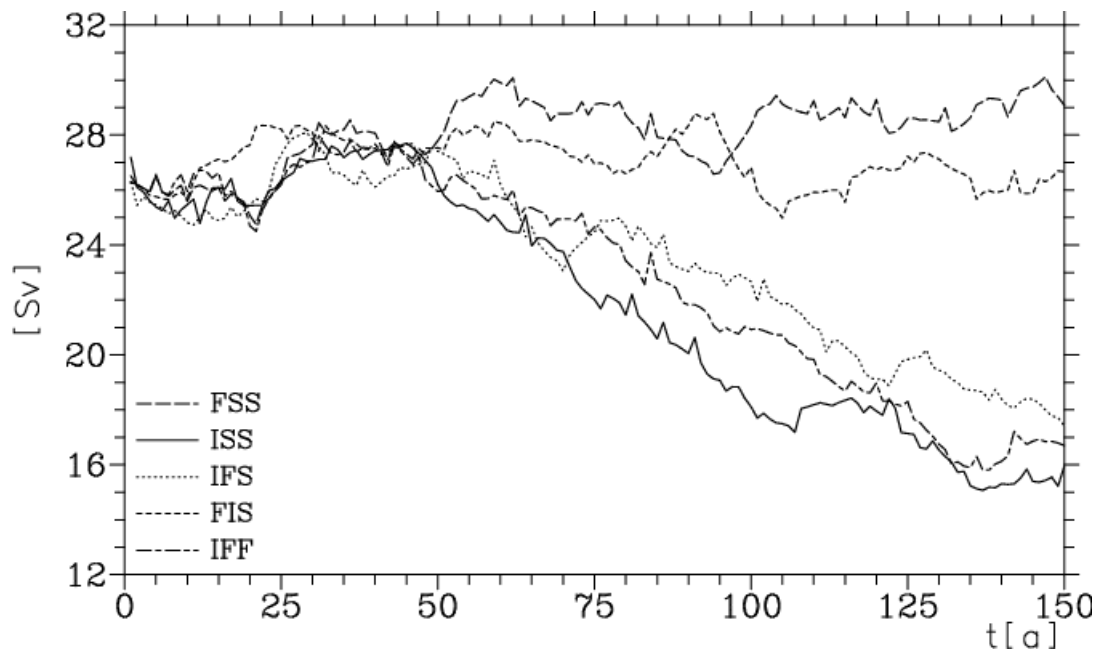


Figure 18: Time series of the zonally integrated Atlantic mass transport stream function at 300 N and 1500 m depth, close to the maximum of the stream function simulated by the ECHAM3/LSG model. For a description of the experiments see Table 4 (from Mikolajewicz and Voss, 1998).

Changes in atmospheric water vapour transport lead to enhanced freshwater input into middle and high latitudes, which weakens the overturning. A stronger export of freshwater from the Atlantic drainage basin to the Indian and Pacific ocean, on the other hand, intensifies the circulation. In total the modified freshwater fluxes slightly weaken the Atlantic thermohaline circulation. The contribution of the modified momentum fluxes has a similar magnitude, but enhances the formation

of North Atlantic deep water.

Salinity anomalies in the Atlantic as a consequence of greenhouse warming stem to almost equal parts from changes in net freshwater fluxes and from changes in ocean circulation caused by the surface warming due to atmospheric heat fluxes. Important effects of the momentum fluxes are a poleward shift of the front between northern hemisphere subtropical and subpolar gyres and a southward shift in the position of the Antarctic circumpolar current, with a clear signal in sea level.

### **3.3. Mid-latitude storm tracks and the North-Atlantic-Oscillation**

Baroclinic wave activity plays a central role for local weather in the mid-latitudes. It can be quantified by considering the locations and intensities of surface cyclones (König et al., 1993; Haak and Ulbrich, 1996, Carnell et al., 1996 and Carnell and Senior, 1998), or (following Blackmon, 1976) by considering the variability of the bandpass (e.g., 2.5-6 day) filtered geopotential height fields at 500 hPa (e.g., Christoph et. al, 1995). Similar to cyclone frequency this latter quantity exhibits two main maxima in boreal winter, one over the North Atlantic (called the Atlantic storm track) and one over the North Pacific (the Pacific storm track). Over the Atlantic, storm tracks and cyclone activity are modulated by the North Atlantic Oscillation (NAO), which itself affects local climate over Europe by changing the mean circulation in the lower troposphere. One example for the joint impact of NAO modulated mean advection and of baroclinic wave activity has been shown for rainfall in Portugal (Ulbrich et al., 1999).

#### **3.3.1 Changes of cyclone- and upper air storm tracks**

A number of climate runs were used for investigating present day mid-latitude baroclinic activity and the imposed anthropogenic changes. Distributions of surface cyclones produced by model control runs with present day greenhouse gases (HadCM2 CON, see Johns et al., 1997; ECHAM4+OPYC, see Roeckner et al., 1998) give a reasonable representation of the observed distribution (e.g., **Fig. 19**).

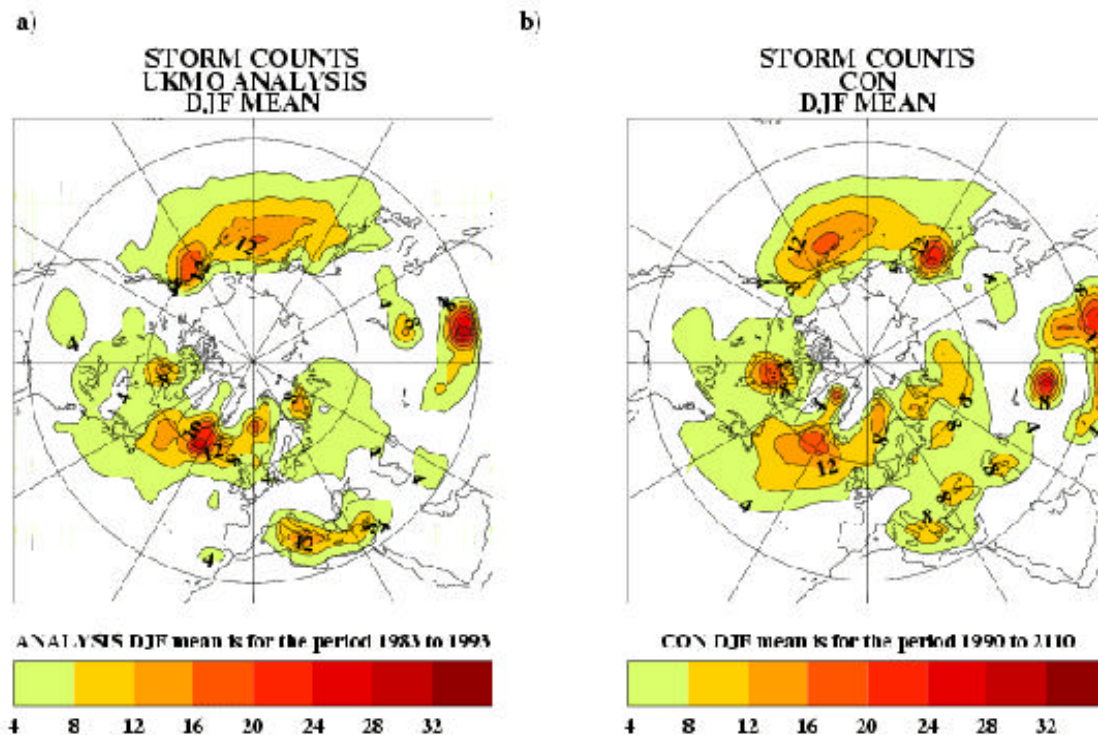


Figure 19: Seasonal (December, January, February, DJF) mean storm counts. The data has been smoothed (9 point centre weighted average) and area weighted prior to plotting to give the number of storms per 1,000,000 km<sup>2</sup>. The contours are at 4 storms per season per 1,000,000 km<sup>2</sup> intervals. Left: UKMO analyses, 1983 to 1993. Right: Control run, 120 winters.

The scenario runs used include

- historical CO<sub>2</sub> increases from 1860 to 1990 followed by a further 1% per year compound increase in CO<sub>2</sub> from 1990 (HadCM2 GHG),
- historical CO<sub>2</sub> increases from 1860 to 1990 followed by a radiative forcing given by the IPCC IS92a scenario-A (ECHAM4+OPYC),
- effects of greenhouse gases as in GHG and the direct radiative forcing due to anthropogenic sulphate aerosols (HadCM2 SUL).

For each of the HadCM2 GHG and SUL experiments ensembles of four members were run for two 30 DJF periods: double CO<sub>2</sub> (2006-2036) and quadruple CO<sub>2</sub> (2070-2100). The ensemble mean cyclone tracks were calculated. Each track was classified by its lowest central pressure into shallow, medium or deep storms (**Fig. 20**). When greenhouse gases and anthropogenic sulphate aerosols are increased there are more deep storms in the Northern Hemisphere winter.

The positions of the cyclone tracks when CO<sub>2</sub> is doubled in GHG are similar to their positions in CON and the differences in the total number of storms is small. When CO<sub>2</sub> is quadrupled the magnitude of the changes increases but the pattern of changes is similar to the earlier period. The changes in SUL are similar to those in GHG.

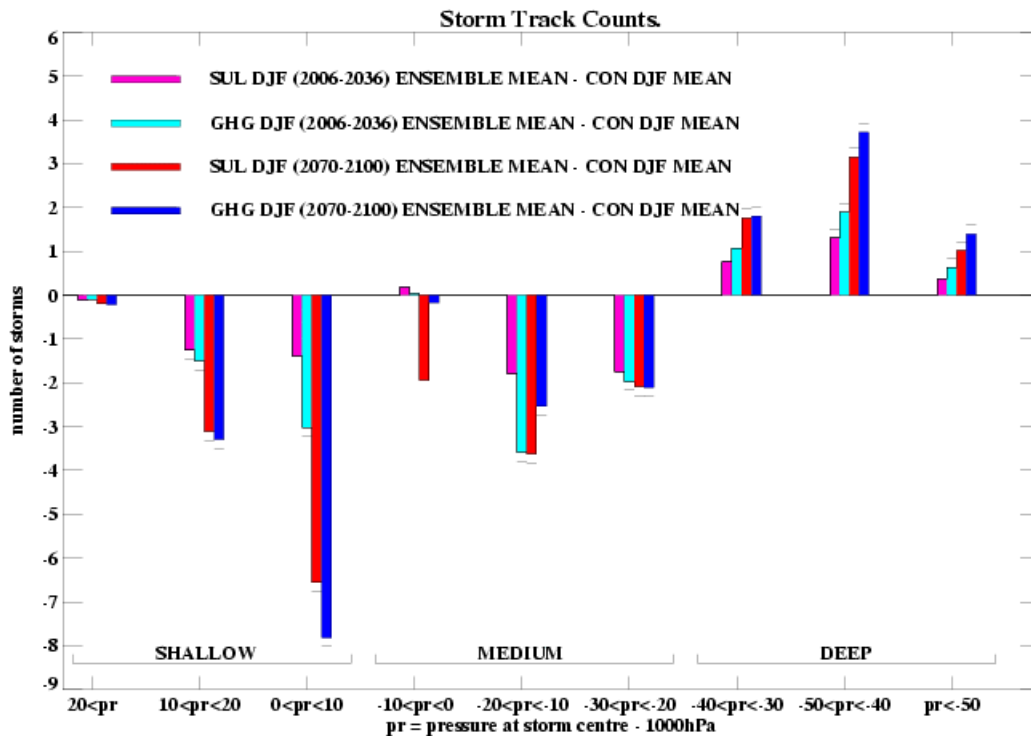
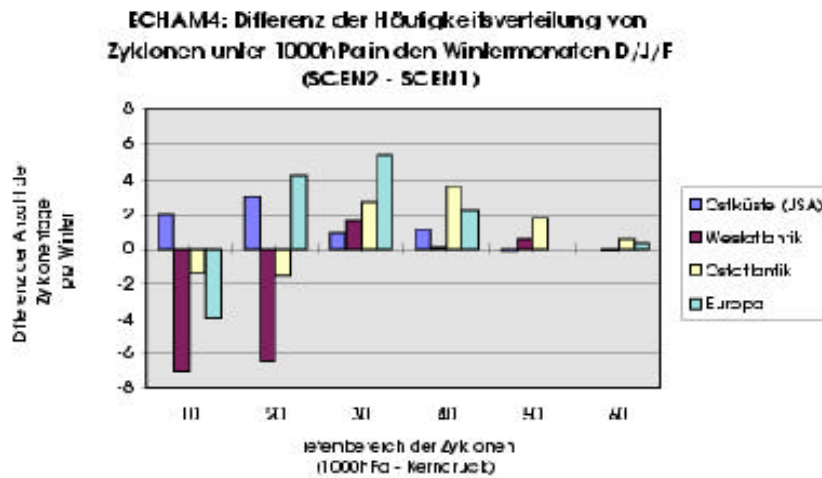


Figure 20: Number of storm tracks per 90 day DJF season in each central pressure band (pr = pressure at storm centre - 1000 hPa). Different colours represent deviations of specific ensembles from the 120 winter mean of the control run CON: Magenta (1st peak from left of each group): SUL (years 2006-2036) deviations; Cyan (2nd from left): GHG (2006-2036) deviations. Red (3rd from left): SUL (2070-2100) deviations. Blue (4th from left): GHG (2070-2100) deviations. Horizontal bars at the end of the peaks show changes that are significant at the 1% level when a Student's t test is applied.

There is some disagreement between the HadCM2 and ECHAM4+OPYC changes regarding the surface cyclones at the time of CO<sub>2</sub>-doubling: The HadCM2 GHG ensemble produces a decrease in the number of storms in the North Atlantic storm development region and also in the number reaching the north-eastern end of the climatological track. There are more storms in the central North Atlantic suggesting that the climatological track has shortened. There is an about 2 hPa increase in mean sea level pressure (PMSL) at the end of the storm track over Western Europe corresponding to the decrease in the number of storms (not shown) and a decrease in PMSL in the central Atlantic where the number of storms has increased. The changes produced by this model in the Pacific are qualitatively similar: there are less storms in the source regions off the coast of Asia and in the Sea of Okhotsk and a shortening of the climatological track at the far north-eastern end. PMSL decreases across much of the North Pacific with the largest decrease being where the number of storms has increased.

In contrast, ECHAM4+OPYC produces an increase in the number of deep cyclones over the central North Atlantic and Western Europe longitude sector (**Fig. 21**) as well as over the central north Pacific (not shown) for doubled greenhouse gas forcing. Over the Atlantic, the increase concerns mainly the high latitudes north of 60°N, while the signal is between 45°N and 60°N for the Pacific. There is, however, agreement between the HadCM2 and the ECHAM4+OPYC signals when considering the upper air storm track intensity change over Northern Europe.



**Figure 21: Difference between present day ( $\sim 1.2 \text{ W/m}^2$ ) and doubled green house gas forcing ( $\sim 6 \text{ W/m}^2$ ) with respect to the number distribution of cyclone core pressures. Each period is represented by 10 winters out of the transient ECHAM4+OPYC greenhouse gas run.**

Both models produce a 10-15% increase of winter storm track activity over the north-western Europe (**Fig. 22**). The simulations of the LMD's coupled atmosphere-ocean model also give a very similar location of the greenhouse gas signal over Europe (**Fig. 22, bottom right panel**). This is in spite of the fact that the LMD model's Atlantic storm track has its maximum at a position east of southern Greenland, i.e. downstream of the observed location. Comparing these results with previous simulations for anthropogenic climate change (Cubasch et al., 1997), the increase of upper air storm track activity over Northern Europe is a common signal, while the amount of this change is variable and in many cases the statistical significance is comparatively low (90-95% level). This effect may be assigned to the low frequency variability in the models. **Fig. 25** shows this variability for storm track activity over Europe in the ECHAM4+OPYC simulation. Depending on the exact choice of a relatively short averaging periods (e.g., 10 winters) out of this run very large or small estimates of a greenhouse gas induced increase of activity can be produced. The longer timescale, however, clearly indicates the dominance of a long term trend. This is further elucidated by a global EOF analysis of the bandpass filtered geopotential heights over all 240 boreal winters. The principal component (PC) associated with the first EOF (explaining 34% of the total variance) reveals a non-linear trend closely following the anthropogenic greenhouse gas forcing function of the run (not shown). While there are also large contributions of the EOF over the Southern Hemisphere, one particular change suggested by the EOF is the increase of storm track intensities over the eastern North Atlantic and Europe. The resemblance between the time series of storm track activity averaged over Europe (**Fig. 25**) and the first PC of the global storm track suggests that storm track intensification over Europe is indeed a stable feature of anthropogenic climate change.

The same kind of analysis was performed for the winter means of sea level pressure. The first PC (explaining 79% of the total variance, also develops in parallel to the radiative forcing. The EOF shows decreasing surface pressure towards the Northeast Atlantic. This change in mean pressures will contribute to a trend in surface cyclone core pressures, which is which is particularly evident in the Eastern Atlantic and European sector in the ECHAM4+OPYC scenario run (Fig. 22).

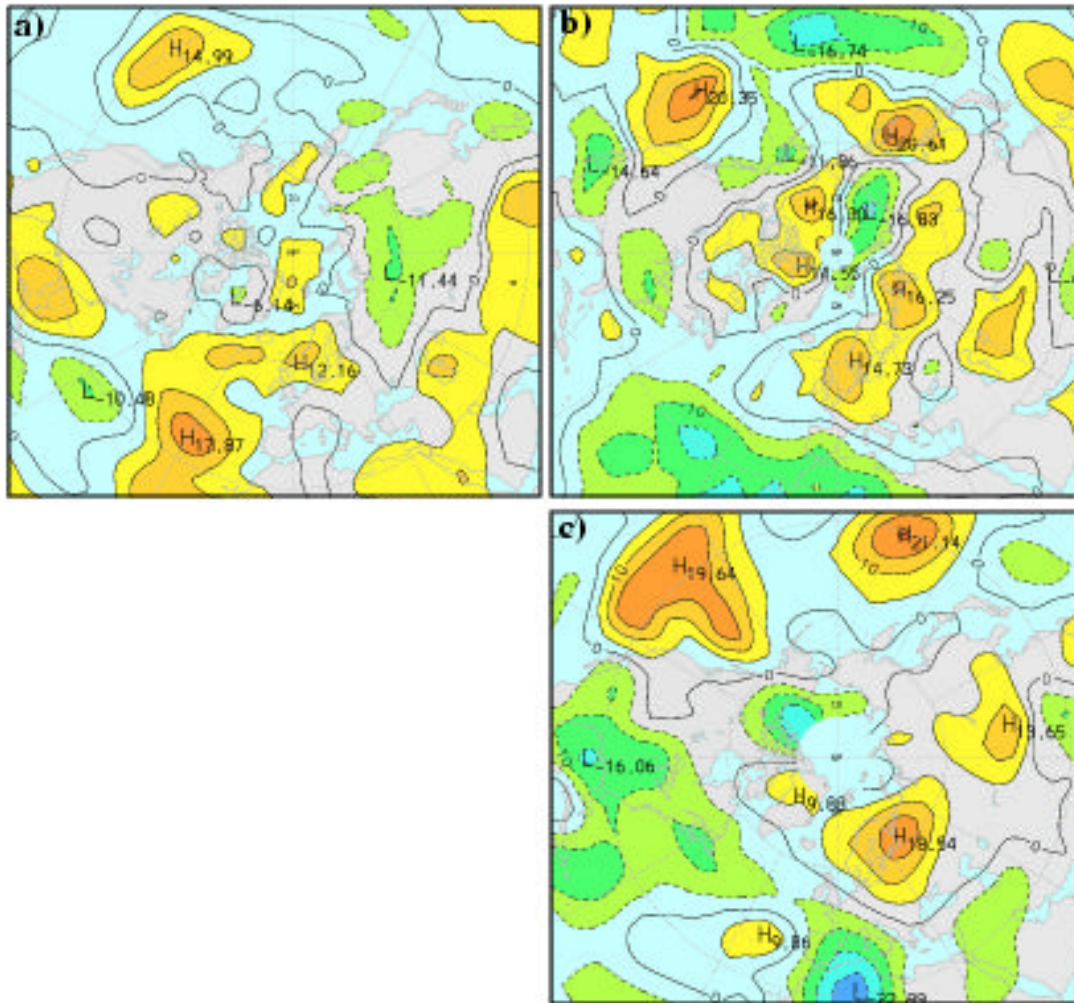
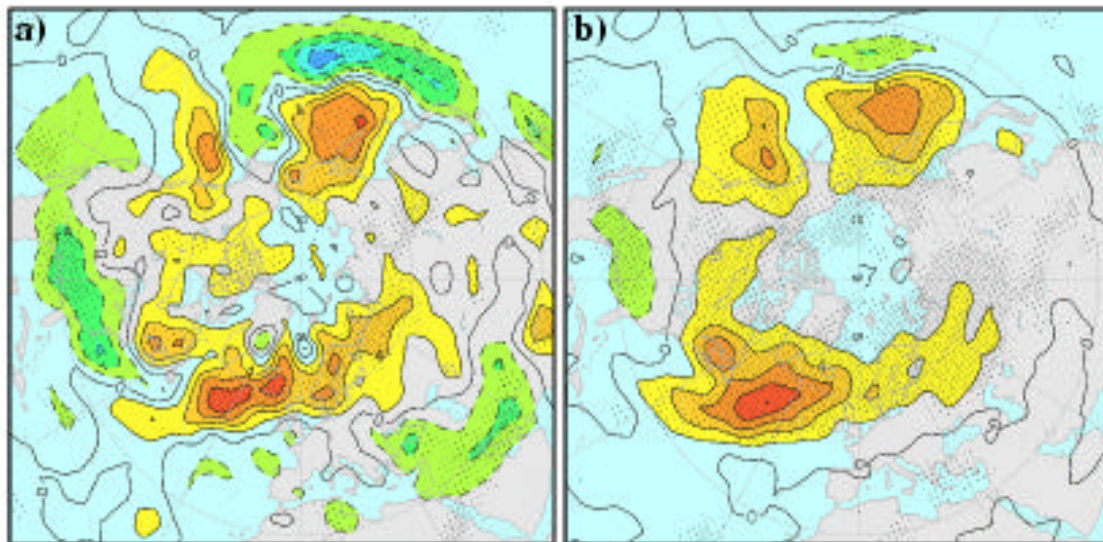


Figure 22: Relative change of winter storm track activity in the scenario runs in per cent. Top left: HadCM2, four-member 30 year ensembles for 2\*CO<sub>2</sub> and 1\*CO<sub>2</sub>. Top right: 10 year periods out of the ECHAM4+OPYC3 transient greenhouse gas Scenario Run, representing a radiative forcing at the tropopause of ~ 1.2 W/m<sup>2</sup> (model years 1965 - 1974) and ~ 6 W/m<sup>2</sup> (model years 2060 - 2069) are compared. Bottom right: Same results for the model LMD version 5.3, 2\*CO<sub>2</sub> (model winters 80/81 to 88/89) - control (model winters 9/10 to 17/18).

Considering potential physical mechanisms for the increase in storm track activity, increasing baroclinicity over the entire north-east Atlantic (estimated by the maximum Eady growth rates) was found for the ECHAM4+OPYC scenario, with main changes occurring in the upper troposphere.

In a warmer climate an increase in storm intensity may also be expected due to a larger amount of water vapour in the atmosphere. The role of diabatic processes in supplying energy within baroclinic waves is estimated by covariances of the transient diabatic heating and temperatures (more specifically: contributions to the generation of eddy available potential energy  $GE_T$  are considered, see Lorenz, 1955, Arpe et al., 1986). The conversion of this energy due to warm air rising and cold air sinking ( $CE_T$ ) leads to an enhancement of the kinetic energy of the storm systems. The largest Northern Hemisphere greenhouse-gas signals for both quantities are found at 400 hPa. They are of similar magnitude. With respect to the horizontal distribution of changes, ECHAM4/OPYC produces different structures for the Pacific and the Atlantic (**Fig. 23a**). Over the Pacific, a northward shift dominates, while the strongest signal over the Atlantic is an intensification of both quantities at the stormtrack exit region (Norwegian sea and Scandinavia, with relative changes up to 50%). The increases of the contribution of  $GE_T$  are dominated by increases in large-scale latent heat release (**Fig. 23b**). They are reflected by increasing precipitation rates over the storm track area. Corresponding results are also found for HadCM2, leading to the interpretation that increases in the upper air wave activity and increases in the number of deep of the storms may be due to an increase in energy from increased latent heating in the warmer, moister atmosphere.



**Figure 23:** Difference between  $2*CO_2$  and  $1*CO_2$  forcing for boreal winter (DJF) in a) baroclinic conversion term  $CE_T$  and b) generation of transient available potential energy ( $GE_T$ ) in units of  $10^6 Wm^2Pa^{-1}$  in 400 hPa. Contour interval is 15 units for a) and b). Values greater 15 or less than  $-15$  units are coloured. Light/heavy shading indicates statistical significance at the 95%/99% level.

### 3.3.2 Variability and anthropogenic changes of the NAO

The observed variability of the NAO index (based on the index of Hurrell, 1995) between 1970 and 1993 shows a significant 8-year oscillation in wavelet analysis (Appenzeller et al., 1998). This oscillation was correlated with the mean DJFM-sea level pressure fields. A comparison shows that the 8-year oscillating signal correlates better with the western part of the NAO pattern and the remaining part of the NAO index with the eastern part of NAO pattern. The underlying SST also correlates very closely ( $> 0.8$ ) with the sine function, but it lags with 2 years or with a phase shift of 90 degrees. So a direct relationship between the oscillation in SLP and SST can almost be

excluded. While the very simple decomposition of the NAO index is able to separate two significant sub-patterns for the period between 1970 and 1993, it is not able to explain the physical mechanism behind the eight-year oscillation.

The NAO index was also investigated using the 300 year control simulation of the ECHAM4+OPYC model (see Ulbrich and Christoph, 1999). It was obtained as the difference between area averaged and normalised monthly mean sea level pressure (SLP) anomalies north-west of Portugal [11-14<sup>0</sup>W, 40-43<sup>0</sup>N] and over Iceland [17-20<sup>0</sup>W, 65-68<sup>0</sup>N]. These locations represent the teleconnectivity centres over the North Atlantic in the simulation. They agree closely with the observed centres. As in the observational data, the teleconnectivity maxima are found in the vicinity of the variability maxima obtained from an EOF analysis of the SLP over the North Atlantic. The first EOF (explaining 46% of the total variance in winter) produces the typical NAO pattern whose subarctic centre possesses a zonally elongated structure, with a primary maximum over south-east Greenland and a secondary maximum over Iceland. This structure agrees well with the leading EOF of observational SLP data from the North Atlantic sector in January (Glowienka-Hense, 1990).

The observed close relationship between the NAO index and the Atlantic storm track intensity is confirmed by the distribution of correlation coefficients (**Fig. 24**), which reaches values of +0.7. The NAO pattern was examined by an EOF analyses of monthly mean SLP fields for 10-year periods with winter storm track activity over central Europe above / below one standard deviation. The positions of the northern centre was found to be rather insensitive with respect to the European storm track intensity, while the southern centres are much closer to the Azores region during intense storm track decades, and closer to gulf of Biscay for weak storm track decades.

In the ECHAM4+OPYC greenhouse gas scenario experiment, there is only a small systematic increase of the spatially fixed NAO index with respect to the control run. It is not before the end of the run that the quadratic curve fit emerges from the band of the control run's standard deviation. The number of winters, however, with index values exceeding the upper margin of the band is much larger towards the end than at the beginning of the run (**Fig. 25**).

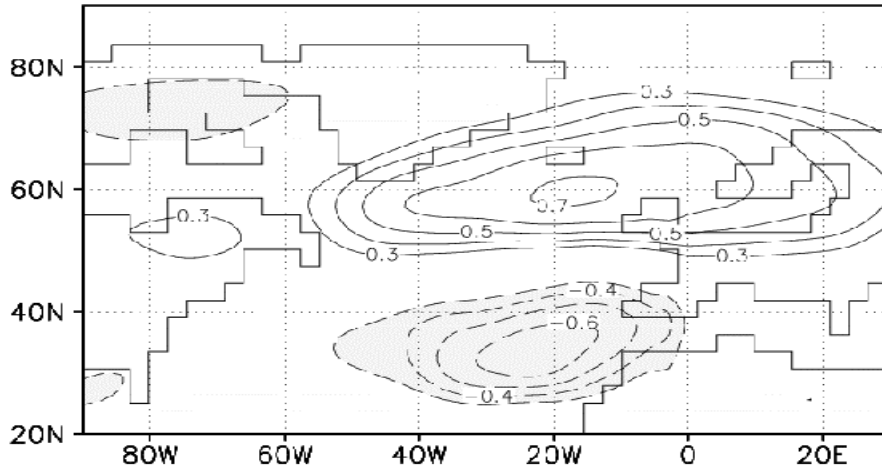


Figure 24: Distribution of correlation coefficients between the NAO index and the storm track for the ECHAM4+OPYC control run in winter (DJF). Contour interval is 0.1. Negative values below -0.3 are shaded. Absolute values of coefficients greater than 0.3 are statistically significant at the 99% confidence level.

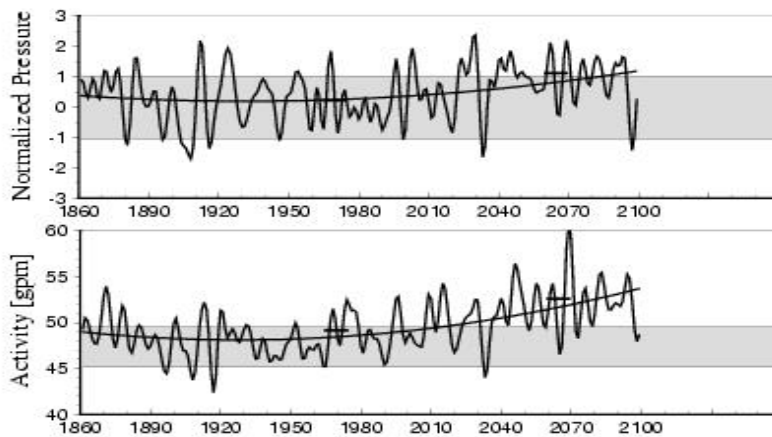
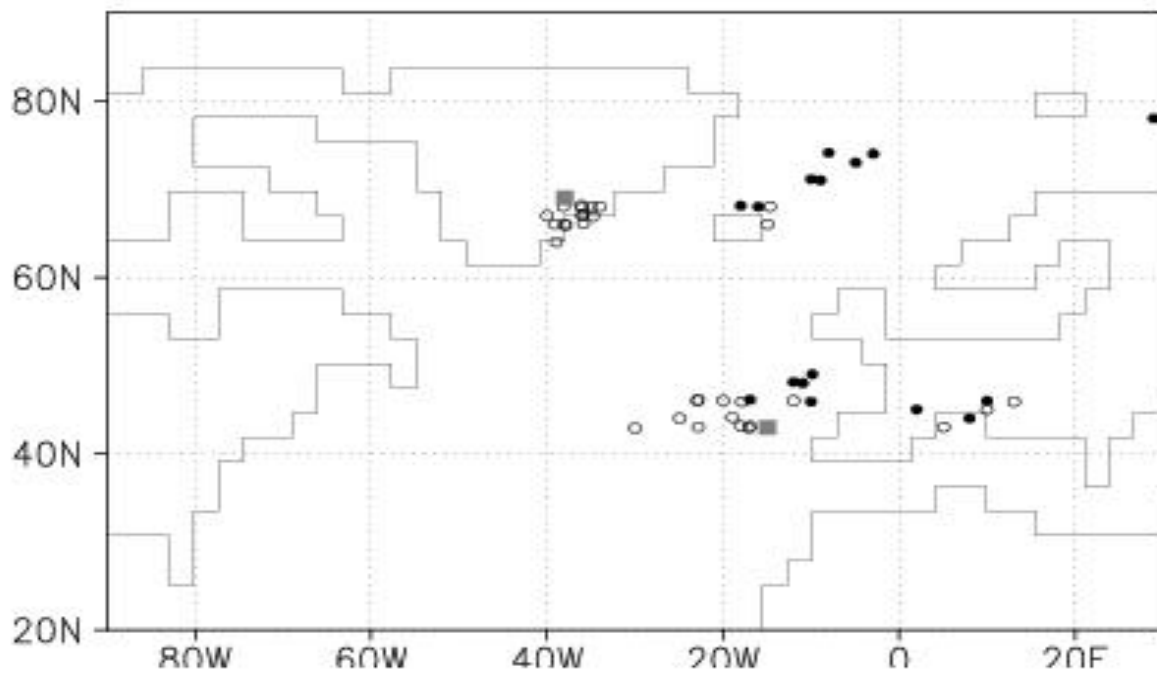


Figure 25: Top panel: Winter NAO index for the scenario run, computed using sea-level-pressure variances from the control run. Bottom panel: Storm track activity over northwestern Europe [60°W - 20°E, 40° - 70° N] in the scenario run in [gpm]. A 4-year low pass filter is applied for smoother display. The grey bands indicate the variability in the control run as measured by the standard deviation. The non-linear climate trends obtained from quadratic curve fitting are marked by the dashed lines.

The fact that the change of the NAO index with increasing greenhouse gas forcing is much less pronounced than that of the European storm track activity may be assigned to a change in the spatial characteristics of the NAO. Centres of variability produced from EOF analyses for 24 subsequent

10-year periods (each comprising 120 monthly means from the scenario run) are shown in **Fig. 26**. The subpolar centres from the first decades of the scenario run (with small to moderate forcing) are located closely to the centre determined for the entire control run, while those from the later decades (moderate to strong forcing exceeding  $3 \text{ W/m}^2$ , around year 2020) reveal a movement towards more easterly positions. Thus, consideration of a spatially fixed NAO index is inadequate for an appraisal of greenhouse gas induced changes



**Figure 26:** Locations of NAO centres as computed from EOF analyses of sea level pressure fields from the ECHAM4+OPYC scenario experiment. The mean positions in the entire control run (using winter means) are marked by grey squares, those of consecutive decades in the scenario run (using all individual months) are marked by open circles before year 2020 and by black dots thereafter.

### 3.4. Convective activity

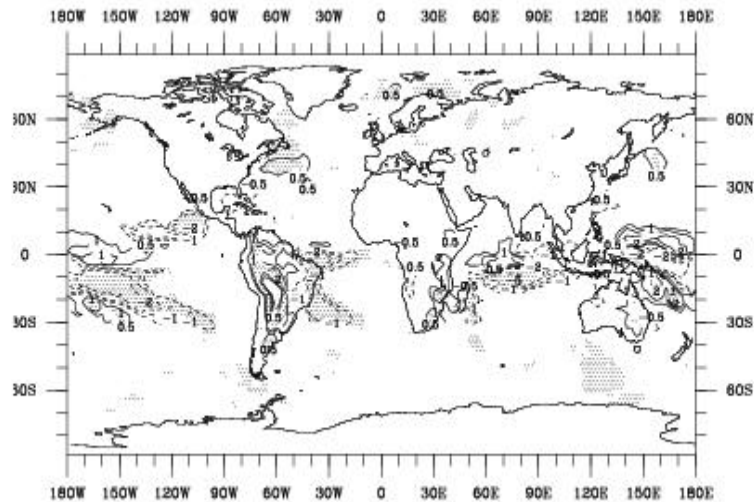


Figure 27: Change of mean convective rain rate [mm/day] in northern winter (DJF). Difference between decade 1981-90 and 2071-80 of the ECHAM4+OPYC scenario run. 99% significance level is shaded area.

It is expected that in a warmer climate the storm intensity increases due to higher sea surface temperatures and a larger amount of water vapour in the atmosphere. Recent studies indicate, at least for certain regions, an increase in storminess and cyclonic activity in a warmer climate (Lunkeit et al., 1996b). With respect to tropical cyclones Royer et al. (1998) found an increase of the total cyclogenesis frequency, but without extension of the area of possible cyclone genesis. We focus on changes in convective activity.

Data of convective and large-scale rain rates of the ECHAM4/OPYC model run IS92a for the 1981-90 decade and the 2071-80 decade (representing 1·CO<sub>2</sub> and 2·CO<sub>2</sub>-forcing, respectively) were analysed. The frequency distribution of convective rain rates and the precipitation intensity (categorised in severity classes) are estimated from daily mean values for the summer (JJA) and winter (DJF) season. In the tropics and subtropics, changes in convective (Fig. 27) and large-scale precipitation rate (not shown) from the 1·CO<sub>2</sub> to the 2·CO<sub>2</sub>-forcing period show similar patterns for both seasons considered. The difference patterns are characterised by shifts of local maxima and minima in regions of generally strong convective activity, in particular in the Western and Central Pacific and the Indian ocean. In the subtropics mainly a decrease of convective rain over sea can be identified, more pronounced on the southern hemisphere. The origin of these changes is not yet clear. However, local changes in sea surface temperature corresponding to the change patterns of the rain rate cannot be recognised. The increase of convective rain rates over land areas on the respective summer hemisphere can be attributed to the higher surface temperature in a warmer climate. In both seasons the global mean convective rain rate decreases by about 4-5 % resulting from a strong decrease of the frequency of deep convective events. Globally, for rain rates between 5 and 40 mm/day we found a decrease of both frequency and the respective mean daily rain rates. However, for convective rain rates larger than 40 mm/day both frequency and mean

daily rain rate increase indicating an increase of strong rain events.

### 3.5. High latitude processes

High latitude processes and their potential changes in a warming climate were investigated using

- a transient greenhouse gas forcing run using the HadCM3 model,
- and
- ten year „time-slice,, high resolution (1.1<sup>0</sup>, T106) GCM runs (Cubasch et al., 1995, Wild et al., 1997) for present day and for approximately doubled CO<sub>2</sub>-concentrations using the ECHAM model.

These latter experiments use prescribed boundary conditions of sea surface temperature and sea ice distribution predicted by lower resolution, transient coupled atmosphere-ocean scenario runs: The T106 (1.1<sup>0</sup>) version of the ECHAM4 model has been integrated using values from the transient ECHAM4 T42/OPYC scenario run; an analogous experiment was performed with the precursor model version ECHAM3 T106, using the boundary conditions from the ECHAM1/LSG scenario run (Ohmura et al. 1996a,b).

The high horizontal resolution is particularly well suited for investigations of the mass balance of the polar ice sheets due to the following two reasons:

- The precipitation distribution over the polar ice sheets is strongly dependent on the orographic forcing. The representation of orography improves considerably with higher resolution (cf. **Fig. 28**). Ohmura et al. (1996b) found a substantial improvement in precipitation over the polar ice sheets in the T106 simulations compared to lower resolution integrations with the same model.
- The ablation areas on the steep margins of the ice-sheets are much better resolved in higher resolution models, allowing for a more appropriate calculation of melt. The accurate calculation of melt in the high resolution ECHAM3 T106 model was documented in Ohmura et al. (1996a).

The accumulation calculated in ECHAM4 T106 under present day conditions integrated over both Greenland and Antarctica is in excellent agreement with observations: Over Antarctica 166 mm/y are simulated, while observational estimates cover the range from 147 to 184 mm/y (cf. Table 4 of Ohmura et al. 1996a and references therein). Over Greenland the simulated amount of 331 mm/y is very close to the observational estimate of 317 mm/y given in Ohmura et al. (1996a). Note that this quantity has improved compared to ECHAM3 T106. In HadCM3, the area-average solid precipitation over Greenland is 440 mm/y, about 30% larger than the estimates given in IPCC (1996). The geographical distribution is good, with the highest rates around the coasts, especially the south-east. In Antarctica area-average precipitation, which is practically all solid, amounts to 170 mm/y. Again, the distribution is good, although the coastal gradient is not as tight as it should be.

	<b>ECHAM3</b>	<b>ECHAM4</b>	<b>HadCM3</b>
<b>Greenland ice mass:</b>			
Accumulation change	-21	+92	+35
Ablation change	-208	-155	-111
Mass balance change	-229	-63	-77
<b>Greenland contribution to sea level change</b>	+1.13	+0.31	+0.43
<b>Antarctic ice mass:</b>			
Accumulation change	+23	+22	+16
Ablation change	0	0	-8
Mass balance change	+23	+22	+8
<b>Antarctic contribution to sea level change</b>	-0.90	-0.86	-0.29
<b>Net contribution of polar ice sheets to sea level change</b>	+0.23	-0.55	+0.14

**Table 5: Change in mass balance of the polar ice sheets and contribution to sea level changes as projected in 2\*CO<sub>2</sub>-scenarios: high resolution (T106) time-slice experiments with the ECHAM3 and ECHAM4, difference years 2050-2070 minus 1980-2000 in the HadCM3 GHG run. Units in mm/y.**

## GREENLAND MODEL TOPOGRAPHY

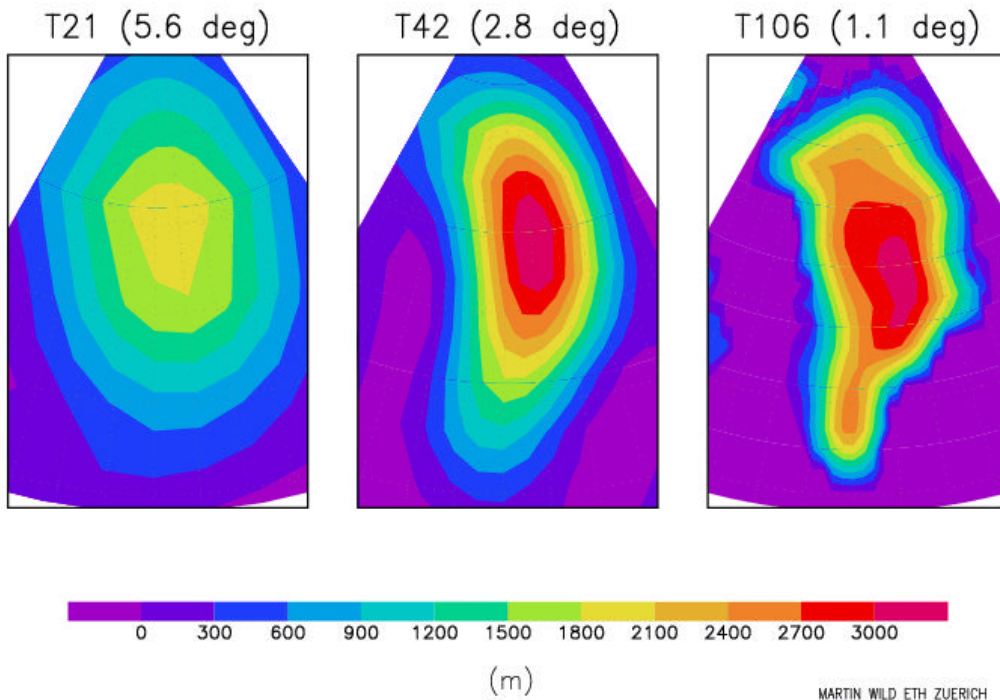


**Figure 28: Representation of the Greenland orography in models with various horizontal resolutions: T21 (5.6°), T42 (2.8°) and T106 (1.1°). Units m.**

In the ECHAM4 T106 2\*CO<sub>2</sub> scenario, the accumulation over Antarctica (**Fig. 29**) increases by 23 mm/y, an amount almost identical to the ECHAM3 scenario (22 mm/y), but about 50% higher than the HadCM3 value (see **Table 5**). Accumulation over Greenland in the ECHAM4 scenario increases by 92 mm/y. For the HadCM3 GHG scenario, the warmer climate in Greenland also leads to precipitation increases. These results are in contrast to the change predicted in the ECHAM3 scenario, which shows a decrease of 21 mm/y.

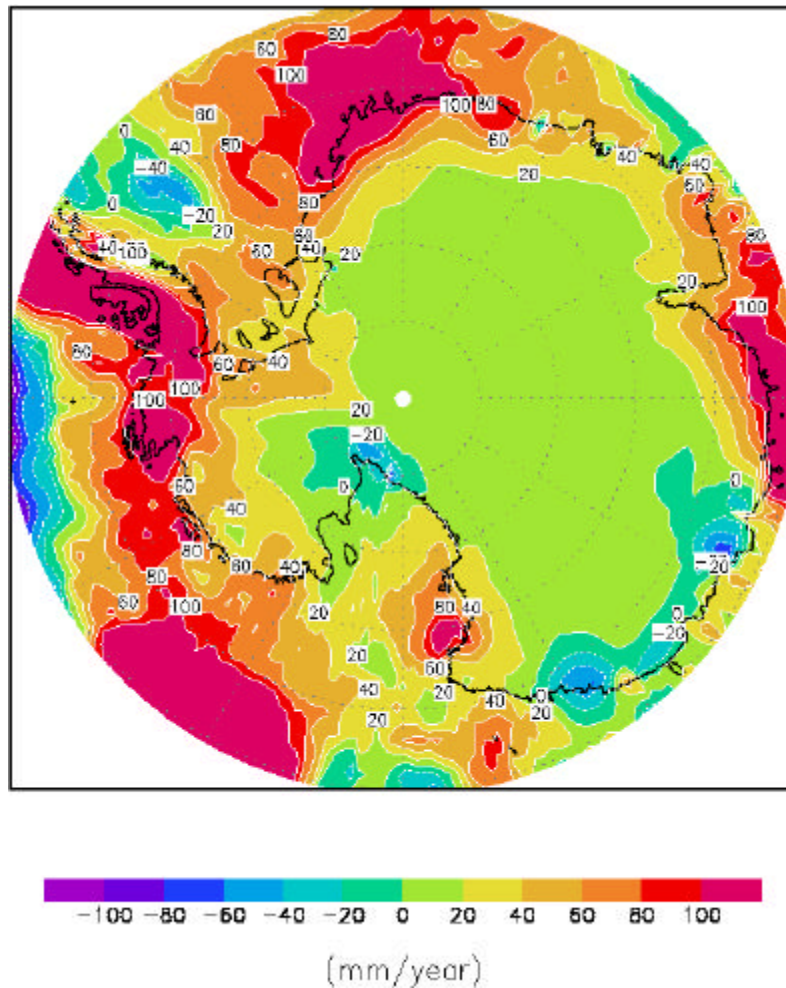


**Figure 29: Change in accumulation over Antarctica as projected in the 2\*CO<sub>2</sub> time-slice scenario with ECHAM4 T106. Units mm/y.**

Since ablation is not explicitly calculated in the ECHAM model, a linear relationship between summer temperature and ablation based on observations on Greenland (Ohmura et al. 1996a) has been used. Ablation deduced this way from ECHAM4 T106 for present day conditions in Greenland shows some biases caused by excessively warm ice sheet margins, which needs further investigation. Still, the projected change in ablation in the ECHAM4 2\*CO<sub>2</sub>-scenario is of a comparable magnitude to the ECHAM3 scenario (cf. **Table 5**). In HadCM3, the ablation over Greenland is also confined to coastal regions, and although the model resolution is not sufficient to resolve the ablation zone as it actually is, the area-average ablation is well simulated at 250 mm/y.

Temperatures over Antarctica are too low for significant melt both under present day and under scenario conditions in the ECHAM runs. The reason is that the -2<sup>0</sup>C isoline, which marks the lowest summer (DJF) temperature where ablation can occur (Ohmura et al. 1996a), does not reach the Antarctic ice sheet even under 2\*CO<sub>2</sub>-conditions. In contrast, the HadCM3 scenario produces an ablation increase amounting 50% of the simulated accumulation change.

The aforementioned changes towards the GHG scenario lead to a net mass loss of about 70 mm/y over Greenland in the ECHAM4 and HadCM3 scenarios. This is significantly less than in the ECHAM3 scenario. Over Antarctica, the mass balance increases by 23 mm/y in the ECHAM4

scenario, an amount almost identical to the ECHAM3 scenario, but 3 times the amount simulated by HadCM3.

There is no agreement about the net influence of glacier mass gain in Antarctica and mass loss in Greenland on sea level change between the different simulations. In the ECHAM3 and HadCM3 scenario experiments mass loss in Greenland and the mass gain in Antarctica are nearly compensated, while there is a negative influence on sea level in the ECHAM4 scenario. The disagreement between the results reflects the large uncertainties still present: For ECHAM4, the contribution from the Greenland ice sheet needs further investigation (accumulation changes and the calculation of ablation). In all models considered the mass balance is not closed over either ice-sheet due to the missing production of icebergs in the models. The contributions to sea level quoted in **Table 5** assume that there is no change in calving rates.

#### **4. Detection and Attribution of Climate Change**

In the previous project (Cubasch et al., 1997), an optimal detection method has been applied to detecting greenhouse gas-induced climate change in near surface temperature trends over 15, 20 and 30 years (Hegerl et al., 1996). This work has been updated applying an optimal fingerprint for greenhouse gas - plus-sulphate aerosol forced climate change from an average of two simulations with ECHAM3/LSG (Hegerl et al., 1997). Results indicated that the previously found very significant detection of climate change in 30-year annual mean trends of surface temperature was confirmed (**Fig. 30**). Additionally, a new attribution method (Hasselmann, 1997) has been applied to 50-year trend patterns of NH summer (JJA; Hegerl et al., 1997). The results indicate that while the observations are consistent with greenhouse gas and aerosol forced climate change, they disagree significantly from greenhouse gas only climate change and marginally from solar forced climate change (as simulated with ECHAM3/LSG; **Fig 31**). The results further suggest that the unusually strong global mean warming in the middle of this century may have been influenced by an early greenhouse gas response, and possibly also by a solar irradiance increase (Cubasch et al., 1997).

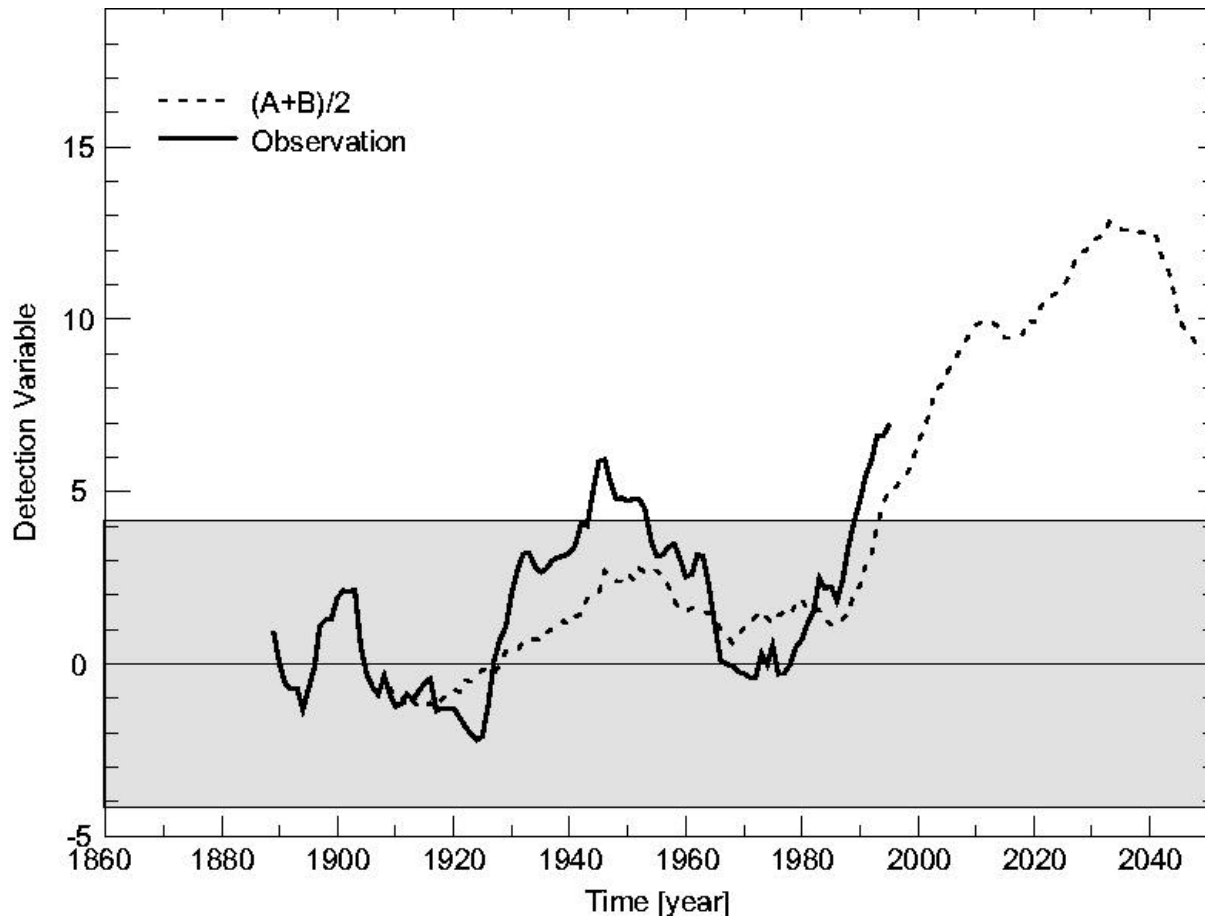


Figure 30: Evolution of the detection variable (computed with the optimal fingerprint for greenhouse gas-plus sulphate aerosol forced climate change) for 30-year trend patterns from the observations, and the average  $(A+B)/2$  of the simulations A and B. The time refers to the final year of the 30-year interval used to compute the trend pattern. A 95% confidence intervals derived from the largest interval computed from four sets of variability data is also indicated. For the present one-tailed test (the signal is known to be positive) the positive confidence limit corresponds to the 97.5% significance level. The recent observed trends exceed this limit, indicating that they represent a significant climate change at the 97.5% confidence level.

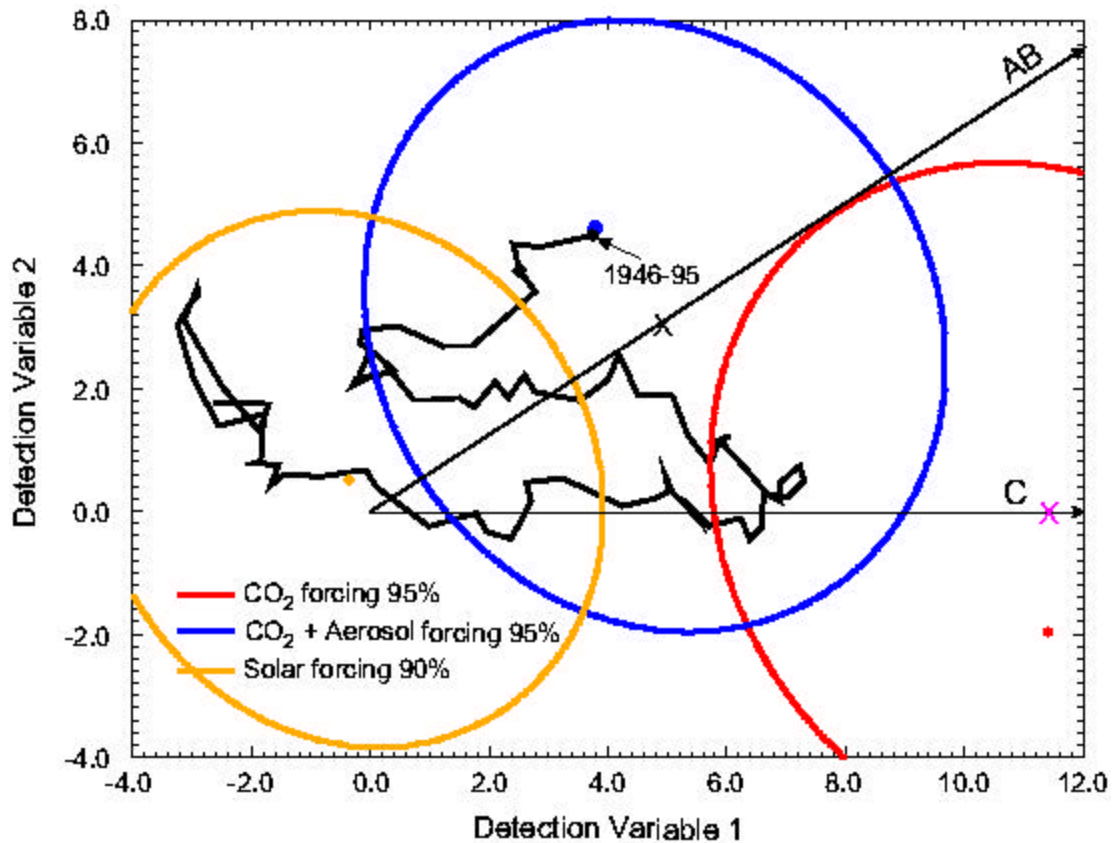


Figure 31: Attribution diagram for observed 50-year northern summer surface temperature trends. The evolution path of the observed detection vector in phase space is indicated by the black line, the latest trend for the period 1946-1995 being represented by a large black dot. The corresponding model predictions and associated 90% confidence ellipses for the difference between the observed and predicted detection vectors are also shown for the three different forcing mechanisms. For the model simulations used to compute the basic signal patterns of the phase space, the confidence ellipses are centred on a projection (denoted by X) of the model values for the trend period 1946-1995 (indicated by an appropriately coloured dot) onto the respective pattern direction, since the noise-free model climate change signal should lie in this direction. The detection variable for the latest observed 50-year trend lies inside the confidence ellipse for the combined forcing signal, but outside the confidence ellipse of the greenhouse gas only signal. The observed trend ending in 1992 is also marginally inconsistent with the respective trend of the solar simulation (black diamond). Thus the observations are inconsistent (at a 90% confidence level) with a pure greenhouse gas or solar forced climate change signal but consistent with a greenhouse gas-plus-aerosol climate change signal.

However, these results rely upon estimates of natural climate variability on timescales of several decades, which are obtained from several multi-century control simulations with different coupled climate models (a 1000 year simulation with the GFDL model, a 1200 simulation with the UKMO model HADCM2 model and an 800 year simulation with a version of the MPI model ECHAM3/LSG) and from observations (Stouffer et al., 1998). The variability of these control simulations has been intercompared. The results show broad scale agreement, but also some level of differences. The HADCM2 model (which has finer resolution than both other, older modes) exhibits over most time scales and spatial structures the largest variability. The ECHAM3/LSG variability of global mean temperature is smaller than that of the GFDL model, but ECHAM3/LSG exhibits larger naturally occurring hemispheric temperature asymmetry. While the strongest contribution to interannual global mean temperature fluctuations in the HADCM2 model comes from tropical Pacific variability, the largest contribution in both other models comes from patterns

exhibiting simultaneous warming of the Northern Hemispheric large land masses, which has been previously found in observations. Additionally, a revised estimate of natural variability has been derived from the observations after subtraction of an estimated anthropogenic climate change signal (Jones and Hegerl, 1998).

The effect of GCM uncertainty on the detection of climate change has been assessed by a pilot study using AMIP-simulations (Barnett et al., 1998). The study applied an estimate of model error by applying the difference between AMP-type atmospheric model simulations and observations. Note that these differences contain both atmospheric internal variability and model error. Furthermore, several approaches for optimal detection of anthropogenic climate change have been intercompared and have been found to be mathematically identical (Hegerl and North, 1997). The different approaches, however, show how optimal fingerprint detection can also be interpreted as optimal averaging and applying an optimal filter to the detection of climate change.

#### 4.1. Fingerprint analysis

Further studies attempting detection and attribution of climate change have been performed at Hadley Centre. As several previous studies, „fingerprinting“ was used to detect climate change (e.g. Stouffer et al. 1994; Hegerl et al. 1996; Santer et al. 1996). In this method an expected signal of climate change („fingerprint,“), due to some forcing, is compared with observations of climate change. If the match is better than expected by chance then detection is claimed. If no other plausible cause could lead to such a signal then the climate change is attributed to that forcing.

A fingerprinting strategy has four components:

1. Fingerprints of possible climate changes. Normally these are taken from simulations of climate models in which the model is given different forcing agents. At the Hadley Centre these fingerprints were generated from ensembles of coupled simulations, over the historical period, using historical forcings and the coupled model HadCM2 (Johns et al. 1997)
2. Observations.
3. Methods of comparison between the fingerprints and the observations.
4. Estimates of internal variability.

In the studies reported here all estimates of internal variability have been taken from a 1000+ year coupled control simulation of HadCM2 (Johns et al. 1997; Tett et al. 1997). On timescales less than a decade the influence of external forcings is likely to be small compared to the internal variability. On annual to decadal timescales the surface temperature variability of HadCM2 compares well with observations (Tett et al. 1997). The power spectrum of the global mean temperature is at least as large as that observed on scales less than 20 years.

Karoly et al. (1994) claimed that the effect of greenhouse gases on the free atmosphere is to warm the troposphere and to cool the stratosphere. Such a fingerprint is a good candidate for determining whether or not there is an anthropogenic CO<sub>2</sub> -effect on climate. To see how well the model-simulated climate change due to different forcings agrees with reality three ensembles, each of four simulations, were carried out using HadCM2 (Tett et al. 1996). The ensembles were forced with historical changes in greenhouse gases, sulphate aerosols and stratospheric ozone depletion. The results of the simulations were compared (**Fig. 32**) with an observational radiosonde dataset of temperature changes throughout the atmosphere (Parker et al., 1997). The simulations were compared using correlation and congruence statistics (Tett et al., 1996). The results of the study were that, on balance, agreement between the simulations and observations is best for a combination of greenhouse gas, aerosol and ozone forcing. Uncertainties remain due to imperfect knowledge of radiative forcing, natural climate variability, and errors in observations and model

response.

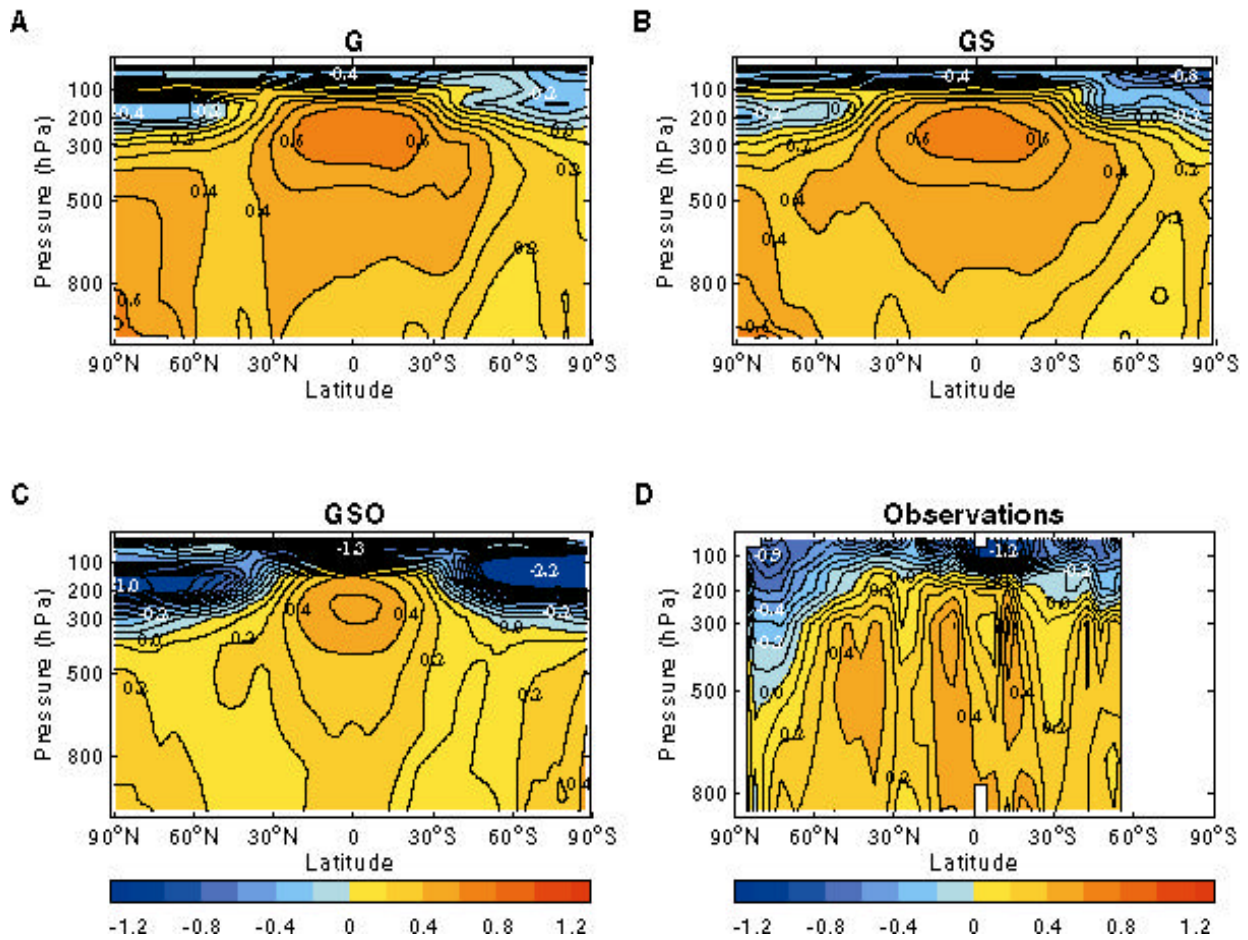


**Figure 32:** Simulated and observed zonal-mean temperature changes (contour interval of 0.1 K) between the decadal 1986-95 mean and the 20-year 1961-80 mean. G - Greenhouse gases alone, GS - Greenhouse gases and Sulphate aerosols, GSO Greenhouse gases, sulphate aerosols and stratospheric ozone.

Work by Allen and Tett (1998) has extended this study using an optimal detection algorithm to show that both the effect of greenhouse gases and stratospheric ozone depletion can be detected. However Gillet et al. (1998) show that there may be problems with the simulation of stratospheric variability in HadCM2.

An investigation was conducted into the spatial and temporal scales on which it is possible to detect a significant change in climate at present, taking into account the climatic effects of greenhouse gases and sulphate aerosols (Stott and Tett, 1998). The simulated response fingerprint was projected onto the observations and compared with the projection of the fingerprints onto the internal climate variability simulated by HadCM2. No significant change was found on timescales of 10 years. For trends of length 30 years only the global mean change was found to be significant. Only for trends of 50 years were significant sub-global scale changes found and even so the changes are only significant for spatial scales greater than 5,000 km.

## 4.2. Causes of twentieth century temperature change:

Observations of near-surface temperature show a global-mean warming of approximately 0.6 K since 1900 (Parker et al., 1994), consistent with proxy evidence suggesting that this century has been unusually warm (Mann et al. 1998). This warming occurred between 1910-1940 and since 1970. To investigate the probable causes of these temperature changes we used results from four HadCM2 ensembles, each of four simulations. The ensembles in this case were:

**G:** Changes in well mixed greenhouse gases from 1860-1995. (Mitchell et al. 1995; Johns et al. 1997; Mitchell and Johns 1997),

**GS:** As G but with changes in surface albedo representing the effects of anthropogenic sulphate aerosols from 1860-1995 (Mitchell et al. 1995; Johns et al. 1997; Mitchell and Johns 1997),

**VOL:** Changes in stratospheric volcanic aerosols from 1850-1995 using an updated version of a previously published timeseries (Sato et al. 1993),

**SOL:** Changes in total solar irradiance from 1700-1995 using a timeseries of solar irradiance variations (Hoyt and Schatten 1993) for the 1700-1991 period based on proxy data and extended to 1995 using satellite observations (Willson, 1997).

Five 50-year segments of data (1905-1955, 1915-1965, 1925-1975, 1935-1985 and 1945-1995) were considered. In each segment the amplitude of the simulated spatio-temporal signals in the observational record of near surface temperature changes were estimated using an „optimal fingerprinting,, algorithm (Hasselmann, 1993, 1997; North et al. 1995; Allen and Tett 1998), a form of multivariate regression. Because of signal degeneracy, no more than two signals could be considered simultaneously in the analysis. Internal variability alone could explain neither the early century warming (1905-1955 and 1915-1965) nor the late century warming (1945-1995). Furthermore, no combination of only natural signals could explain the warming since 1945 - the period when the observational coverage is best. As no restriction was placed on the amplitudes of the simulated signals this result holds even if HadCM2 is missing an important mechanism or feedback affecting the amplitude of the climate response to solar (e.g. ozone amplification of solar irradiance changes (Haigh, 1996, 1994) or volcanic activity.

Of the possible combinations of signals that were considered, only two combinations were satisfactory explanations for temperature changes over the entire century: G vs GS (or GHG vs SUL) and GS vs. Sol, i.e. a combination of greenhouse gases and sulphate aerosol signal, or greenhouse gas plus sulphate aerosol signal plus solar variations. Having estimated the amplitude of the simulated signals in the observations they were then used to reconstruct the contributions to global mean temperature in two periods of significant change during the century. The results suggest that the recent warming can be explained by the climatic response to anthropogenic changes in greenhouse gas concentrations partly offset by cooling due to anthropogenic sulphate aerosols which results in little net temperature change from 1945 to 1975. They also show that the early century warming can also be explained by anthropogenic causes and internal variability. However, solar irradiance changes could have made a significant contribution if there were no error in the relative forcing by sulphates and greenhouse gases as prescribed in HadCM2.

## 5. Summary and conclusions

Climate responses under various anthropogenic and natural forcing scenarios have been studied and intercompared with several independent models and with different experimental strategies.

One strategy, which has been used, are the scenario calculations. Here an increase with time of the greenhouse gases according to an idealised (typically 1% greenhouse gas increase) or an IPCC scenario (scenario A 1990 or IS92 a) have been used to force the models:

The model simulated patterns of temperature and precipitation responses to increases in the greenhouse gas concentration are related to the model feedbacks, and therefore differ in detail between models. Nevertheless, some broad features of the responses; amplification of warming in high latitudes, marked land-sea contrast with land warming more than the ocean surface, and intensified hydrological cycle (more evaporation and rainfall, with largest increases in the Tropics); are common to all models.

The models produce a 10-15% increase of winter storm track activity over the north-western Europe at the time of CO<sub>2</sub>-doubling. Comparing these results with previous simulations for anthropogenic climate change (Cubasch et al., 1997), the increase of upper air storm track activity over Northern Europe is a common signal, while the amount of this change is variable and in many cases the statistical significance is comparatively low (90-95% level). This effect may be assigned to the low frequency variability in the models.

Depending on the exact choice of a relatively short averaging periods (e.g., 10 winters) out of this run very large or small estimates of a greenhouse gas induced increase of storm-activity can be produced. The longer timescale, however, clearly indicates the dominance of a long term trend. This is further elucidated by a global EOF analysis of the bandpass filtered geopotential heights over the boreal winters. The principal component (PC) associated with the first EOF reveals a non-linear trend closely following the anthropogenic greenhouse gas forcing function of the run. While there are also large contributions of the EOF over the Southern Hemisphere, one particular change suggested by the EOF is the increase of storm track intensities over the eastern North Atlantic and Europe. The resemblance between the time series of storm track activity averaged over Europe and the first PC of the global storm track suggests that storm track intensification over Europe is indeed a stable feature of anthropogenic climate change.

The increase in storm track activity is caused by an increasing baroclinicity over the entire north-east Atlantic (estimated by the maximum Eady growth rates) with main changes occurring in the upper troposphere. In a warmer climate increases in storm intensity is due to a larger amount of water vapour in the atmosphere, as an analysis of the role of diabatic processes in supplying energy within baroclinic waves by calculating covariances of the transient diabatic heating and temperatures has shown. The conversion of this energy due to warm air rising and cold air sinking leads to an enhancement of the kinetic energy of the storm systems.

The observed close relationship between the NAO index and the Atlantic storm track intensity is confirmed in the model simulations by the distribution of correlation. The positions of the northern centre was found to be rather insensitive with respect to the European storm track intensity, while the southern centres are much closer to the Azores region during intense storm track decades, and closer to gulf of Biscay for weak storm track decades.

The fact that the change of the NAO index with increasing greenhouse gas forcing is much less pronounced than that of the European storm track activity may be assigned to a change in the spatial characteristics of the NAO. Centres of variability in the subpolar regions from the first decades of a scenario run (with small to moderate forcing) are located closely to the centre determined for the entire control run, while those from the later decades reveal a movement towards more easterly positions. Thus, consideration of a spatially fixed NAO index is inadequate for an appraisal of greenhouse gas induced changes.

The frequency distribution of convective rain rates and the precipitation intensity (categorised in severity classes) are estimated from daily mean values for the summer (JJA) and winter (DJF)

season. In the tropics and subtropics, changes in convective and large-scale precipitation rate from the 1\*CO<sub>2</sub> to the 2\*CO<sub>2</sub>-forcing period show similar patterns for both seasons considered. The difference patterns are characterised by shifts of local maxima and minima in regions of generally strong convective activity, in particular in the Western and Central Pacific and the Indian ocean. In the subtropics mainly a decrease of convective rain over sea can be identified, more pronounced on the southern hemisphere. The origin of these changes is not yet clear. Local changes in sea surface temperature corresponding to the change patterns of the rain rate cannot be recognised. The increase of convective rain rates over land areas on the respective summer hemisphere can be attributed to the higher surface temperature in a warmer climate. In both seasons the global mean convective rain rate decreases by about 4-5 % resulting from a strong decrease of the frequency of deep convective events. Globally, for rain rates between 5 and 40 mm/day a decrease of both frequency and the respective mean daily rain rates is found. However, for convective rain rates larger than 40 mm/day both frequency and mean daily rain rate increase indicating an increase of strong rain events.

There is no agreement about the net influence of glacier mass gain in Antarctica and mass loss in Greenland on sea level change between the different simulations. The disagreement between the results reflects the large uncertainties still present: In all models considered the mass balance is not closed over either ice-sheet due to the missing production of icebergs in the models.

Another strategy is followed in the stabilisation experiments: Anticipating an eventual stabilisation of the greenhouse gas concentration in the atmosphere, a set of experiments has been run where the greenhouse gas concentration is increased until it has doubled or quadrupled and then kept constant. Common to all these stabilising experiments is a strong warming during the years, while the greenhouse gas concentration is still increasing, followed by a weaker, but still considerable, warming during the period with fixed concentrations. This warming continues to the end of the long simulations (i.e. in one case even 850 years).

This continuing slow increase is due to adjustment processes of the ocean. For instance, in one of the simulations, the temperature increase in the deep ocean is much stronger during the last hundred years (751-850) than in the first century. The long-term adjustment is also visible in the sea-level change due to thermal expansion. After 850 years the sea level has risen for more than 75 cm in the CO<sub>2</sub>-doubling case and more than 150 cm in the CO<sub>2</sub>-quadrupling case. Due to the large heat capacity of the deep ocean the changes are still strong at the final century of the experiments (5 cm/century in the CO<sub>2</sub>-doubling run and 12 cm/century in the CO<sub>2</sub>-quadrupling run).

The overturning circulation weakens during the first 100 years of these experiments by 15% to 20%. In these runs the intensity slowly recovers after reaching the minimum, once the greenhouse gas concentration has stabilised. In the CO<sub>2</sub>-quadrupling experiments the reduction is so strong that at the end of the runs even after the recovery the intensity is still significantly weaker than in the control simulation. Nevertheless, in the quadrupling experiments an Atlantic conveyor belt-type overturning circulation pattern is present throughout the full simulation period. This is in contrast to a corresponding CO<sub>2</sub>-quadrupling experiment of Manabe and Stouffer (1994) where the thermohaline circulation totally collapses.

In order to find out, what causes this reduction, a set of sensitivity experiments has been performed, in which either the freshwater and/or momentum fluxes were no longer simulated, but prescribed according to one of the fully coupled baseline experiments. This approach gives a direct estimate of the contribution from the individual flux components. The direct effect of surface warming and the associated feedbacks in ocean circulation are the dominant processes in weakening the Atlantic thermohaline circulation in the model. The relative contribution of momentum and freshwater fluxes

to the total response turned out to be less than 25%.

One key element of this study was to investigate, to what extent man-kind has already influenced the climate and to what extent the changes which are seen, are just indicators of natural variability. If one just studies global mean quantities, a 2D-model offers itself as sensible tool:

The response of such a model to the combination of all, i. e. natural and anthropogenic forcings suggests that the observed temperature trends are the result of a subtle combination between naturally driven climate fluctuations and effects of industrialisation. As an example, the warming trend 1920-1940 which coincides with a warm stage of a Gleissberg cycle (an 80- to 90-year quasi-periodic variation in sunspot number and other solar indices) and with the lack of large volcanic events after the Katmai eruption (Alaska) in 1912 is strengthened by industrialisation in Western Europe and the US. The period of relatively low volcanic activity holds until the Agung eruption (Bali) in 1963. This resurgence of volcanic activity combined with a decreasing solar output allows to offset and overcome the greenhouse warming signal (partly counteracted by sulphate aerosols) during a few years. The rapid warming after 1970 appears to be the response to accelerated greenhouse warming and a slower rate of increase in cooling from sulphate aerosols. This last period is clearly dominated by the greenhouse warming which seems to be the largest climate forcing except for short time periods linked with volcanic events like El Chichon (Mexico, 1982) or Pinatubo (Philippines, 1991). Therefore, it seems impossible to simulate the 20th century climate warming without the inclusion of the greenhouse-gas releases connected to human activities, unless this warming is due to the internally driven natural variability of the climate system.

With the coupled OAGCMs it is possible, to use also the horizontal and vertical structure of the response to an increase in greenhouse gases to analyse this problem:

First results indicate that the previously found very significant detection of climate change in 30-year annual mean trends of surface temperature can be confirmed. Additionally, a new attribution method (Hasselmann, 1997) has been applied to 50-year trend patterns of NH summer (JJA; Hegerl et al., 1997). The results indicate that while the observations are consistent with greenhouse gas and aerosol forced climate change, they disagree significantly from greenhouse gas only climate change and marginally from solar forced climate change. No significant change was found on timescales of 10 years. For trends of length 30 years only the global mean change was found to be significant. Only for trends of 50 years were significant sub-global scale changes found and even so the changes are only significant for spatial scales greater than 5,000 km. The results further suggest that the unusually strong global mean warming in the middle of this century may have been influenced by an early greenhouse gas response, and possibly also by a solar irradiance increase (Cubasch et al., 1997).

On the whole, the diversity of the models employed to perform the studies in this project adds confidence to the results.

## **6. Exploitation of model results**

Results from some of the coupled models discussed here formed an integral part of the IPCC 1995 scientific assessment report (Houghton et al., 1996), and in particular were an important strand in the scientific evidence behind the main conclusion of 'a discernible human influence' on climate.

Dissemination of data continues from the UKMO (Hadley Centre) and DKRZ models to other scientists, particularly impacts researchers, both within Europe and world-wide. This activity is being further co-ordinated and strengthened by the IPCC-based Data Distribution Centre, built on

Web-sites at DKRZ and the University of East Anglia Link project. The DDC already has databases for several of the models in SIDDACLICH, as well as several other qualifying models from around the world, and more model data (e.g. HadCM3) will be added in due course.

Most coupled models (or preliminary versions) developed and run under SIDDACLICH have also been submitted to the CMIP 1 and CMIP 2 Coupled Model Intercomparison Projects co-ordinated by PCMDI at Lawrence Livermore (<http://www-pcmdi.llnl.gov/cmip/>). Only preliminary analysis has been performed on the control runs and idealised scenario runs so far, but it is expected that a range of future diagnostic projects will make use of more of the data over the next several years. It is hoped that CMIP projects will eventually feed back information of relevance to improving the basic simulations and climate sensitivities.

Political negotiations under the auspices of the United Nations Framework Convention on Climate Change (UNFCCC) have also been informed directly by recent climate change modelling work sponsored partly by the SIDDACLICH contract, through IPCC reports and other means. For example, presentations and reports were prepared for the Third and Fourth Conferences of the Parties to the UNFCCC (cop Kyoto December 1997; cop Buenos Aires November 1998) by the Hadley Centre (1997, 1998), in which recent model-generated climate change scenarios were assessed both in terms of global climate changes and their implied impacts. Conclusions concerning the probable fingerprint of anthropogenic climate change; the likelihood of significant ongoing sea level rise for many centuries into the future even after stabilising GHGs; and local impacts on water resources, ecosystems and agriculture, including the possibility of dramatic die-back of Amazonian forests after 2050 seen in the latest HadCM3 business-as-usual scenario; have been particularly relevant to these discussions.

## 7. References

\* - published during and partly sponsored by SIDDACLICH

\*Airey, M.J., Hulme, M. and Johns, T.C., 1996: Evaluation of simulations of terrestrial precipitation in the UK Met Office/Hadley centre climate change experiments. *Geophys. Res. Lett.*, 23, 1657-1660.

Allen, M.R. and S.F.B.Tett, 1998; Checking for model consistency in optimal fingerprinting. *Climate Dynamics* (submitted)

Appenzeller, C., Stocker, T. F. and Anklin, M. 1998: North Atlantic Oscillation dynamics recorded in Greenland ice cores, *Science*, conditional accepted.

Barnett T., Hegerl G. C., Santer B. D. and Taylor K. (1998): The potential effect of GCM uncertainties and internal atmospheric variability on anthropogenic signal detection. *J. Climate*, 11: 659-675.

\*Barthelet, P., S. Bony, P. Braconnot, A. Braun, D. Cariolle, E. Cohen-Solal, J-L. Dufresne, P. Delecluse, M. Deque, L. Fairhead, M. Filiberti, M. Forichon, J. Grandpeix, E. Guilyardi, M. Houssais, M. Imbard, H. Le Treut, C. Levy, Z. Li, G. Madec, P. Marquet, O. Marti, S. Planton, L. Terray, O. Thual, and S. Valcke, 1998. Simulations couplées globales des changements climatiques associés à une augmentation de la teneur atmosphérique en CO<sub>2</sub>. *C. R. Acad. Sci. Paris*, 326: 677-684.

\* Barthelet, P., L. Terray, and S. Valcke, 1998. Transient CO<sub>2</sub> experiment using the ARPEGE/OPAICE non flux corrected coupled model. *Geophys. Res. Lett.*, 25, 2277-2280.

Berger, A., 1978. Long-term variations of daily insolation and Quaternary climatic changes. *J. Atmos. Sci.*, 35: 2362-2367.

Blackmon, M.L., 1976: A climatological spectral study of the 500 mb geopotential height of the Northern Hemisphere. *J. Atmos. Sci.*, 33, 1607-1623.

Campin J.M., 1997. Modélisation tridimensionnelle de la circulation générale océanique lors du dernier maximum glaciaire. *PhD Thesis*, Université catholique de Louvain, Louvain-la-Neuve, Belgium, 342pp.

- Campin J.M., and H. Goosse, 1999. Parameterization of density-driven downsloping flow for a coarse-resolution ocean model in z-coordinate. *Tellus*, 51A, pp. 412-430.
- \*Carnell, R.E., C.A. Senior, and J.F.B. Mitchell, 1996: An assessment of measures of storminess: simulated changes in northern hemisphere winter due to increasing CO<sub>2</sub>. *Climate Dynamics*, 12, 467-476.
- \*Carnell RE and Senior CA (1998): Changes in mid-latitude variability due to increasing greenhouse gases and sulfate aerosols. *Clim Dyn* 14: 369-383
- Cox, P., R. Betts, C. Bunton, R. Essery, P.R. Rowntree, and J. Smith, 1998; The impact of new land surface physics on the GCM simulation of climate and climate sensitivity. *Climate Dynamics* (to appear).
- \*Christoph, M., U. Ulbrich, and U. Haak, 1995: Faster determination of the intraseasonal variability of storm tracks using Murakami's recursive filter. *Mon. Wea. Rev.*, 123, 578 - 581.
- Cubasch, U., K. Hasselmann, H. Hoeck, E. Maier-Reimer, U. Mikolajewicz, B. D. Santer and R. Sausen, 1992: Time-dependent greenhouse warming computations with a coupled ocean-atmosphere model; *Climate Dynamics*, 8, 55-69.
- \*Cubasch, U., Waszkewitz J., Hegerl G.C., and Perlwitz J., 1995: Regional climate changes as simulated in time-slice experiments. *Climatic Change*, 31, 273-304.
- Cubasch, U. (ed.), J.-Y. Caneill, M.A. Filiberti, G. Hegerl, T.C. Johns, A. Keen, S. Parey, O. Thual, U. Ulbrich, R. Voss, J. Waszkewitz, M. Wild, J.P. van Ypersele, 1997: Anthropogenic climate change. Project No. EV5V-CT92-0123 final report. Office for Official Publications of the European Commission No. EUR 17466EN Luxembourg, ISBN92-827-9728-7, 73 pp.
- Cusack S., A. Slingo, J.M. Edwards, and M. Wild, 1998; The radiative impact of a simple aerosol climatology on the Hadley Centre GCM. *QJR Meteor. Soc.* (to appear).
- Da Silva, A. M., C.C. Young and S. Levitus, 1995: Atlas of surface marine data 1994, US Dept. of Commerce, NOAA, NESDIS
- Delecluse P., G. Madec, M. Imbard and C. Levy, 1993. OPA version 7, Ocean General Circulation Model reference manual. *LODYC internal report 93/05*.
- Deleersnijder E., J.P. van Ypersele and J.M. Campin, 1993. An orthogonal curvilinear coordinate system for a World Ocean model. *Ocean Modelling*, 100, pp. 7-10 (+ figures).
- \* Delobbe, L., C. Tricot, and J.-P. van Ypersele, 1997: Tropopause-height feedback and radiative forcing in 2D climate simulations. *Atmosfera*, 10, 75-99
- \* de Montety, A., T. Fichet, and C. Poncin, 1998: Impact of the horizontal grid in an atmospheric model. *Ann. Geophysicae, Part II: Hydrology, Oceans, and Atmosphere, Supplement II to volume 16*, C643.
- Déqué M., Devreton C., Braun A. and D. Cariolle, 1994. The ARPEGE/IFS atmosphere model: a contribution to the French Community Climate Modelling. *Climate Dynamics*, 10, pp. 249-266.
- Ducoudré N.I., Laval K. and A. Perrier, 1993. Sechiba, a new set of parameterizations of the hydrologic exchanges at the land/atmosphere interface within the lmd atmospheric general circulation model. *J. Climate*, 6, pp. 248-273.
- Edwards, J.M. and A. Slingo, 1996; Studies with a flexible new radiation code. I: Choosing a configuration for a large scale model. *QJR Meteor. Soc.*, 122: 689-719.
- Fichet Th., Tricot, Ch., 1992. Influence of the starting date of model integration on projections of greenhouse-gas-induced climatic change. *Geophys. Res. Letters*, vol. 19 n°17, pp. 1771-1774.
- Fichet, Th., 1995. Solar radiation and global climate change: some experiments with a two-dimensional climate model. In: Solar output and climate during the Holocene, B. Frenzel (ed.), Gustav Fischer Verlag, Stuttgart New York, vol. 16, pp. 161-184, Special issue: ESF Project, European Palaeoclimate and Man 11.

- \* Fichefet, T., C. Poncin, and H. Grenier, 1997: A coupled atmosphere–ocean general circulation model for climate studies. *Ann. Geophysicae, Part II: Hydrology, Oceans, Atmosphere and Nonlinear Geophysics, Supplement II to volume 15*, C496.
- Fichefet T. and M.A. Morales Maqueda, 1997. Sensitivity of a global sea ice model to the treatment of ice thermodynamics and dynamics. *J. Geophys. Res.*, 102, pp. 12609-12646.
- \* Fichefet, T., H. Goosse, and M. A. Morales Maqueda, 1998: On the large-scale modeling of sea ice and sea ice-ocean interactions. In *Ocean Modeling and Parameterization*, E. P. Chassignet and J. Verron (eds.), Kluwer Academic Publishers, The Netherlands, p. 399-422.
- Filiberti M.A., Dufresne J.L., Houssais M.N., M. Imbard, and G. Madec, 1997: Some aspects of the thermodynamic ice-ocean interaction in a global OGCM. European Geophysical Society, XXII General Assembly, Vienna, Austria.
- \*Filiberti, M. A., Dufresne, J. L., Grandpeix J. Y., 1999: The IGLOO sea-ice model, IPSL technical note, 30pp.
- Fouquart Y. and B. Bonnel, 1980 : Computations of solar heating of the Earth's atmosphere: a new parameterization. *Beitr. Phys. Atmos.*, 53, pp. 35-62.
- Frey, H., M. Latif and T. Stockdale, 1997: The coupled GCM ECHO-2. Part I: The tropical Pacific. *Mon. Wea. Rev.*, 125, 703-720.
- Gallée H., van Ypersele J.P., Fichefet Th., Tricot Ch., Berger A., 1991. Simulation of the last glacial cycle by a coupled sectorially, averaged climate-ice-sheet model. I. The Climate Model. *J. Geophys. Res.*, 96, pp. 13,139-13,161.
- Gent, P.R. and J.C.McWilliams, 1990. Isopycnal mixing in ocean circulation models. *J. Phys.Oceanogr.* 20: 150-155.
- Glowienka-Hense, R., 1990: the North Atlantic Oscillation in the Atlantic-European SLP. *Tellus*, 42A, 497-507.
- Goosse H., Campin J.M., Fichefet T., and E. Deleersnijder, 1997a. Sensitivity of a global ice-ocean model to the Bering Strait throughflow. *Clim. Dyn.*, 13, pp. 349-358.
- \* Goosse H., Campin J.M., Fichefet T. and E. Deleersnijder, 1997b. Impact of sea-ice formation on the properties of Antarctic bottom water. *Annals of Glaciology*, 25, pp. 276-281.
- \* Goosse, H., T. Fichefet, and B. Tartinville, 1998. Simulation de la Polynie de la mer de Ross dans un modèle à grande échelle. In *Convection - cryosphere*. Proceedings of the Atelier de modélisation de l'atmosphère 1998, Toulouse, 8-9 December 1998, p. 174-177.
- \* Goosse, H., and T. Fichefet, 1999. Importance of ice-ocean interactions for the global ocean circulation: a model study. (*J. Geophysical Research -Oceans-*, under revision).
- Gordon, C., C. Cooper, C.A. Senior, H. Banks, J.M. Gregory, T.C. Johns, J.F.B. Mitchell and R.A. Wood, 1999; The simulation of SST, sea ice extents and ocean heat transports in a version of the Hadley Centre coupled model without flux adjustments. *Climate Dynamics* (accepted).
- Gregory D., R. Kershaw and P.M. Inness, 1997; Parametrization of momentum transport by convection. II: tests in single column and general circulation models. *QJR Meteor. Soc.* 123: 1153-1183.
- \*Gregory, J. M. and Mitchell, J. F. B, 1997. The climate response to CO<sub>2</sub> of the Hadley Centre coupled AOGCM with and without flux adjustment. *Geophysical Research Letters*, 24, 1943-1946.
- Gregory D., G.J. Shutts and J.R. Mitchell, 1998; A new gravity wave drag scheme incorporating anisotropic orography and low level wave breaking: Impact upon the climate of the UK Meteorological Office Unified Model. *QJR Meteor. Soc.* 124: 463-493.
- Grenier H., 1995. Grid connection and related sub-grid motions in a global climate model. *Progress Report 1995/8*, Université catholique de Louvain, Institut d'Astronomie et de Géophysique G. Lemaître.
- \* Grenier H., 1997. Les interactions air-mer dans le système climatique: une étude à l'aide d'un modèle couplé tridimensionnel océan-atmosphère-glace marine. *Thèse de doctorat*, Université catholique de Louvain, Louvain-la-Neuve, Belgium.

- \* Grenier, H., H. Le Treut, and T. Fichefet, 1999. Ocean-atmosphere interactions and climate drift in a coupled general circulation model. (*Climate Dynamics*, under revision).
- \*Hadley Centre 1997. Climate Change and its impacts: a global perspective. Department of the Environment, Transport and the Regions /UK Met Office, 16 pp.
- \*Hadley Centre 1998. Climate Change and its impacts. Some highlights from the ongoing UK research programme: a first look at results from the Hadley Centre's new climate model. Department of the Environment, Transport and the Regions/UK Met Office, 11 pp.
- Haigh, J.D., 1996; Impact of solar variability on climate. *Science* 272: 981-984.
- Haigh, J.D., 1994; The role of stratospheric ozone in modulating the solar radiative forcing of climate. *Nature* 370: 544-546.
- Haney, R. L., 1971: Surface thermal boundary conditions for ocean circulation models. *J. Phys. Oceanogr.*, 1, 241-248.
- Hansen J.E., Fung I., Lacis A.A., Ring D., Lebedeff S., Ruedy R., and G. Russell, 1988: Global climate changes as forecast by Goddard Institute for Space Studies three-dimensional model. *J. Geophys. Res.*, 93, pp. 9341-9364.
- Harzallah, A. and R. Sadourny, 1995. Internal versus SST-forced atmospheric variability as simulated by an atmospheric General Circulation Model. *J. Climate*, 8, pp. 474-495.
- Hibler III, W. D., 1979: A dynamic thermodynamic sea ice model, *J. Phys. Oceanogr.*, 9, 815-846.
- Hasselmann, K., 1993; Optimal fingerprints for the detection of time-dependent climate change. *J. Climate* 6: 1957-1971.
- \*Hasselmann, K., 1997; Multi-pattern fingerprint method for detection and attribution of climate change. *Climate Dynamics* 13: 601-611.
- \*Hegerl, G.C., H. von Storch, K.Hasselmann, B.D.Santer, U.Cubasch and P.D.Jones, 1996; Detecting greenhouse gas induced climate change with an optimal fingerprint method. *J. Clim.* 9: 2281-2306.
- \*Hegerl G.C. and North, G. R. (1997): Comparison of statistically optimal approaches to detecting anthropogenic climate change. *J. Climate*, 10, 1125-1133.
- \*Hegerl G. C., Hasselmann K., Cubasch U., Mitchell, J. F. B., Roeckner, E., Voss, R. and Waszkewitz J. (1997): On multi-fingerprint detection and attribution of greenhouse gas- and aerosol forced climate change. *Climate Dynamics*, 13: 612-634.
- Houghton J.T., G.J. Jenkins, J.J. Ephraums, (eds) 1990: Climate change: The IPCC scientific assessment. Cambridge University Press, Cambridge
- Houghton J.T., L.G. Meira Filho, J. Bruce, H. Lee, B.A. Callander, E. Haites, N. Harries and K. Maskell, (eds) 1995: Climate Change 1994 Radiative forcing of climate change and an evaluation of the IPCC IS92 emission scenarios. Cambridge University Press, Cambridge
- Houghton, J.T., L.G. Meir a Filho, B.A. Callander, N. Harris, A. Kattenberg and K. Maskell (editors), 1996. Climate Change 1995. The science of climate change. Cambridge University Press, Cambridge.
- Hoyt, D.V. and K.H.Schatten, 1993; A discussion of plausible solar irradiance variations, 1700-1992. *J. Geophys. Res* 98: 18895-18906.
- Hurrell, J.W., 1995: Decadal trends in the North Atlantic Oscillation: regional temperatures and precipitation. *Science*, 269, 676-679.
- \*Hulme, M., T.J. Osborn and T.C. Johns, 1998. Precipitation sensitivity to global warming: Comparison of observations with HadCM2 simulations. *Geophys. Res. Let.* 25, 3379-3382.
- IPCC, 1996. Climate Change 1995: The Science of Climate Change. J.T. Houghton, L.G. Meira Filho, B.A. Callander, N. Harris, A. Kattenberg, and K. Maskell (eds.), Cambridge University Press, Cambridge, UK, 572 pp.

- Johns, T.C., 1996; A description of the second Hadley Centre coupled model (HADCM2). *Climate Research Technical Note 71*, UK Meteorological Office, Bracknell.
- \*Johns, T.C., Carnell, R.E., Crossley, J.F., Gregory, J.M., Mitchell, J.F.B., Senior, C.A., Tett, S.F.B. and Wood, R.A., 1997: The Second Hadley Centre Coupled Ocean-Atmosphere GCM: Model Description, Spinup and Validation. *Climate Dynamics*, 13, 103-134.
- \*Jones P. D. and Hegerl G. C. (1998): Comparisons of two methods of removing anthropogenically related variability from the near-surface observational temperature field. *JGR* 103: 13777-13786
- Kantha L.H. and C.A. Clayson, 1994. An improved mixed layer model for geophysical applications. *J. Geophys. Res.*, 99(C12), pp. 25235-25266.
- Karoly, D.J., J.A.Cohen, G.A.Meehl, J.F.B.Mitchell, A.H.Oort, R.J.Stouffer and R.T.Wetherald, 1994; An example of fingerprint detection of greenhouse climate change. *Climate Dynamics*, 10: 97-105.
- \*Keen, A.B. and Murphy, J.M., 1997: Influence of natural variability and the cold start problem on the simulated transient response to increasing CO<sub>2</sub>. *Climate Dynamics*, 13, 847-864.
- Kraus, E.B. and J.S. Turner, 1967; A one dimensional model of the seasonal thermocline. Part II. *Tellus*, 19: 98-105.
- Kuo H.L., 1965 ; On the formation and intensification of tropical cyclones through latent heat release by cumulus convection. *J. Atmospheric Sci.*, 22, pp. 40-63.
- Langner, J., and H. Rodhe, 1991. A Global Three-Dimensional Model of the Tropospheric Sulphur Cycle. *J. Atmos. Chemistry*, 13: 225-263.
- König W, Sausen R, Sielmann F (1993): Objective identification of cyclones in GCM simulations. *J. Climate*, 6: 2217-2231
- Lean, J., J. Beer and R. Bradley, 1995: Reconstruction of solar irradiance since 1600: Implications for climate change. *Geophys. Res. Lett.*, 22, 3195-3198.
- Le Treut H. and X.S. Li, 1991. Sensitivity of an atmospheric general circulation model to prescribed SST changes: feedback effects associated with the simulation of cloud optical properties. *Clim. Dyn.*, 5, pp. 175-187.
- Levitus S., 1982. Climatological Atlas of the world ocean, 173pp., *NOAA professional paper 13*.
- Levitus, S. and T.P. Boyer, 1994; World Ocean Atlas 1994, Volume 4: Temperature. NOAA/NESDIS E/OC21, US Department of Commerce, Washington, DC, 117pp.
- Louis J.F., 1979. A parametric model of vertical eddy fluxes in the atmosphere. *Bound. Layer Meteo.*, 17, pp. 187-202.
- \*Lunkeit F, Sausen R, Oberhuber JM, 1996a: Climate simulations with the global coupled atmosphere-ocean model ECHAM2/OPYC. Part I: present-day climate and ENSO events. *Clim Dyn* 12: 195-212
- \*Lunkeit, F., M. Ponater, R. Sausen, M. Sogalla, U. Ulbrich, and M. Windelband, 1996b: Cyclonic activity in a warmer climate. *Beitr. Phys. Atmosphäre*, 69, 393 - 407
- Madec G. and M. Imbard, 1996. A global ocean mesh to overcome the North Pole singularity. *Climate Dynamics*, 12, pp. 381-388.
- Maier-Reimer, E., U. Mikolajewicz and K. Hasselmann, 1993: Mean circulations the Hamburg LSG OGCM and its sensitivity to the thermohaline forcing. *J. Phys. Oceanogr.*, 23, 731-757.
- Manabe S. and R.F. Strickler, 1964. On the thermal equilibrium of the atmosphere with convective adjustment. *J. Atmos. Sci.*, 21, pp. 361-385.
- Manabe, S., and R.J. Stouffer, 1994: Multiple-century response of a coupled ocean-atmosphere model to an increase of the atmospheric carbon dioxide. *J. Clim.*, 7, 5-23.

- Mann, M.E., R.S.Bradley and M.K.Hughes, 1998; Global-scale temperature patterns and climate forcing over the past six centuries. *Nature* 392: 779-787.
- Mellor G.L. and T. Yamada, 1974. A hierarchy of turbulence closure models for planetary boundary layers. *J. Atmos. Sci.*, 31, pp. 1791-1806.
- Mellor G.L. and T. Yamada, 1982. Development of a turbulence closure model for geophysical fluid problems. *Rev. Geophys. Spac. Phys.*, 20(4), pp. 851-875.
- Météo-France/CNRM, 1996. ARPEGE-Climat version 2 (4 volumes). Available on query at M. Déqué, CNRM 42 avenue Coriolis Cedex 1, 31057 Toulouse, France.
- \*Mikolajewicz, U., R. Voss, 1998: The role of individual air-sea flux components in CO<sub>2</sub>-induced changes of the ocean's circulation and climate. Report No. 263, Max-Planck-Institut für Meteorologie, Hamburg, Germany.
- Milton, S.F. and C.A.Wilson, 1996; The impact of parametrized sub-grid scale orographic forcing on systematic errors in a global NWP model. *Mon. Weath. Rev.* 124: 2023-2045.
- \*Mitchell, J.F.B. and Johns, T.C. 1997: On modification of global warming by sulfate aerosols. *J. Climate*, 10, 245-267.
- \*Mitchell, J.F.B., Johns, T.C. and Senior, C.A. 1998: Transient response to increasing greenhouse gases using models with and without flux adjustment. Hadley Centre Technical Note No. 2, Meteorological Office, Bracknell, UK.
- Mitchell, J.F.B., R.A.Davis, W.J.Ingram and C.A.Senior, 1995; On Surface Temperature, Greenhouse Gases, and Aerosols: Models and Observations. *J. Climate* 10: 2364-2386.
- Mitchell, J.F.B, T.C.Johns, J.M.Gregory and S.F.B.Tett, 1995; Climate response to increasing levels of greenhouse gases and sulfate aerosols. *Nature* 376: 501-504.
- Mitchell, J.F.B. and T.C.Johns, 1997; On modification of global warming by sulfate aerosols. *J. Climate*, 10: 245-267.
- Neelin, J. D., M. Latif, M. A. F. Allaart, M. A. Cane, U. Cubasch, W. L. Gates, P. R. Gent, M. Ghil, C. Gordon, N. C. Lau, G. A. Meehl, C. R. Mechoso, J. M. Oberhuber, S. G. H. Philander, P. S. Schopf, K. R. Sperber, A. Sterl, T. Tokioka, J. Tribbia und E. Zebiak, 1992: Tropical air-sea-interaction in general circulation models; *Climate Dynamics*, 7, 73-104.
- North, G.R., K.-K. Kim, S.S.P.Shen and J.W.Hardin, 1995; Detection of Forced Climate Signals. Part I: Filter Theory. *J. Climate* 8: 401-408.
- Morcrette J.J., 1990. Impact of changes to the radiation transfer parameterizations plus cloud optical properties in the ECMWF model. *Monthly Weather Review*, 118, pp. 847-873.
- Oberhuber, J. M., 1988: An atlas based on the COADS data set: The budgets of heat, buoyancy and turbulent kinetic energy at the surface of the global ocean. Report No. 15, MPI für Meteorologie, Hamburg, FRG.
- Oberhuber, J. M., 1993a: Simulation of the Atlantic circulation with a coupled sea-ice-mixed layer-isopycnal general circulation model. Part I: Model description. *J. Phys. Oceanogr.*, 23, 808-829.
- Oberhuber, J. M., 1993b: Simulation of the Atlantic circulation with a coupled sea-ice-mixed layer-isopycnal general circulation model. Part II: Model experiment. *J. Phys. Oceanogr.*, 23, 830-845.
- \*Ohmura, A., Wild, M., and Bengtsson, L. 1996a: A possible change in mass balance of greenland and antarctic ice sheets in the coming century. *J. of Climate*, 9, 2124-2135.
- \*Ohmura, A., Wild, M., and Bengtsson, L. 1996b: Present and future mass balance of the ice sheets simulated with GCM. *Annals of Glaciology* 23, 187-193.
- Overpeck, J., K. Hughen, D. Hardy, R. Bradley, R. Case, M. Douglas, B. Finney, K. Gajewski, G. Jacoby, A. Jennings, S. Lamoureux, A. Lasca, G. MacDonald, J. Moore, M. Retelle, S. Smith, A. Wolfe, and G. Zielinski, 1997. Arctic environmental change of the last four centuries. *Science*, 278: 1251-1256.

- Pacanowski, R.C. and S. G. Philander, 1981; Parametrization of vertical mixing in numerical models of tropical oceans. *J. Phys. Oceanogr. 11*: 1443-1451.
- Parker, D.E., M.Gordon, D.P.N.Cullum, D.M.H.Sexton, C.K.Folland and N.Rayner, 1997; A new global gridded radiosonde temperature data base and recent temperature trends. *Geophys. Res. Lett. 24*; 1499-1502.
- Parker, D.E., P.D.Jones, C.K.Folland and A.Bevan, 1994; Interdecadal changes of surface temperature since the late nineteenth century, *J. Geophys. Res 99*: 14373-14399.
- \* Poncin, C., T. Fichefet, and H. Grenier, 1997: A coupled atmosphere--ocean general circulation model for climate studies. Dans : IAMAS--IAPSO, Melbourne 1997, Earth--Ocean--Atmosphere Forces for Changes, Abstracts, pp. JPM9--2.
- \* Poncin, C., T. Fichefet, and H. Goosse, 1998: Sensitivity experiments with a coupled atmosphere--ocean general circulation model. *Ann. Geophysicae, Part II: Hydrology, Oceans, and Atmosphere, Supplement II to volume 16*, C650.
- \* Poncin, C., and T. Fichefet, 1999. Sensitivity experiments with the UCL's coupled atmosphere-ocean general circulation model. *Geophysical Research Abstracts, vol. 1(2)*, 24<sup>th</sup> General Assembly Hydrology, Oceans and Atmosphere, p.569.
- Rahmstorf, S. 1994: Rapid climate transitions in a coupled ocean-atmosphere model. *Nature*, 372, 82-85.
- Rahmstorf, S. 1995: Bifurcations of the Atlantic thermohaline circulation in response to changes in the hydrological cycle. *Nature*, 378, 145-149.
- Ritter B., and J.F. Geleyn, 1992. A comprehensive radiation scheme for numerical weather prediction models with potential applications in climate simulations. *Mon. Wea. Rev.*, 120, pp. 303-325.
- Roeckner, E., K. Arpe, L. Bengtsson; S. Brinkop, L. Dümenil, M. Esch, E. Kirk, F. Lunkeit, M. Ponater, B. Rockel, R. Sausen, U. Schlese, S. Schubert and M. Windelband, 1992: Simulation of the present-day climate with ECHAM model: impact of model physics and resolution. *Max-Planck-Institut für Meteorologie, Report No. 93*, 171 p.
- Roeckner, E., T. Siebert and H. Feichter, 1995: Climatic response to anthropogenic sulphate forcing simulated with a general circulation model. In: *Aerosol Forcing of Climate*, Ed. R. J. Charlson and J. Heintzenberg, Eds., John Wiley & Sons, Cichester, pp. 349-362.
- Roeckner, E., K. Arpe, L. Bengtsson, M. Christoph, M. Claussen, L. Dümenil, M. Esch, M. Giorgetta, U. Schlese and U. Schulzweida, 1996: The atmospheric general circulation model ECHAM4: model description and simulation of present-day climate. *Max-Planck-Institut für Meteorologie, Hamburg, Report No. 218*.
- Roeckner, E., L. Bengtsson, J. Feichter, J. Lelieveld, and H. Rodhe, 1998: Transient climate change simulations with a coupled atmosphere-ocean GCM including the tropospheric sulfur cycle. MPI Report No. 266, 48 pp [available from Max-Planck-Institute for Meteorology, Bundesstrasse 55, 20146 Hamburg, Germany].
- Royer, J.-F., F. Chauvin, B. Timbal, P. Araspin and D. Grimal, 1998: A GCM Study of the Impact of Greenhouse Gas Increase on the Frequency of Occurrence of Tropical Cyclones. *Climatic Change 38*, 307-343.
- Sadourny R., 1975a. The dynamics of finite difference models of the shallow water equations. *J. Atmos. Sci.*, 32, pp. 680-689.
- Sadourny R., 1975b. Compressible model flows on the sphere. *J. Atmos. Sci.*, 32, pp. 2103-2110.
- Sadourny R. and K. Laval, 1984. January and July performance of the LMD General Circulation Model. In: *New Perspectives in Climate Modelling*, pp. 173-198, Elsevier Science Publishers, Amsterdam.
- Santer, B.D., K.E.Taylor, T.M.L.Wigley, T.C.Johns, P.D.Jones, D.J.Karoly, J.F.B.Mitchell, A.H.Oort, J.E.Penner, V.Ramaswamy, M.D.Schwarzkopf, R.J.Stouffer and S. Tett, 1996; A Search for Human Influences on the Thermal Structure of the Atmosphere. *Nature 382*: 39-45.
- Sato, M., J.E.Hansen, M.P.McCormick and J.B.Pollack, 1993; Stratospheric aerosol optical depths (1850-1990). *J. Geophys. Res. 98*: 22987-22994.

- Sausen, R., K. Barthel, K. Hasselmann, 1988 : Coupled ocean-atmosphere models with flux correction. *Clim. Dyn.*, 2, 145-163.
- Semtner A.J., 1976. A model for the thermodynamic growth of sea ice in numerical investigations of climate. *J. Phys. Oceanogr.*, 6, pp. 379-389.
- Stott, P.A. and S.F.B.Tett, 1998; Scale-dependent detection of climate change. *J. Climate*, 11, 3282-3294.
- Stouffer, R.J., S.Manabe and K.Ya.Vinnikov, 1994; Model assessment of the role of natural variability in recent global warming. *Nature* 367: 634-636.
- Stouffer, R.J., Hegerl G. C. and Tett S. F. B. (1998): A comparison of surface air temperature variability in three 1000-year coupled ocean-atmosphere model integrations. Submitted for publication.
- Terray L., E. Sevault, E. Guilyardi, and O. Thual, 1995. The OASIS coupler user guide version 2.0, CERFACS technical report TR/CMGC/95-46.
- Taylor, K., and J. E. Penner, 1994: Response of the climate system to atmospheric aerosols and greenhouse gases. *Nature*, 380, 419-422.
- Terray L., S. Valcke, A. Piacentini, 1998. OASIS 2.2, Ocean atmosphere sea ice soil, User's Guide and Reference Manual. CERFACS technical report TR/CGMC/98-05.
- \*Tett, S.F.B., T.C.Johns and J.F.B.Mitchell, 1997; Global and regional variability in a coupled AOGCM. *Climate Dynamics* 13: 303-323.
- Tett, S.F.B., J.F.B.Mitchell, D.E.Parker and M.R.Allen, 1996; Human influence on the atmospheric vertical temperature Structure: detection and observations. *Science* 247: 1170-1173.
- \*Timbal B., J-F. Mahfouf, J-F. Royer, U. Cubasch and J.M. Murphy, 1997. Comparison between doubled CO2 time slice and coupled experiments. *J Climate*, 10, 1463-1469.
- \*Ulbrich, U., M. Christoph , J.G. Pinto and J. Corte-Real, 1998: Dependence of winter precipitation over Portugal on NAO and baroclinic wave activity. *Int. J. Climatol.*, in press.
- \*Ulbrich, U., M. Christoph , J.G. Pinto and J. Corte-Real, 1999: Dependence of Winter Precipitation over Portugal on NAO and Baroclinic Wave Activity. *Int. J. Climatol.*, 19, 379-390.
- \*Ulbrich, U., and M. Christoph, 1999: A Shift of the NAO and Increasing Storm Track Activity over Europe due to Anthropogenic Greenhouse Gas Forcing. *Climate Dynamics*, 15, 551-559.
- Unesco, 1983. Algorithms for computation of fundamental property of sea water. Unesco Techn. Pap. Mar. Sci., 44.
- Visbeck, M., J. Marshall, T. Haine and M. Spall, 1997; On the specification of eddy transfer coefficients in coarse resolution ocean circulation models. *J. Phys. Oceanogr.* 27: 381-402.
- Voss R, 1996: Entwicklung eines Kopplungsverfahrens zur Reduzierung der Rechenzeit von Atmosphäre-Ozean-Modellen. Max-Planck-Institut für Meteorologie, Hamburg, Examensarbeit Nr 38 (ISSN 0938-5177), 123 pp
- \*Voss, R., R. Sausen and U. Cubasch, 1998: Periodically synchronously coupled integrations with the atmosphere-ocean general circulation model ECHAM3/LSG. *Clim. Dyn.*, 14, 249-266
- \*Voss, R. U. Mikolajewicz, 1999: Long-term climate changes due to increased CO<sub>2</sub>-concentration in the coupled atmosphere-ocean general circulation model ECHAM3/LSG. In prep.
- \*Wild M., Ohmura A., and Cubasch U., 1997: GCM simulated surface energy fluxes in climate change experiments. *J. Climate*, 10, 3093-3110.
- Willson, R.C., 1997; Total solar irradiance trend during solar cycles 21 and 22. *Science* 277: 1963-1965.
- Wolff, J.-O., E. Maier-Reimer, and S. Legutke, 1997: The Hamburg Ocean Primitive Equation Model, *Technical report, No.*

13, German Climate Computer Center (DKRZ), Hamburg, 98pp.

Wright, D.K., 1997; A new eddy mixing parametrization and ocean general circulation model. *International WOCE newsletter*, 26: 27-29.

Zielinski, G.A., 1995. Stratospheric loading and optical depth estimates of explosive volcanism over the last 2100 years derived from the Greenland Ice Sheet Project 2 Ice core. *J. Geophys. Res.*, 100: 20,937-20,955.